

Review

Plant-Derived Metal Nanoparticles (PDMNPs): Synthesis, Characterization, and Oxidative Stress-Mediated Therapeutic Actions

Mohammad Faheem Khan ^{1,2,*}  and Mohd Aamish Khan ^{1,2}

¹ Department of Biotechnology, Era's Lucknow Medical College & Hospital, Era University, Sarfarazganj, Hardoi Road, Lucknow 226003, India

² Department of Chemistry, Era University, Sarfarazganj, Hardoi Road, Lucknow 226003, India

* Correspondence: faheemkhan35@gmail.com

Abstract: In the 21st century, plant-derived metal nanoparticles (PDMNPs) have gained considerable interest because of their tremendous and remarkable potential as therapeutic agents as well as development of less expensive, safer, and easier biomedical equipment. PDMNPs are synthesized from metal salts or oxides by using plant extracts because plants have diversified bioactive compounds that can act as reducing and stabilizing agents at the time of nanoparticle synthesis. Besides, PDMNPs take advantages over the nanoparticles synthesized by other methods because of their low cost, environmental friendliness, and sustainability. The present review explains the synthesis of PDMNPs, their characterization techniques, and oxidative stress-mediated pharmacological effects. The mode of actions for antioxidant, antimicrobial, and anticancer properties has also been critically explored. Due to the plethora of data on plant-derived nanoparticles and their pharmacological properties, we have highlighted PDMNPs' shape, size, metals of use, and experimental findings regarding their antioxidant, anti-microbial, and anticancer properties in a tabulated form for studies conducted in the last five years, from 2018 to 2022. Because of our review study, we, herein, contemplate that the scientific community as a whole will get a greater comprehension of PDMNPs and their numerous therapeutic applications in a single window.

Keywords: plant-derived metal nanoparticles; reactive oxygen species (ROS); antioxidant; antimicrobial; anticancer



Citation: Khan, M.F.; Khan, M.A. Plant-Derived Metal Nanoparticles (PDMNPs): Synthesis, Characterization, and Oxidative Stress-Mediated Therapeutic Actions.

Future Pharmacol. **2023**, *3*, 252–295.

<https://doi.org/10.3390/futurepharmacol3010018>

Academic Editor: Fabrizio Schifano

Received: 24 December 2022

Revised: 13 February 2023

Accepted: 17 February 2023

Published: 1 March 2023



Copyright: © 2023 by the authors. Licensee MDPI, Basel, Switzerland. This article is an open access article distributed under the terms and conditions of the Creative Commons Attribution (CC BY) license (<https://creativecommons.org/licenses/by/4.0/>).

1. Introduction

The burgeoning branch of science based on nanoparticles (NPs), known as nanoscience and nanotechnology, has attracted a lot of study attention over the past few decades. NPs have been developed widely with unique and dazzling properties ranging in size from 1.0 to 100 nm because they provide the way for advancing multidisciplinary research ranging from medicine to engineering, physics, and chemistry [1]. For several years, NPs have been employed in the manufacture of nanodevices, nanotherapeutics, nanoelectronics, and engineered biological structures, with applications in pharmaceuticals, foods, agriculture, energy, environment, cosmetics, electronics, and catalysis [2]. Because of their tiny size, diverse structure, and numerous biological and physicochemical features, NPs have increasingly caught the attention of the research community over the past two decades [3]. In most of the cases, metal salts/oxides-mediated NPs outperform other nanoparticles due to their huge surface area to volume ratio, excellent biocompatibility, adjustable production, and high stability, making them appropriate for a wide range of applications [3]. Depending on the synthesis methods, NPs may be obtained in various forms, including nanotubes, nanorods, nanoparticles, and nano-sheets, which differ in morphology, size, and form along with optical properties, but they excel in a variety of applications in diverse sectors [4]. The top-down strategy and bottom-up approach are two methods used to create

nanoparticles. The techniques that use chemical reactions to generate nanoparticles are commonly known as bottom-up approaches. These processes can also be used to grow thin films in some cases. For generating thin films when bulk material is used for depositions, top-down techniques are preferable. Radio frequency sputtering, pulsed laser deposition, molecular beam epitaxy, and e-beam evaporation are the techniques that are often utilized. NPs are sometimes grown using techniques like mechanical milling and high-energy ball milling [5].

Furthermore, due to significant energy consumption, environmental contamination, and detrimental impacts on humans, physical and chemical procedures are not regarded as an optimal and significant strategy for manufacturing NPs [6]. To address these inadequacies, green methods are preferable since they are environmentally friendly, save energy, and have no hazardous side effects. There are numerous green and sustainable methods for producing NPs, including microorganisms (bacteria, fungi, and yeast), biomolecules, and plants [7]. Plant-derived metal nanoparticles (PDMNPs) are among those that have gained recognition as nanomedicine in recent years and have advantages over synthetic NPs. Plants' bioactive compounds serve as reducing, capping, and stabilizing agents by converting the metal sources into NPs [8]. Although PDMNPs are biologically efficient as therapeutics at the target sites of protein receptors, they may exhibit several types of toxicity influenced by their size, shape, surface area, crystallinity, agglomeration as well as dissolution [9]. However, they are quite effective for a variety of therapeutic applications [10]. Thus, PDMNPs' ability to turn bioactive compounds that are poorly soluble and poorly absorbed into promising deliverable substances has enormous potential in the pharmaceutical and biomedical sectors. PDMNPs could lead to the development of cost-effective and safer therapeutic as well as drug-delivery agents against various diseases.

Oxidative stress, a global health concern, is a redox imbalance in between the generation and accumulation of reactive oxygen species (ROS) during the metabolic processes [11]. Oxidative stress is primarily caused by oxygen free radicals such as hydrogen peroxide, superoxide, and hydroxyl groups, which are produced as byproducts of molecular oxygen through oxidative reactions, catalyzed by endothelial nitric oxide synthase (eNOS), xanthine oxidase (XO), and NADPH oxidases enzymes [12]. Based on types and sources, oxidative stress signaling causes metabolic dysfunctions and inflammatory responses. Consequently, increased inflammatory signaling is linked to altered redox balance, which leads to metabolic dysfunctions such as cardiovascular stroke, atherosclerosis, and diabetes [13]. On the other side, ROS overproduction causes oxidative damage to biomembranes, lipids, fats, proteins, and nucleic acids, which leads to aging, inflammation, pain, and the onset of various diseases such as diabetes, cancer, cardiovascular, neurodegenerative, and metabolic disorders [14]. Naturally, the human body has a number of independent cellular mechanisms that work together to counteract the negative effects of oxidative stress. Antioxidants, whether produced endogenously or taken as supplements, are helpful in reducing oxidative stress [15]. Thus, managing ROS may be an important therapeutic pursuit to prevent various diseases. PDMNPs have a well-established role in the prevention of oxidative stress-related diseases [16]. PDMNPs exposure may significantly increase ROS generation because PDMNPs release metal ions, which promote ROS overexpression by impairing mitochondrial function via targeting electron transport chain (ETC) reactions [17]. Additionally, at higher doses, PDMNPs may cause pathophysiological toxicity, including genotoxicity, inflammation, carcinogenesis, and cell necrosis [18]. PDMNPs, on the other side, release metal ions at very low doses, which interfere with the redox reaction and produce the Fenton reaction, e.g., $H_2O_2 + M^{n+} \rightarrow M^{n+} + HO^- + \bullet OH$. This entire cascade suppresses the mitochondrial membrane potential and the electron shuttle chain, as well as blocking the enzymes that denature the proteins of the cell membrane [19]. Because of this process, PDMNPs exhibit antioxidant, antibacterial, and anticancer properties.

Thus, keeping all these points in mind, we envisioned the PDMNPs in a concise manner through this study which is focused on their synthesis, characterization techniques, and pharmacological properties in a lucid approach (Figure 1). For many decades, a huge

number of publications on various pharmacological properties of plant-derived NPs have been published but addressing the mode of action and mechanism is very limited. Due to this rationale, the antioxidant, antimicrobial, and anticancer activities have been provided in a tabular form for the last 5 years from the year of 2018 to the year-end of 2022. More importantly, in-depth mechanisms of oxidative stress-mediated pharmacological actions are also covered. We hope that the scientific community will get a deeper understanding of the physicochemical profile of PDMNPs and their therapeutic applications as a result of this review.

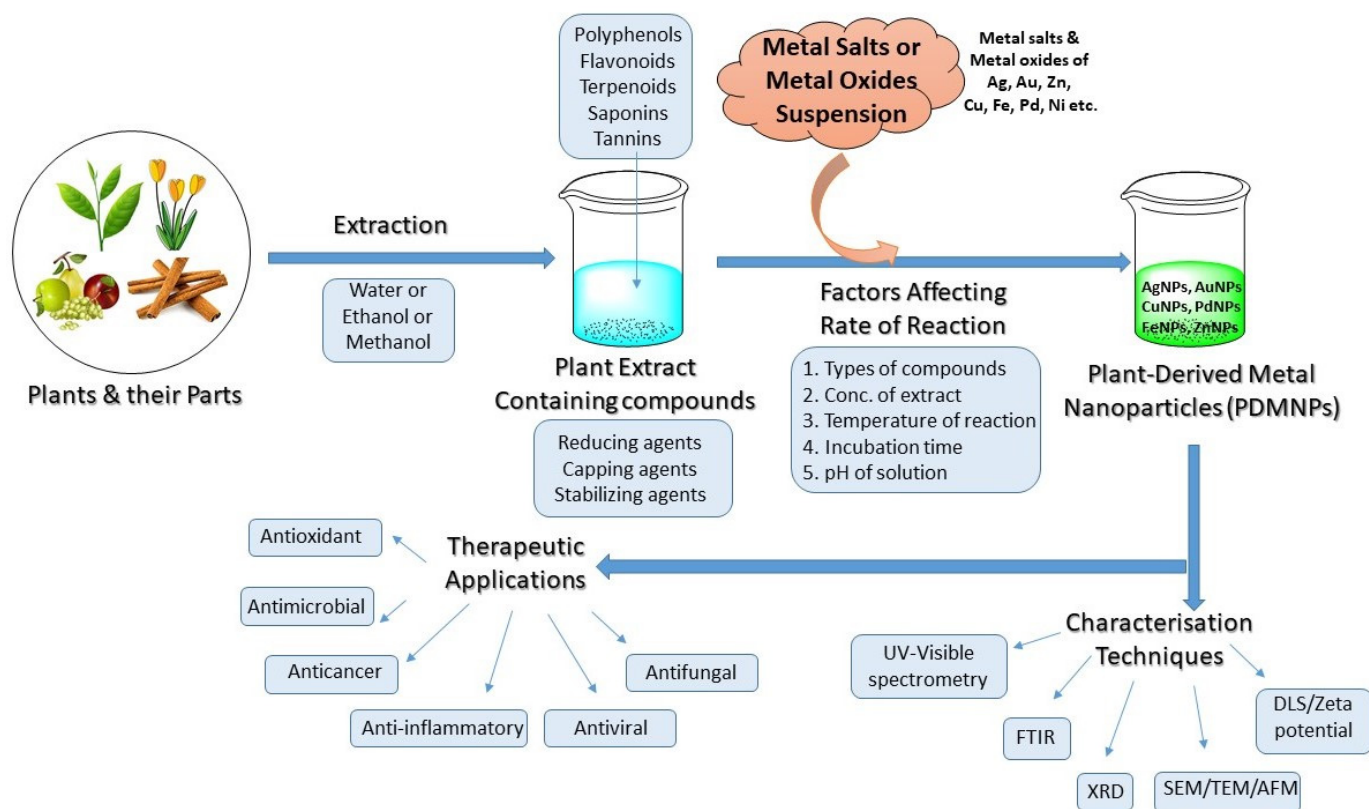


Figure 1. Schematic diagram showing the strategies for the synthesis, optimization of reactions, characterization, and therapeutic applications of PDMNPs.

2. Overview of Nanoparticles

2.1. History and Development of Nanoparticles

NPs made of carbon or other materials such as silver (Ag), gold (Au), or iron (Fe) metals have nanoscopic dimensions ranging from 1 to 100 nanometers in size [20]. They cannot be seen with the naked eye or even a standard microscope [21]. Because of their small size, NPs exhibit high surface energy, and huge surface area, and thus, they have unique and distinct physical and chemical properties from their bulk counterparts [22]. NPs can be made artificially as by-products or by modifying/engineering raw materials that have specific functions. The chemical synthesis of metal-based NPs, including Ag, Au, Fe, copper (Cu), zinc (Zn), palladium (Pd), platinum (Pt), and cobalt (Co) comes to mind when we discuss the different types of nanoparticles [23]. Materials like metal salts, metal oxide, silicates, polymers, organics, carbon, and others are also tuned into nano-size on a large scale using physical, mechanical, and chemical approaches [24]. Depending on the material from which they are made, nanomaterials can adopt a variety of morphologies such as spheres, cylinders, sheets, or tubes [25]. Nanomaterials can take many different forms, such as zero-dimensional (colloids, quantum dots, nanoclusters, etc.), one-dimensional (nanowires, nanotubes, nanobelts, and nanorod, etc.), two-dimensional (quantum wells, super lattices, and bio membranes, etc.), and three-dimensional (nanocomposites, filamentary composites,

cellular materials, porous materials, hybrids, and nanocrystal array) [26–28]. The synthesis of metal nanoparticles in suspension was made by Faraday in 1857, and Mie characterized the quantitative color change of nanoparticles in suspension in 1908 [29]. Metal-based nanomaterials are superior to other nanomaterials due to their high area-to-volume ratio, high surface energy, and distinctive electronic structure, which are formed via simple electronic transitions between various energy levels [30]. Ag is one of the metals that is frequently used to create nanomaterials using a variety of techniques because it is simple to convert from Ag^+ ion to zero valent Ag^0 . As a result, silver has many excellent uses in the fields of medicine, catalysis, biotechnology, the environment, and the textile industry. According to a literature review, Au is also used in the synthesis of nanomaterials to a significant level, followed by other metals, viz., Cu, Zn, Fe, Pd, Pt, and Co but to a lesser extent [31]. Nanomaterials based on metal oxide are used to create nano-polymers because they have an M-O-M bridge connecting the metal to the oxygen atom [32]. Alloy-based nanomaterials are also created with specialized qualities, like the preservation of atomic ordering, lusters, and more cluster shining, to improve the metal properties in electronic appliances. Additionally, magnetic nanoparticles have a magnetic component (such as Fe, Co, or Ni) and a chemical component to modify their magnetic characteristics, which are widely used in industries for catalysis [33].

2.2. Methodology

The electronic search engines like SciFinder, Google Search, Google Scholar, National Center for Biotechnology Information (NCBI), PubMed, EMBASE (biomedical and pharmacological bibliographic database of published literature), and clinicaltrials.org were used to collect the scientific data based on PDMNPs and their therapeutic applications. In order to get the published papers, we also looked for publications including ScienceDirect, the American chemical society (ACS), Royal society of chemistry (RSC), Springer Nature, Elsevier, Taylor & Francis, and Bentham Sciences. The key terms, like Nanoparticles, plant-derived nanoparticles, plant-based nanoparticles, metal nanoparticles, therapeutic applications of nanoparticles, antioxidant properties of nanoparticles, antimicrobial properties of nanoparticles, and anticancer properties of nanoparticles, were used to search the literature for this review article.

3. Synthesis of PDMNPs

3.1. General Synthesis

The properties and therapeutic applications of NPs or PDMNPs depend on their synthesis method. They are often synthesized using the top-down approach and the bottom-up approach [34,35]. As shown in Figure 2, to make nanoparticles, both approaches include physical, chemical, and biological processes [36]. The bulk material under study is broken down into fine particles using suitable techniques such as mechanical grinding, thermal evaporation, sputtering, and ball-milling in the top-down approach, whereas in the bottom-up approach, nanomaterials are synthesized by assembling atoms or molecules into new or novel material in the nano-size using chemical and biological methods [37]. Condensation and evaporation are two important physical processes that generate metal NPs in a furnace tube at atmospheric pressure. These processes mostly follow the top-down method, utilizing electrical or mechanical energy to grind materials into minute NPs. Even though physical techniques do not involve hazardous materials, they nonetheless cost more to produce nanoparticles since they need expensive and energy-intensive equipment [38]. Chemical methods include the reduction, precipitation, hydrothermal, sol-gel, emulsion, and micro-emulsion processes. The most widely used technology among them is sol-gel because of its flexible implementation and high yield. Chemical processes are faster at producing bulk materials, but they also require expensive, hazardous substances that are detrimental to the environment and our health [39]. The synthesis of NPs using salts or oxides of metals such as Ag, Au, Pt, and Pd has attracted a lot of attention in recent decades due to the need to create materials that are safe for the environment, society, and economy,

as well as for use in everyday items like electrical appliances, vehicles, aircraft, biomedical devices, and medications [40]. Because they are uniform in size, shape, composition, surface charge, and optical properties, metal-based NPs have many advantageous medical and industrial applications. However, the high cost and purity of metals during synthesis is a major concern in the biomedical and pharmaceutical sectors [41,42]. Greener approaches to synthesizing biogenic NPs are constantly in demand by researchers to reduce toxic effects and maintain a green environment because of their biocompatible, clean, cost-effective, and eco-friendly properties [43,44].

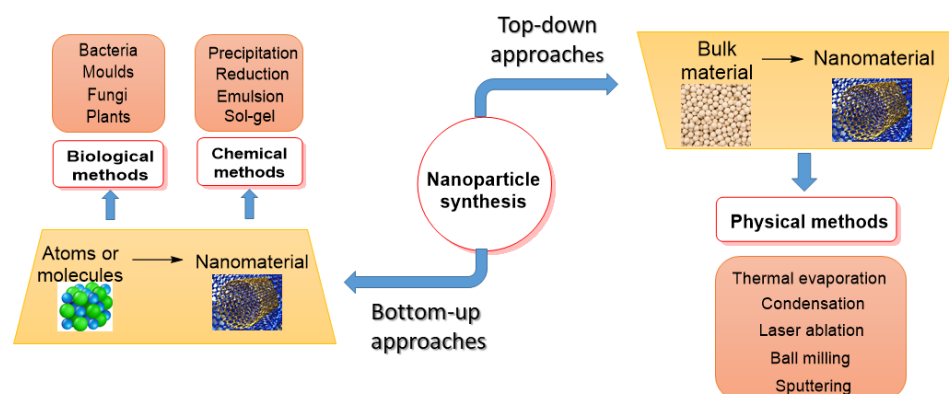


Figure 2. A flow chart showing the synthesis of PDMNPs by applying top-down and bottom-up approaches.

3.2. Plant Mediated Synthesis

Use of fungi, bacteria, plant, and plant-derived products are the best examples and best studied topics currently to synthesize green NPs over conventionally synthesized NPs [45]. However, the production of NPs by microorganisms like bacteria and fungi is a costly and time-consuming process, and since microbes are the main contributor to many diseases, high-grade care is always needed. PDMNPs do not pose these dangers and typically preserve positive health effects. In the suspension of plant extracts and metal salts/oxides, the synthesis of PDMNPs is completed in three steps, viz., activation, growth, and termination [46]. The synthesis begins with the activation of metal salts/oxides by reducing them followed by the growth of smaller nanoparticles into larger NPs, and finally, with the production of desired nanoparticles [47]. The usage of plant extract helps to overcome the poor solubility, decreased stability, and extended duration, which are the main drawbacks of the synthesis of metal NPs (Figure 3). The aqueous extracts of the leaves of numerous plants have received the most attention among plant extracts for the production of metal-chelated NPs [48]. Given the rapid rate of synthesis, short reaction times, and repeatable yields of Ag and Au, these metals are excellent choices for creating plant-based NPs [49]. All plant parts, including the flowers, leaves, stems, fruits, and roots, are abundant sources of bioactive compounds, which include terpenoids, polyphenols, flavonoids, and tannins. Numerous studies have demonstrated that various plant extracts contain polyphenols, flavonoids, tannins, quinol, chlorophyll, and saponin, contributing as reducing, capping, and stabilizing agents to improve the stability of PDMNPs [50].

When PDMNPs are synthesized, the bioactive compounds found in plant extracts provide great stability, reduce the clumping, as well as inhibiting the agglomeration, which promotes good dispersion and more active sites in the suspension [51]. These bioactive compounds have a variety of functional groups, including carboxylic acid (-COOH), aldehyde (-CHO), hydroxyl (-OH), nitrile (-CN), and amines (-NH₂), which are engaged in reducing metal ions into free metals (Figure 4) like $\text{Ag}^+ \rightarrow \text{Ag}^0$, $\text{Au}^+ \rightarrow \text{Au}^0$, $\text{Cu}^{2+} \rightarrow \text{Cu}^0$, $\text{Zn}^{2+} \rightarrow \text{Zn}^0$, and $\text{Pt}^+ \rightarrow \text{Pt}^0$ [52]. Bioactive compounds also improve the adsorption ability of NPs by increasing the surface area of PDMNPs through molecular interactions such as electrostatic interaction, dipole-dipole induction, π - π interaction, and hydrogen bonding [53]. According to research studies, functional groups of bioactive compounds are

4. Factors Affecting the Synthesis of PDMNPs

There are some challenges during the synthesis of PDMNPs, particularly, non-uniformity in the particle's shape and size, that need to be overcome in order to maintain monodispersity in the suspension phase. There are also some other factors that cause delays in the production rate, reaction time, and overall yield of synthesized nanoparticles. These factors include the concentration of plant extract, metal salt concentration, incubation time, pH, temperature, types of bioactive compounds, and agitation processes to make the plant extract and suspension of nanoparticles [60].

4.1. Effect of Extract Concentration

The concentration of extracts is one of the most important factors that influence the synthesis of PDMNPs as well as the time required for their formation [61]. In most of the studies, generally, the extract volume ranges from 1 mL to 250 mL have been applied to observe their effects on the synthesis [62]. The effects of extract concentration can be easily observed by changes in color while synthesizing PDMNPs. Moreover, color changes have been observed as the ratio of concentrations of plant extract varies, indicating variations in the size of nanoparticles. When the concentration of plant extract containing significant number of bioactive compounds is high, a sharp peak (small particle size) is observed. A broad peak is observed as the concentration of extract decreases, indicating that the size of the nanoparticle is large [63]. Furthermore, Adeyemia et al. synthesized the bimetallic Ag and Au nanoparticles by using different concentrations (50, 100, and 250 mL) of *Dovyalis caffra* (Kei apple) fruit extract. This study demonstrated that different concentrations of extracts affect the shape and size of nanoparticles with a low reaction time in 250 mL volume [64]. Other researchers also reported the different extract concentrations regarding the best synthesis of PDMNPs using *Ocimum sanctum* (Tulsi) leaves extract (0.1, 0.2, 0.3, 0.4, and 0.5 mL), *Aegle marmelose* leaves extract (10, 20, and 30 mL), and *Aloe barbadensis* Mill. (Aloe Vera) leaves extract (5, 10, and 15 mL) concentrations [65–67].

4.2. Effect of Time

The incubation period of suspension containing plant extract and metal salts/oxides is a vital period that influences the synthesis of PDMNPs in an appropriate time. Smaller-size nanoparticles are produced by using a short incubation time, but larger nanoparticles with a propensity to assemble are often produced by employing a longer incubation time [68]. Numerous investigations have shown that the ideal incubation time, during which all essential reaction steps are properly carried out, is in between 30 min and 2 h. By using *Garcinia indica* fruit extract, Sangaonkar et al. successfully carried out the experiment of UV spectroscopy to investigate the incubation time from 2.0 to 120 h in a reaction mixture and then found that 24 h was the ideal incubation time for the synthesis of Ag nanoparticles. Similar to this, when fruit extract from *Garcinia indica* was utilized as a reducing agent, the Au ions are reduced, followed by transformation into nanoparticles in less than two hours [69,70]. In the earlier studies, by using the extracts of Chenopodium leaf and Tansy fruits, Ag and Au nanoparticles started to appear within 10 min of the reaction started and increased up to 2 h by the time the reaction was finished [71,72]. In contrast, other research indicated that the incubation period was slightly longer than the recommended 2 h [73,74]. Additionally, several reports indicated that the ideal incubation duration for the nucleation reactions used to generate metal nanoparticles from plant extracts is 60 min, indicating great stability of the metal nanoparticles [75,76].

4.3. Effect of pH

The parameter of pH cannot be ignored at the time of nanoparticle synthesis because it affects the morphology of nanoparticles in terms of shape and size [77]. The absorbance peaks in UV-Visible absorption spectra throughout their investigation make it simple to see changes caused by pH variations [78]. The formation of big-sized nanoparticles at pH 2.0 and large amounts of smaller-sized nanoparticles at pH 3.0 to 4.0 during the synthesis of

gold nanoparticles using *Avena sativa* plant extract demonstrate the strong pH dependence of nanoparticle size [79]. Another study found that increasing the pH from 3.0 to 7.0 causes nanoparticle size to decrease, whereas increasing the pH from 7 to 11 causes nanoparticle size to rise [80]. Similarly, by using some other plant extracts, studies hypothesized that higher pH (alkaline) values produce small, mostly spherical nanoparticles whereas lower pH (acidic) values produce big, ellipsoidal nanoparticles [81–84]. According to an experiment performed by Chitra and Annadurai, the size of Ag nanoparticles synthesized using *Bacillus brevis* cell culture was highly dependent on pH changes, with larger size (60–110 nm) at pH 5 and smaller size (10–40 nm) at pH 9 [85]. Moreover, Suresh et al. reported the synthesis of smaller size nanoparticles derived from low-pH ginger extract, which was attributed to the presence of the highest total phenolic content as compared to neutral and alkaline pH extracts [86]. Overall, pH influences the size and shape of PDMNPs because exposure of polar functional groups such as carbonyl and hydroxyl groups increase the stability as well as binding ability of metal ions during the nucleation and growth phases, which encourages less aggregation of synthesized nanoparticles [87].

4.4. Effect of Temperature

Another crucial factor that must be monitored throughout the synthesis of nanoparticles is temperature. A rise in temperature typically speeds up the reaction, increasing the amount of product produced. For instance, the rate of nanoparticles formation is higher at high temperatures than it is at normal temperature [88]. The greater yield of synthesized nanoparticles is made possible by an increase in metal reduction and homogenous nucleation, both of which are influenced by temperature. It is interesting to note that the temperature range needed for the synthesis of PDMNPs is lower (37–100 °C) than the temperature range needed for synthesis using physical and chemical methods, which is around 350 °C [89]. Because of the increment in surface plasmon resonance and sharpness of peak by increasing temperature, Ag and Au nanoparticles have been synthesized at higher rates at higher temperatures, transitioning from nanorod to platelet-shaped size, as reported in various research [90–93]. Additionally, some research used spectrophotometers to analyze the strong peaks of absorbance, which directly linked the experiment's increased temperature to the nanoparticle's rapid growth [94]. The sharpness of the absorbance relies on the size of the synthesized nanoparticles.

4.5. Effect of Types of Bioactive Compounds

Plant extracts rich in bioactive compounds (polyphenols, flavonoids, tannins, saponin, etc.), which function as reducing and stabilizing agents, influence the reduction of metal ions, the size, shape, processing, and stability of the PDMNPs [95]. These variations are explained by the presence of varying amounts of phytochemicals, which rely on extract preparation techniques, species variances within the same plant, and geographical and seasonal variations [96]. There are many publications on PDMNPs that reported the use of bioactive compounds as reducing, capping, and stabilizing agents, but no clear study is available so far on which types of phytochemicals are responsible for these properties. Most often, the reported bioactive compounds are polyphenols, flavonoids, terpenoids, and alkaloids, which contain oxygen functionalities and could act as reductants of metal ions for the synthesis of PDMNPs [97,98]. Some publications showed that ascorbic acid and glucose could reduce some metals like Au and Ag into their zero valent states, leading to PDMNPs synthesis [99]. Proteins, enzymes, and sugars found in plant extracts also lead to bio reduction of metals as well as agglomeration of synthesized nanoparticles [100,101]. Thus, the various types of bioactive compounds, which are good reducing and capping agents, may enhance the yield of synthesized PDMNPs by inhibiting the aggregation of the nanoparticles.

4.6. Effect of Agitation

Naturally, bioactive compounds are synthesized in cytoplasm or in specific cells and organelles, followed by transportation to other organs. Among them, terpenoids and alkaloids are synthesized in chloroplast whereas the endoplasmic reticulum contains the steroids and sesquiterpenoids. Plant vacuoles contain water-soluble compounds like polyphenols, flavonoids, saponins, and tannins. Lipid soluble compounds such as monoterpenoids and fats are transported through resin ducts and lactiferous glands from their origin sites to storage locations [102]. Most of the compounds are synthesized in the leaves and aerial parts and stored in other parts like roots, fruits, and stems. Thus, a metabolic profile based on bioactive compounds that varies from species to species of plants depends upon season, time, and stage of development [103]. It also depends on the location and types of compounds by which extraction should be done so that we can obtain bioactive compounds in good yield [104]. Agitation during extraction is a very important aspect that should be done because most of the bioactive compounds are enclosed within the cells or vacuoles. Usually, proper agitation causes the breakdown of the cell walls or vacuole rupturing, followed by enhancing the squeezing out of the compounds [105]. Hot aqueous extraction, among them, is the best way for easy preparation of PDMNPs. In this type of extraction, polar compounds are widely extracted, the majority of which are polyphenols and flavonoids, along with their glycosides. Further, when compounds are extracted for an extended time of period, their yield improves [106–108]. In addition, pressurized agitation of plant material is very important; applying pressure increases extraction yield [109].

5. Structural Characterization of PDMNPs

To ensure the reproducibility in terms of therapeutic potential, production, and safety after the completion of synthesis, thorough characterization of synthesized nanoparticles is crucial [110]. Basic physicochemical techniques such as UV-Visible absorption spectroscopy, Fourier Transform Infrared Spectroscopy (FTIR), Raman spectroscopy, Scanning Electron Microscopy (SEM), Transmission Electron Microscopy (TEM), and powder X-ray Diffraction (XRD) are used to characterize the NPs based on their shape, dispersity, size, and surface area. There are also some more recent methods that are available and frequently used in modern times, including X-ray photoelectron spectroscopy (XPS), dynamic light scattering (DLS), energy dispersive X-ray spectroscopy (EDX), field emission scanning electron microscopy (FE-SEM), etc. (Table 1) [111].

5.1. Ultra Violet-Visible Spectroscopy

UV-Visible absorption spectroscopy is an easy-to-use technique that clearly displays the peak's absorbance. Strong or weak bands on the peak indicate how stable a synthesized nanoparticle is, and these optical features include reaction time, temperature, pH, and concentration of suspension [112]. For Ag and Au metals, the majority of the synthesized nanoparticles are visible at wavelength ranges of 400–450 nm and 500–550 nm, respectively [113].

5.2. X-ray Crystallography

X-ray crystallography is a powerful method to characterize the crystal structure and phase identification of synthesized nanoparticles in which X-rays strike the crystal surface and then interact with the atoms to measure the crystallinity [114]. On the crystalline plane, the atoms organize themselves properly and display a diffraction pattern [115]. According to multiple research papers, several PDMNPs have resulted in crystalline structures with average particle sizes of about 25–30 nm [116–120].

5.3. Fourier-Transform Infrared Spectroscopy (FTIR)

Fourier-transform infrared spectroscopy (FTIR) is used to depict the chemical information, particularly functional groups (amide, hydroxyl, and carboxyl groups), along with bonds parameters [121]. By locating the bioactive compounds present in plant extracts,

which may serve as coating/capping and stabilizing agents during the reduction processes of metal into their respective ions, FTIR is used to extract useful information about the surface chemistry of synthesized PDMNPs [122]. In addition to identifying functional groups, FTIR also identifies stretching and vibrational frequencies, such as C=O, C=C, C-H, and C-O, demonstrating that a functional group can change from a raw plant extract to a synthesized nanoparticle [123]. The chemical behavior of PDMNPs has been well documented in the literatures [124–128].

5.4. Microscopic Techniques

High-resolution microscopies such as SEM, TEM, and AFM depict the morphological characterization of nanoparticles. Data are collected in two-dimensional images using the SEM technique via a selection of areas under study. The generated image depicts spatial variations in morphological properties (size distribution, shape, aggregation, and dispersion), as well as information on the sample's qualitative chemical composition [129]. There is also a high-resolution SEM technique called FE-SEM that offers deeper pictures of molecules in their native condition. The direct imaging method TEM, on the other hand, shows particle size, size distribution, and morphology. It has a resolution that is around one million times better than the wavelength in simple light microscopy [130]. Numerous scientists and researchers have used SEM and TEM to characterize numerous examples of PDMNPs in terms of particle size, distribution, aggregation, and chemical contents [131–133]. The AFM technique, which analyses 3D pictures of samples with information on size, shape, sorption, dispersion, and aggregation as well as surface properties of particles, is an improvement over the SEM and TEM approaches [134].

5.5. Powder XRD Technique

By examining the crystalline structure (orientation, phases, and lattice parameters) of samples in powder form, this approach may characterize the NPs and compare them to established structural databases. Because atoms in a crystal are arranged at the proper distance, when X-rays hit the crystal surface and interact with the atoms, they produce a diffraction pattern [135]. The XRD experiment yields two peaks, where a broad peak denotes amorphous powder and a sharp peak denotes the crystalline form of synthesized NPs [136]. The XRD method has been used in numerous studies to characterize the PDMNPs in order to ascertain the crystalline properties of samples, and in the majority of cases, samples displayed a strong diffraction pattern that was closely correlated with the emergence of NPs [137–140]. In contrast, EDX is a unique and adaptable tool for obtaining a sample's composition map or performing an area-specific elemental analysis. This method involves stimulating samples with electrons or high-energy photons and then detecting the spectrum of the released photons [141].

5.6. Light Scattering Methods and Zeta-Potential (ζ)

Two significant non-destructive/invasive methods that are based on the light scattering concept are dynamic light scattering (DLS) and zeta-potential to determine the physicochemical properties of NPs. When they are distributed in colloidal suspension under various conditions, including concentration, pH, temperature, and time, DLS assesses the diameter and stability of the NPs. DLS also relies on the particle's diffusive motion. Particles that are more massive will move more slowly than those that are smaller. Zeta potential, on the other hand, is used to describe the surface charge of NPs and learn more about their physical stability and interactions with other molecules on their surfaces [142]. DLS has been widely used in recent years to measure the size of PDMNPs that have been reduced to nano-size ranges between 1.0 and 200 nm [143,144]. The values of Zeta potential are crucial indicators of a nanoparticle's stability. NPs have a tendency to aggregate at 0–5 mV values, whereas 5–20 mV values indicate that they are poorly stable. The maximum stability of NPs is shown by Zeta potential values above 40 mV [145].

Table 1. The details of techniques that are widely used to characterize the PDMNPs [146].

Name of Technique	Source of Detection	Study
UV-Visible absorption spectroscopy	Monochromatic wavelength	For identifying, characterizing, and studying nanomaterials in terms of size, shape, concentration, and agglomeration state
Fourier-Transform Infrared (FTIR) spectroscopy	Infrared radiations	Identifying the surface adsorption of functional groups on nanoparticles
Scanning Electron Microscopy (SEM)	Electron beam	Characterization of size (below 1.0 nm) and shape of nanoparticles
Transmission Electron Microscopy (TEM)	Electron beam	Measurement of nanoparticle's size, distribution, and morphology
Atomic Force Microscopy (AFM)	Electron beam from the laser light	Evaluation of size and shape of nanoparticles in three dimensions. It also determines the surface morphology and elemental composition in a very quick time
Dynamic Light Scattering (DLS)	Scattered light from a laser	Studying the aggregation and colloidal state of nanoparticles in suspension
Zeta Potential Measurement	Free ions	Studying the physical stability in terms of surface charge of colloidal nanoparticles

6. Assessment of Oxidative Stress-Mediated Therapeutic Actions

6.1. Antioxidant Action

Living cells undergo metabolic reactions and generate free radical species, which cause human diseases (cardiovascular, neurodegeneration, inflammation, and cancer, among others) and ageing by damaging proteins, nucleic acids, lipids, and carbohydrates [147]. Chemicals like propyl gallate (PG), tertiary butyl hydroquinone (TBHQ), butylated hydroxyanisole (BHA), and butylated hydroxytoluene (BHT) are widely used as antioxidants that inhibit degenerative reactions in processed foods, drinks, juice, and the edible items but, when used for a long time, they have negative impacts on the human body [148]. Despite the availability of chemical antioxidants, there is growing interest in the development of nano-antioxidants due to their low cost as well as lack of deleterious side effects. Many researchers have synthesized a large number of metal NPs from plant extract for their antioxidant properties because medicinal plants as well as metals such as Ag, Au, Cu, Zn, Fe, and Pd have been well known for their antioxidant properties in traditional medicines since antiquity [149]. Many bioactive compounds, including polyphenols, flavonoids, terpenoids, tannins, and saponins, are abundant in plants and act as reducing, capping, and stabilizing agents for the synthesis of PDMNPs by reducing the metal ions into their zero-valent state. Because of fine-tuning in surface area, particle size, and surface activity, PDMNPs have attracted a lot of attention recently for their powerful antioxidant effects. These agents exhibit good biocompatibility and action stability [150]. As shown in Figure 5, metals can readily donate an electron to quench free radicals, according to their chemical structure, and act as powerful antioxidants on their own in nature. For their antioxidant activity, metals salts of Ag, Au, Pd, Pt, Zn, Cu, and metal oxides like copper oxide (CuO), zinc oxide (ZnO), nickel oxide (NiO), and magnesium oxide (MgO) are frequently utilized [151]. Numerous medicinal plants and nanoparticles synthesized by their extracts along with free radical scavenging properties are well studied [152–156]. It has been considered that antioxidants remove the free radicals by converting $O_2^{\cdot-}$, H_2O_2 , and OH^{\cdot} into O_2 , H_2O , and O_2 , respectively [157,158]. Nanoparticles derived ROS that facilitate the damaging of the cell membrane of microorganisms, as well as cancerous cells, are resulted into antimicrobial and anticancer effects. The scavenging capacity of ROS derived from PDMNPs, can be easily determined by using ROS or other free radical quenching-based assays including 2,2-diphenyl-1-picrylhydrazyl (DPPH), ferric reducing antioxidant power (FRAP), trolox equivalent antioxidant capacity (TEAC), oxygen radical absorbance capacity (ORAC), total oxy radical scavenging capacity (TOSC), total radical-trapping antioxidant parameter

(TRAP), cupric-reducing antioxidant capacity (CUPRAC), and chemiluminescence methods [159]. Although DPPH, FRAP, TEAC, TOSC, ORAC, TRAP, and CUPRAC methods are simple, standardized, and the most recognized antioxidant assays, the chemiluminescence methods have advantage over them because they are a highly sensitive analytical method that gives quenching capacity of ROS at very low concentration [160]. Due to the low detection limit, luminol, lucigenin, pholasin, and peroxyoxalate are used as chemiluminescence reagents to generate the excited state by producing light which is diminished by the oxidant initiator such as HO^\bullet , O_2^\bullet , ROO^\bullet , ONOO^- , or HOCl [161]. The total antioxidant capacity of various plant extracts and their NPs by the chemiluminescence method was also reported in many studies [162]. Most of the methods are based on luminol- H_2O_2 chemiluminescence, lucigenin- H_2O_2 chemiluminescence nano-enzyme based sensor, and NaHCO_3 - H_2O_2 - Co^{2+} chemiluminescence reactions to measure the antioxidant activities of various fruit, herbs, and medicinal plants extracts along with dietary substances such as soft drinks and wines [163–167]. The chemiluminescence assay is also reported to evaluate the antioxidant activity in pomegranate and honey samples [168]. Additionally, herein, we present an in-depth mechanism of ROS-mediated antimicrobial and anticancer properties of PDMNPs. Table 2 shows the antimicrobial and anticancer activities of PDMNPs over the last five years (2018–2022).

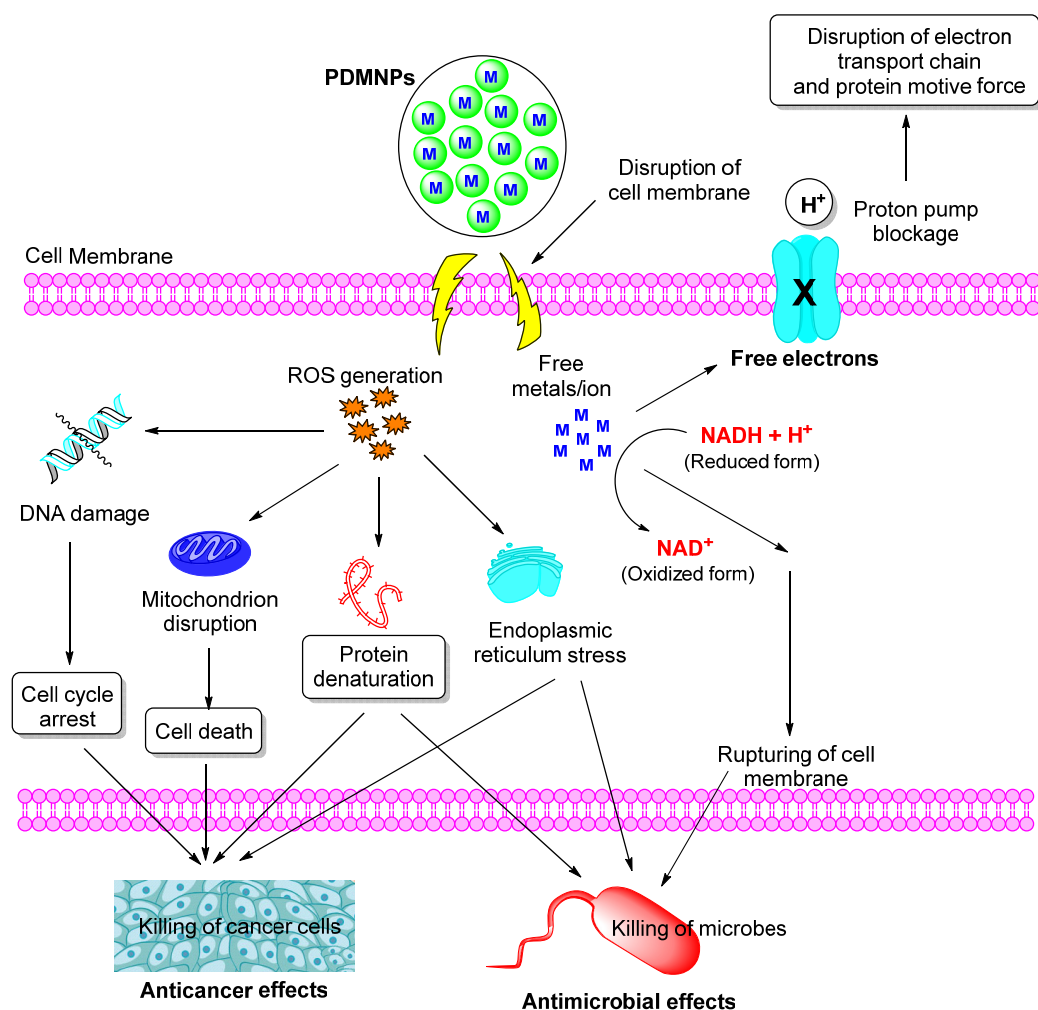


Figure 5. The representation of pathways involved in oxidative stress-mediated anticancer and antimicrobial properties given by PDMNPs.

6.2. Antimicrobial Action

Infections caused by various pathogenic microorganisms have become a major challenge for the entire world, and the problem is worsening due to the uncontrolled and indiscriminate use of antibiotics to prevent the infections. Since multidrug resistance (MDR) poses a severe threat to the spread of epidemic infections, the researchers' extensive efforts to find new medicines have been insufficient [169]. The development of sustainable, alternative techniques to reduce antibiotic exposure and their resistance has recently attracted a lot of attention and it is unsurprisingly growing quickly [170]. PDMNPs have been noteworthy as emerging antibacterial agents in the current context because of their high surface area to volume ratio and distinctive chemical diversity. PDMNPs are observed in a variety of shapes when reactions are completed, including spherical, hexagonal, triangular, truncated, octahedral, rod-shaped, and flower-shaped. PDMNPs with different shapes have a large surface-volume area, which facilitates their antimicrobial actions by interacting with biological components of microorganisms via various mechanisms such as membrane disintegration, cellular component damage (DNA, protein, lipids, and electron transport chain), and the generation of ROS (Figure 5) [171]. Thus, PDMNPs may be promising options for combating MDR microorganisms and overcoming microbial resistance. PDMNPs have shown inhibitory activities against both Gram-positive and Gram-negative bacteria, fungi, and various viruses as a safe, eco-friendly, and simple platform for developing anti-microbial agents [172].

However, many reports have proposed antimicrobial mechanisms mediated by NPs, but the precise mechanism is unknown. PDMNPs have antimicrobial activity because they release metal ions. Metal ions interact with the cell membrane to form pits or gaps, which cause cell membrane damage by deactivating enzyme functions [173]. They also interact with the sulfur or phosphorus functionalities of proteins or DNA, causing metabolic processes to breakdown. Similarly, PDMNPs can cause ROS formation due to lipid/phospholipid membrane oxidation, which leads to the collapse of DNA/RNA/protein architecture within the bacterium cell [174]. The mechanism underlying the nanoparticle's antibacterial action was recently revealed by a study. In this study, PDMNPs were exposed to solar energy, which causes electrons to move from the band gap to the conduction band and produce both free electrons and holes. OH^- combines with a hole to make OH^\bullet , while free electrons react with O_2 to create O_2^\bullet . ROS that was produced as a result of this antibacterial activity disrupted cell membranes, allowed cytoplasm to leak out, damaged mitochondria and DNA, and ultimately caused cell death [175]. According to a literature review, due to the high toxicity of Ag ions or Ag-based products against microbes, Ag is the most commonly employed metal for the synthesis of PDMNPs as antibacterial agents [176]. Ag and Ag-products in the form of nanoparticles have been or are being employed as preservatives in the development of nanomedicine, cosmetics, and the food sector due to their small size and huge surface area [177].

Additionally, due to the existence of a thick peptidoglycan layer that serves as a barrier to the penetration of nanoparticles, Gram-positive and Gram-negative bacteria demonstrated different antibacterial efficacy [178]. Most studies concluded that Ag nanoparticles are more effective antibacterial agents against Gram-positive bacteria than Gram-negative bacteria. Some studies, however, have speculated that Ag is more effective for Gram-negative bacteria [179]. According to a different study carried out by Singh and colleagues, Gram-positive bacteria are covered in a thick layer of peptidoglycans and straight-chain polysaccharides that are cross-linked with embedded proteins, giving the cell stiffness and making it difficult for PDMNPs to bind to the cell surface. In contrast, Gram-negative bacteria have negatively charged lipopolysaccharides that are bonded to positively charged silver metal [180]. Tiwari et al. discovered the mechanism by which Zn-based PDMNPs generate ROS. These ROS increase lipid peroxidation, DNA damage, protein, and nucleic acid leakage, as well as reducing the microorganism cell viability. Furthermore, the Zn^{2+} ions released by PDMNPs contribute to the damage of microorganism cell membranes during molecular interactions [181]. When Zn nanoparticles bind with biomolecules through

electrostatic interactions, Zn^{2+} ions are released at the target site, where they cause the oxidation of proteins and lipids, which damages cells [182]. Similar to this, it has been revealed that nanoparticles made of Ti metal generate ROS, when exposed to ultraviolet light. According to this study, ROS prevent oxidative phosphorylation from occurring in the cell membrane, which results in cell death [183]. PDMNPs use a similar antibacterial mechanism to destroy fungal species by releasing metal ions that produce ROS and other free radicals [184]. The enzymatic action of glucan synthase or N-acetyl glucosamine on components such as mannoproteins, 1,3-D-glucan, 1,6-D-glucan proteins, chitin, as well as polysaccharides like chitin, glucan, and mannan or galactomannan, is what creates the cell walls of fungi. These enzymes interact with the metal ions and ROS produced by PDMNPs to display antifungal action [185]. Figure 5 also depicts the antifungal activity of PDMNPs when they interact with the cell membrane or cell wall, allowing intracellular components to leak out. Free radicals, in particular, react with sulfur and phosphorus functionalities in the cell wall to disrupt redox homeostasis. Furthermore, free radicals disrupt fungal growth by interfering with DNA replication, protein synthesis, and enzymatic activity [186]. PDMNPs also interact with glutathione-producing enzymes (antioxidants), reducing fungi resistance [187]. Despite these findings, a more detailed mechanism for the action of PDMNPs against pathogenic bacteria (both Gram-positive and Gram-negative) and fungi is still required. Table 2 shows the antimicrobial activities of PDMNPs over the last five years (2018–2022).

6.3. Anticancer Action

According to the WHO database, cancer is currently the world's top cause of death, accounting for close to 10 million deaths globally in 2020. By 2025, it is anticipated that this number would rise to 19.3 million, with the majority of the patients being from emerging nations [188]. Therefore, it is vital that focus be given globally to accurate cancer detection and subsequent therapy. There are numerous medicines available to treat the various forms of cancer, but these treatments have side effects, particularly when they harm healthy cells, tissues, and organs, which lower down the quality and length of life [189]. Anticancer agents have essentially demonstrated three proposed mechanisms for combating various types of cancer. The first is the apoptotic pathway's target, which is dependent on an increased level of ROS, which causes oxidative stress and DNA fragmentation in the cancerous cell. The second is the interaction of cancer cell proteins/DNA, and the last is anticancer agents interacting with cell membranes to alter cell permeability and mitochondrial dysfunction [190]. The diagnosis of cancer is also a crucial step before treatment, which involves the common use of methods including tissue biopsy, microscopy, and histopathology assay. These techniques, however, only reach a minimal amount of tissue, which causes cells to proliferate quickly and develop into the metastatic stage. While receiving surgical or chemotherapeutic treatment, this cascade makes it difficult to target the cancer cells. However, positron emission tomography (PET), computed tomography (CT) scan, and magnetic resonance imaging (MRI) approaches can detect the cancers more effectively when using NPs-based imaging agents because they can more precisely reach the target areas [191].

Due to the presence of bioactive compounds, the abilities of medicinal plants to treat cancer have been well documented since antiquity [192–194]. The detection, diagnosis, and therapy of cancer have also been investigated using a wide variety of metal NPs. As compared to microbial synthesis of nanoparticles, PDMNPs have recently attracted much greater attention since they are clean, safe, and environmentally friendly while bridging the current gap between physical and chemical techniques of their synthesis [195]. According to studies, PDMNPs have a high level of selectivity between cancer cells and healthy cells, which helps to reduce negative effects and provides protection against healthy cell damages. The broad synthesis of PDMNPs by using various metal oxides/salts and plant extracts as green sources has enormous therapeutic potential for the treatment of cancer. Interestingly, Ovais et al. created Ag and Au nanoparticles based on plant extracts to

observe tumor progression and evaluate it at the cellular level [196,197]. Although the mode of action of PDMNPs is complex and under investigation, some reports claim that their anticancer activity is due to enhanced apoptosis in cancer cells via cell cycle arrest as well as activation of ROS and caspase-3 mediated signaling. Finally, in cancerous cells, they cause mitochondrial depolarization and DNA damage [198]. NPs develop intracellular membrane-bounded vesicles when they are exposed to the cancer cell surface, which permits them to enter the cells and produce reactive oxygen species. These species exhibit a series of abnormal behavior, including mitochondrial dysfunction, enzyme inactivation, protein oxidation, damage to nuclear materials (DNA/RNA), etc., and as a result, develop the cancer disease [199]. The cell cycle is stopped in the growth phase at the time of mitosis and meiosis, based on a 2017 study by Patil and Kim. By increasing the ratio of B-cell lymphoma protein 2-associated X and B-cell lymphoma protein, ROS causes cells to be more susceptible to apoptosis [200]. This one is followed by stimulation of caspase-3, -8, and -9 to help accelerate apoptosis. Two years later, Kim et al. demonstrated in their experiment that ROS increases the quantity of P53, a tumor protein that fights against cancer cells. Researchers noted in the same study that smaller NPs could kill more cancer cells because they can enter the cell membrane more readily and acquire a larger surface area. Therefore, it seems reasonable that ROS production aids PDMNPs in their fight against cancer [201]. Table 2 lists the anticancer investigations of PDMNPs for the last five years (2018–2022).

Table 2. A list of PDMNPs along with their characteristics, antioxidant, antimicrobial, and anticancer properties for the last five years (2018–2022).

Plant Name (Part Used)	Extract	Nanoparticles	Findings	Ref.
<i>Quercus robur</i> , <i>Eucalyptus globulus</i> , <i>Camellia sinensis</i> , <i>Thimus mastichina</i> , <i>Thimus vulgaris</i> , <i>Thuja occidentalis</i> , <i>Mentha</i> sp., <i>Rosmarinus officinalis</i> , <i>Laurus nobilis</i> , <i>Citrus limon</i> (leaves)	Aqueous	Metal: Ag, Cu, Fe, Pd, Ni, Shape: Hexagonal, spherical, triangular, and rod shaped Size: 50 nm	Antioxidant activity: Evaluated by using DPPH, FRAP, FC, and cyclic voltammetry methods	[202]
<i>Camellia sinensis</i> , <i>Ilex paraguariensis</i> , <i>Salvia officinalis</i> , <i>Tilia cordata</i> , <i>Levisticum officinale</i> , <i>Aegopodium podagraria</i> , <i>Urtica dioica</i> , <i>Capsicum baccatum</i> , <i>Viscum album</i> (whole plants)	Methanol	Metal: Ag Shape: spherical, and rod-shaped Size: 100–200 nm	Antioxidant activity: Evaluated by DPPH, CUPRAC, and SNPAC assays	[203]
<i>Phoenix Dactylifera</i> (leaves)	Ethanol/water mixture (70%/30%)	Metal: Cu Shape: spherical and rhombohedral Size: 25–100 nm	Antioxidant activity: Evaluated by using DPPH, phosphomolybdenum, and ferric-reducing antioxidant power (FRAP) assays with IC ₅₀ of 0.39 mg/mL	[204]
<i>Rosa floribunda charisma</i> (flowers)	Phenyl ethyl alcohol	Metal: Mg Shape: Polyhedral Size: 35.25–55.14 nm	Antioxidant activity: Evaluated by using inhibition of superoxide (IC ₅₀ 26.2 µg/mL), nitric oxide (IC ₅₀ 52.9 µg/mL), hydroxyl radical (IC ₅₀ 31.9 µg/mL), and xanthine oxidase (IC ₅₀ 15.9 µg/mL) assays Antibacterial activity: Against <i>Staphylococcus epidermidis</i> (MIC of 15.63), <i>Staphylococcus pyogenes</i> (MIC of 7.81), and <i>Pseudomonas aeruginosa</i> (MIC of 31.25) µg/mL as well as with minimum biofilm inhibitory concentrations 1.95, 1.95, 7.81 µg/mL, respectively	[205]

Table 2. Cont.

Plant Name (Part Used)	Extract	Nanoparticles	Findings	Ref.
<i>Cestrum nocturnum</i> (leaves)	Aqueous	Metal: Ag Shape: spherical Size: 20 nm	Antioxidant activity: Evaluated by DPPH (29.55% inhibition) hydrogen peroxide (45.41% inhibition), hydroxyl radical (20% inhibition), and superoxide radical scavenging (8% inhibition) methods Antibacterial activity: Against <i>Citrobacter</i> , <i>Escherichia faecalis</i> , <i>Salmonella typhi</i> , <i>Escherichia coli</i> , <i>Proteus vulgaris</i> , and <i>Vibrio cholera</i> with MIC values of 16, 4, 16, 8, 8, and 16 µg/mL	[206]
<i>Plantago lanceolate</i> (whole)	Aqueous	Metal: Ag Shape: spherical Size: 30 ± 4 nm	Antioxidant activity: Evaluated by using DPPH assay with IC ₅₀ 369.5 ± 13.42 µg/mL Antibacterial activity: Against <i>Agrobacterium tumefaciens</i> , <i>Proteus vulgaris</i> , <i>Staphylococcus aureus</i> , and <i>Escherichia coli</i> with IC ₅₀ values 08.02 ± 0.68, 55.78 ± 1.01, 12.34 ± 1.35 and 11.68 ± 1.42 µg/mL, respectively	[207]
<i>Flemingia wightiana</i> (leaves)	Aqueous	Metal: Ag Shape: spherical Size: 20–40 nm	Antioxidant activity: Evaluated by using DPPH and H ₂ O ₂ scavenging activity with IC ₅₀ values of 71.96 and 80.59 µg/mL respectively Anticancer activity: Against SKOV3 (inhibition 83.2%) and COLO205 (inhibition 75.9%) cancer cells	[208]
<i>Artemisia absinthium</i> , <i>Humulus lupulus</i> , and <i>Thymus vulgaris</i> (leaves)	Ethanol	Metal: Ag Shape: spherical and wedge Size: 42–48 nm	Antioxidant activity: Evaluated by using DPPH with 0.14 ± 0.00 inhibition for <i>A. absinthium</i> /AgNPs, 0.11 ± 0.00 inhibition for <i>H. lupulus</i> /AgNPs, and 0.14 ± 0.00 mmol/g for <i>T. vulgaris</i> /AgNPs while 0.55 ± 0.05; 0.86 ± 0.05 and 0.55 ± 0.05 mmol/g inhibitions in ABTS method for <i>A. absinthium</i> /AgNPs, <i>H. lupulus</i> /AgNPs, and <i>T. vulgaris</i> /AgNPs samples. Antibacterial activity: Evaluated with inhibition zones in the range 9.0 ± 0.1 to 20.4 ± 0.3 mm for all the samples	[209]
<i>Sesamum indicum</i> (oil cake)	Aqueous	Metal: Ag Shape: spherical Size: 6.6–14.8 nm	Anticancer activity: Against MCF-7 cell lines with 72.02% cell viability, 15.18% late apoptosis, and 1.20% necrosis at 2.5 µg/mL concentration of AgNPs whereas against with 56.97% cell viability, 31.19% late apoptosis, and 4.85% necrosis at 7.5 µg/mL concentration of AgNPs Antibacterial activity: With minimum inhibitory concentration (0.5 µg/mL) against <i>Pseudomonas aeruginosa</i> , <i>Klebsiella pneumoniae</i> , and <i>Escherichia coli</i> .	[210]

Table 2. Cont.

Plant Name (Part Used)	Extract	Nanoparticles	Findings	Ref.
<i>Dodonaea viscosa</i> (leaves)	Aqueous, acetone, methanol, acetonitrile	Metal: Ag Shape: spherical and dendritic Size: 15, 18, 12, and 20 nm	Antibacterial activity: Against <i>Streptococcus pyogenes</i> with a zone of inhibition (20, 16, 13, 18 mm) for AgNPs synthesized by methanol, acetone, acetonitrile, and water extracts nanoparticles, respectively Anticancer activity: Against A549 NSCLC cell lines with IC ₅₀ values 14, 3, 80, and 4 µg/mL for methanol, acetone, acetonitrile, and water extract derived nanoparticles, respectively.	[211]
<i>Mangifera indica</i> (leaves)	Aqueous	Metal: Ag Shape: rod-shaped Size: 500–900 nm	Antioxidant activity: Evaluated by using DPPH with inhibition 83.7 ± 0.2%, 89.8 ± 0.3%, and 96.4 ± 0.3% for 0.1 w/v, 1 w/v, and 10% w/v concentration, respectively. Anticancer activity: Against MCF-7 and HCT-116 cell lines with cell growth 49.1 ± 0.5% and 58.2 ± 0.2%, respectively, at 10% w/v	[212]
<i>Impatiens balsamina</i> and <i>Lantana camara</i> (leaves)	Aqueous	Metal: Ag Shape: spherical Size: <24 nm	Antioxidant activity: Against <i>Staphylococcus aureus</i> and <i>Escherichia coli</i> with average ZOI values 13.8 and 8.9 mm for <i>Impatiens balsamina</i> and 15.8 and 15.4 mm <i>Lantana camara</i> , respectively	[213]
<i>Jasminum auriculatum</i> (leaves)	Aqueous	Metal: Au Shape: spherical Size: 8–37 nm	Anticancer activity: Against cervical cancer Antibacterial activity: Against <i>Streptococcus pyogenes</i> , <i>Staphylococcus aureus</i> , <i>Escherichia coli</i> , and <i>Klebsiella pneumoniae</i> Antifungal activity: Against <i>Candida albicans</i> , <i>Aspergillus fumigatus</i> , <i>Lecanicillium lecanii</i> , and <i>Trichoderma viride</i>	[214]
<i>Alpinia nigra</i> (fruits)	Aqueous	Metal: Ag Shape: spherical Size: 6 nm	Anticancer activity: Against human cervical cancer cell line (HeLa) with the IC ₅₀ value of 104 µg/mL Antibacterial activity: Against <i>Streptococcus pyogenes</i> , <i>Staphylococcus aureus</i> , <i>Escherichia coli</i> , and <i>Klebsiella pneumoniae</i> with ZOI values of 20, 9, 12, and 7 mm, respectively Antifungal activity: <i>Candida Albicans</i> , <i>Aspergillus fumigatus</i> , <i>Lecanicillium lecanii</i> , and <i>Trichoderma viride</i> with ZOI values of 4, 4, 5, and 5 mm, respectively	[215]
<i>Lycium chinense</i> (fruits)	Aqueous	Metal: Au, Ag Shape: spherical Size: 536 and 480 nm	Anticancer activity: Aignificant cytotoxicity to the human breast cancer MCF7 cell line for AgNPs and whereas no toxicity to non-diseased RAW264.7 (murine macrophage) cells, whereas no toxicity on both cell lines for AuNPs	[216]
<i>Garcinia Indica</i> (fruit)	Aqueous	Metal: Au, Ag Shape: spherical Size: 20–30 nm	Antioxidant activity: Evaluated by DPPH assay with 32–72% inhibition	[217]

Table 2. Cont.

Plant Name (Part Used)	Extract	Nanoparticles	Findings	Ref.
<i>Ziziphora clinopodioides</i> (whole plant)	Aqueous	Metal: Ag Shape: spherical Size: 20–45 nm	Antibacterial activity: Against <i>Staphylococcus aureus</i> and <i>Escherichia coli</i> with MIC values at 200 and 400 ppm concentrations, respectively	[218]
<i>Calophyllum tomentosum</i> (leaves)	Aqueous	Metal: Ag Shape: spherical Size: NA	Antioxidant activity: Evaluated by using DPPH (90% inhibition), H ₂ O ₂ scavenging (83.94%), nitric oxide scavenging power (78.4%), reducing power assays Antibacterial activity: Against <i>Klebsiella aerogenes</i> , <i>Staphylococcus aureus</i> , <i>Pseudomonas aeruginosa</i> , and <i>Escherichia coli</i> with a maximum inhibition at 100 µg/mL concentration	[219]
<i>Pistacia atlantica</i> (leaves and fruit)	Aqueous	Metal: Au Shape: spherical Size: 40–50 nm	Antioxidant activity: Evaluated by using DPPH assay Anticancer activity: Against cervical cancer with a maximum inhibition of cells at 200 µg/mL concentration Antibacterial activity: Against <i>Escherichia coli</i> , <i>Pseudomonas aeruginosa</i> , <i>Staphylococcus aureus</i> , and <i>Bacillus subtilis</i> with MIC values 7.81, 3.9, 7.81, and 3.25 µg/mL	[220]
<i>Allium rotundum</i> L., <i>Falcaria vulgaris</i> Bernh. and <i>Ferulago angulate</i> Boiss. (leaves)	Aqueous	Metal: Ag Shape: spherical Size: 20.5 nm	Antimicrobial activity: Against <i>Pseudomonas aeruginosa</i> and <i>Staphylococcus aureus</i>	[221]
<i>Carya illinoensis</i> (leaves)	Methanol	Metal: Ag Shape: spherical Size: 20 nm	Antibacterial activity: Against <i>Saphylococcus aureus</i> (MIC: 128), <i>Listeria monocytogenes</i> (MIC: 64), <i>Escherichia coli</i> (MIC: 16), <i>Pseudomonas aeruginosa</i> (MIC: 32)	[222]
<i>Tasmannia lanceolata</i> and <i>Backhousia citriodora</i> (leaves)	Aqueous	Metal: Au Shape: spherical Size: 7.10 ± 0.66 nm	Anticancer activity: Against liver cancer (HepG2), melanoma cancer (MM418C1), and breast cancer (MCF-7) cell lines. AuNPs showed 20% better inhibition of these cancer cell lines than plant extracts	[223]
<i>Ougeinia oojeinensis</i> (leaves)	Ethanol	Metal: Ag Shape: spherical Size: 5–100 nm	Antioxidant activity: Evaluated by DPPH assay with IC ₅₀ value 21.95 ± 1.02 Antibacterial activity: Against <i>Escherichia coli</i> , <i>Bacillus cereus</i> , <i>Pseudomonas aeruginosa</i> , and <i>Staphylococcus aureus</i> with ZOI values 14.58 ± 0.79, 16.55 ± 0.37, 16.25 ± 0.63, and 23.83 ± 0.44 mm, respectively. Antifungal activity: <i>Aspergillus niger</i> , <i>Rhizopus oryzae</i> , <i>Mucor azygosporus</i> , and <i>Penicillium chrysogenum</i> with a zone of inhibition 20.17 ± 0.6, 16.50 ± 0.29, 20.25 ± 0.38, 21.82 ± 0.43 mm, respectively	[224]

Table 2. Cont.

Plant Name (Part Used)	Extract	Nanoparticles	Findings	Ref.
<i>Holoptelea integrifolia</i> (leaves)	Aqueous	Metal: Ag Shape: spherical Size: 32–38 nm	Antioxidant activity: Evaluated by using DPPH, metal chelating, and nitric oxide assay with inhibition 51.49 ± 3.33 , 41.18 ± 2.27 , and $74.59 \pm 3.08\%$, respectively Antibacterial activity: Against <i>Escherichia coli</i> and <i>Salmonella typhimurium</i> with MIC value ranges from 75 to 150 μ g	[225]
<i>Aesculus hippocastanum</i> (leaves)	Aqueous	Metal: Ag Shape: spherical Size: 50 ± 5 nm	Antioxidant activity: Evaluated by using DPPH and superoxide radical scavenging assays with 54.72% and 62.9% inhibition at the highest concentration of 100 ppm. Antibacterial activity: Against <i>Pseudomonas aeruginosa</i> , <i>Pseudomonas fluorescens</i> , <i>Staphylococcus aureus</i> , <i>Staphylococcus epidermidis</i> , <i>Listeria monocytogenes</i> , <i>Bacillus subtilis</i> , <i>Corynebacterium renale</i> , <i>Micrococcus luteus</i> , <i>Enterococcus faecalis</i> , and <i>Bacillus cereus</i> with ZOI values as 20.0, 8.0, 8.0, 17.5 ± 2.12 , 13 ± 0.00 , 13 ± 0.00 , 15 ± 2.64 , 12 ± 0.00 , 17 ± 0.00 , 10.5 ± 1.41 , 10.5 ± 1.41 mm diameter, respectively	[226]
<i>Punica granatum</i> L. (seeds)	Oil	Metal: Au Shape: elongated, and rectangular Size: 70 nm	Antioxidant activity: Evaluated by using DPPH scavenging (23.6 ± 1.5 to $62.5 \pm 1.8\%$) and H_2O_2 scavenging (21.6 ± 1.3 to $62.8 \pm 1.8\%$) at different concentrations Anticancer activity: Against lung and colon cancer with the cell viability ranging from 80.3 to 25% and 83.3 to 28.4.2%, respectively	[227]
<i>Alternanthera bettzickiana</i> (leaves)	Aqueous	Metal: Au Shape: spherical Size: 80–120 nm	Antibacterial activity: <i>Bacillus subtilis</i> , <i>Staphylococcus aureus</i> , <i>Salmonella typhi</i> , <i>Pseudomonas aeruginosa</i> , <i>Micrococcus luteus</i> , and <i>Enterobacter aerogenes</i> Anticancer activity: Against human lung cancer	[228]
Green tea and black tea (leaves)	Aqueous	Metal: Au, Ag Shape: spherical Size: ~ 10 nm for AuNPs, and ~ 30 nm for AgNPs	Antibacterial activity: Against <i>Bacillus subtilis</i> , <i>Staphylococcus aureus</i> , <i>Salmonella typhi</i> , <i>Pseudomonas aeruginosa</i> , <i>Micrococcus luteus</i> , and <i>Enterobacter aerogenes</i> with ZOI values 14 ± 0.43 , 19 ± 0.33 , 17 ± 0.13 , 28 ± 0.33 , 30 ± 0.33 , 24 ± 0.17 mm diameters for AgNPs while AuNPs show the ZOI values as 16 ± 0.88 , 16 ± 0.44 , 14 ± 0.58 , and 22 ± 0.44 mm diameter against <i>Salmonella typhi</i> , <i>Pseudomonas aeruginosa</i> , <i>Micrococcus luteus</i> , and <i>Enterobacter aerogenes</i> , respectively	[229, 230]
<i>Phoenix dactylifera</i> (root hairs)	Aqueous	Metal: Ag Shape: spherical Size: 15–40 nm	Antibacterial activity: Against <i>Candida albicans</i> and <i>Escherichia coli</i> with 20 and 22 mm ZOI, respectively Anticancer activity: Against MCF7 cell lines with IC_{50} values of 29.6 μ g/mL	[231]

Table 2. Cont.

Plant Name (Part Used)	Extract	Nanoparticles	Findings	Ref.
<i>Sida cordifolia</i> (whole plant)	Aqueous	Metal: Ag Shape: spherical Size: 3–6 nm	Antibacterial activity: Against <i>Escherichia coli</i> , <i>Klebsiella pneumoniae</i> , <i>Bacillus subtilis</i> , and <i>Staphylococcus aureus</i> with ZOI values as 15.0 ± 0.63 , 17.17 ± 0.75 , 18.00 ± 0.63 , and 19.50 ± 0.55 mm, respectively	[232]
<i>Salvia spinose</i> (whole plant)	Aqueous	Metal: Ag Shape: spherical Size: 450 nm	Antibacterial activity: Against <i>Bacillus subtilis</i> , <i>Bacillus vallismortis</i> , and <i>Escherichia coli</i> with zone of inhibition diameters of 15, 16, and 12 mm	[233]
<i>Melaleuca alternifolia</i> (leaves)	Aqueous	Metal: Ag Shape: spherical Size: 11.56 nm	Antimicrobial activity: Against <i>Staphylococcus aureus</i> , <i>Staphylococcus epidermidis</i> , <i>Streptococcus pyogenes</i> , <i>Klebsiella pneumoniae</i> , <i>Pseudomonas aeruginosa</i> , <i>Trichophyton mentagrophytes</i> , and <i>Candida albicans</i> with ZOI values ranges from 14.8 to 24.7 mm	[234]
<i>Parkia speciosa</i> (leaves)	Aqueous	Metal: Ag Shape: spherical Size: 31–35 nm	Antimicrobial activity: Against <i>Escherichia coli</i> , <i>Staphylococcus aureus</i> , <i>Pseudomonas aeruginosa</i> , and <i>Bacillus subtilis</i> with ZOI values ranging from 4.0 to 10 mm in diameter Antioxidant activity: Evaluated by DPPH assay with IC ₅₀ value of 15.26 µg/mL	[235]
<i>Hygrophila spinosa</i> (whole plant)	Aqueous	Metal: Au Shape: spherical Size: 68.44 ± 0.30 nm	Anticancer activity: Against MCF-7 and MDA-MB-231 (breast cancer), SKOV-3 (ovarian cancer) NCI/ADR (multi-drug resistant), and U-87 (glioblastoma, brain cancer) cell lines with significant percentage cell viability 43.78, 39.34, 21.45, 31.48, and 27.89%, respectively	[236]
<i>Clerodendrum phlomidis</i> (leaves)	Aqueous	Metal: Ag Shape: spherical Size: 23–42 nm	Antioxidant activity: Evaluated by using phosphomolybdate (910 AEAA), ferric reducing power (1.63 AU), superoxide radical scavenging (IC ₅₀ 55.86 µg/mL), and DPPH (IC ₅₀ 9.12 µg/mL) assays Anticancer activity: Against Ehrlich ascites carcinoma (EAC) and human colorectal adenocarcinoma (HT29) cell lines with 91.84% and 84.91% inhibition, respectively	[237]
<i>Aconitum toxicum</i> Rchb (rhizome)	Aqueous	Metal: Ag, Au Shape: spherical Size: 9–15 nm for AuNPs and 53–67 nm for AgNPs	Antioxidant activity: Evaluated by using DPPH assay with inhibition in between 78% and 84.32% at different concentrations	[238]

Table 2. Cont.

Plant Name (Part Used)	Extract	Nanoparticles	Findings	Ref.
<i>Musa acuminata colla</i> (flowers)	Aqueous	Metal: Ag, Au Shape: spherical Size: 12.6–15.7 nm for AgNPs and 10.1–15.6 nm for AuNPs	Antibacterial activity: Against <i>Enterococcus faecalis</i> , <i>Staphylococcus aureus</i> , <i>Klebsiella pneumoniae</i> , <i>Salmonella typhi</i> , <i>Escherichia coli</i> , <i>Proteus mirabilis</i> , and <i>Pseudomonas aeruginosa</i> with ZOI values 13, 9, 10, 9, 12, 6, and 12 mm for AgNPs) and 11, 0, 10, 9, 7, 8, and 9 for AuNPs at 1000 µg concentration Anticancer activity: 50% cell viability at 55.0 µg/mL and 35 µg/mL concentrations for AuNPs, and AgNPs respectively	[239]
<i>Allium cepa</i> (cloves)	Aqueous	Metal: Ag Shape: spherical Size: 10–50 nm	Antibacterial activity: Against methicillin-resistant <i>Staphylococcus aureus</i> and <i>Pseudomonas aeruginosa</i> with a maximum inhibition at 100 µg/mL concentration Anticancer activity: Against human breast cancer cells (MCF-7) with a maximum inhibition at 100 µg/mL concentration after 24 h	[240]
<i>Solanum nigrum</i> (leaves)	Aqueous	Metal: Au, Ag, Pd Shape: spherical Size: 3.46 nm for AgNPs, 9.39 nm for AuNPs, and 21.55 nm for PdNPs	Antibacterial activity: Against <i>Escherichia coli</i> with ZOI values 19.2 and 20 mm, 23 and 20 mm, and 18 and 19 mm for AuNPs, AgNPs, and PdNPs, respectively, at 5 and 10 mL concentration	[241]
<i>Carthamus tinctorius</i> L. (flowers)	Aqueous	Metal: Ag Shape: spherical Size: 38 nm	Antibacterial activity: Against <i>Escherichia coli</i> with inhibition of 98% and 85% at 40 °C and 80 °C temperatures	[242]
<i>Carpesium cernuum</i> (whole plant)	Aqueous	Metal: Ag Shape: spherical Size: 13.0 ± 0.2 nm	Antioxidant activity: Evaluated by using DPPH assay with IC ₅₀ value 0.121 ± 0.005 mg/mL Anticancer activity: Against human lung cancer A549 and B16F10 cell lines with 44.5 and 36.0% cytotoxicity on A549 and B16F10 respectively at 100 µg/mL concentration	[243]
<i>Ananas comosus</i> (peels)	Aqueous	Metal: Fe Shape: spherical Size: 17.87 nm	Antifungal activity: Against <i>Fusarium verticillioides</i> , <i>Aspergillus flavus</i> , and <i>Alternaria alternate</i> with inhibition zones ranging from 18.96 to 39.23 mm diameters	[244]
<i>Aaronsohnia factorovskiyi</i> (whole plant)	Aqueous	Metal: Ag Shape: spherical Size: 104–140 nm	Antibacterial activity: Against <i>Staphylococcus aureus</i> , <i>Bacillus subtilis</i> , <i>Pseudomonas aeruginosa</i> , and <i>Escherichia coli</i> with an inhibition zone diameter of about 19.00 ± 2.94 mm Antifungal activity: Against <i>Fusarium oxysporum</i> , <i>Fusarium solani</i> , <i>Helminthosporium rostratum</i> , and <i>Alternaria alternate</i> with reduced the growth of fungal yarn to 1.5 mm.	[245]

Table 2. Cont.

Plant Name (Part Used)	Extract	Nanoparticles	Findings	Ref.
<i>Vernonia amygdalina</i> (leaves)	Aqueous	Metal: CuO Shape: spherical Size: 19.68 nm	Antibacterial activity: Against <i>Staphylococcus aureus</i> , <i>Escherichia coli</i> , <i>Pseudomonas aeruginosa</i> , and <i>Enterobacter aerogenes</i> . The uppermost zone of inhibition of 15 mm was observed for <i>E. aerogenes</i>	[246]
<i>Artemisia ciniformis</i> (leaves)	Aqueous	Metal: Ag Shape: spherical Size: 4–14 nm	Anticancer activity: Against gastric cancer with the highest inhibition of cell proliferation at 100 µg/mL concentration	[247]
<i>Cichorium intybus</i> (leaves)	aqueous	Metal: Ag Shape: spherical Size: 17.17 nm	Anticancer activity: Against human breast cancer (MCF-7) with IC ₅₀ value 507.58 µg/mL after 24 h.	[248]
<i>Rhynchosia suaveolens</i> (leaves)	Aqueous	Metal: Ag Shape: spherical Size: 10–30 nm	Anticancer activity: Against DU145 and PC-3 (human prostate carcinoma cell lines), SKOV3 (human ovarian carcinoma), and A549 (human lung adenocarcinoma) with IC ₅₀ values of 4.35, 7.72, 4.2, and 24.7 µg/mL, respectively	[249]
<i>Solanum lycopersicum</i> (leaves)	Aqueous	Metal: FeO Shape: flower shaped Size: 483.8 nm	Anticancer activity: Against human lung cancer cell line A549 with IC ₅₀ value 69 ± 0.50 µg/mL	[250]
<i>Ageratum conyzoides</i> (leaves)	Aqueous	Metal: Ag Shape: spherical Size: 14–48 nm	Antioxidant activity: Evaluated by using DPPH and ABTS free radical scavenging assays with % inhibition 53.61 ± 0.01 to 89.82 ± 0.017 and 40.16 ± 0.13 to 81.1 ± 0.13 in 31.25 to 500 mg/mL concentrations, respectively.	[251]
<i>Blumea eriantha</i> DC (whole plant)	Ethanol	Metal: Ag, Fe Shape: spherical Size: 50 nm	Antioxidant activity: Evaluated by using DPPH (% inhibition 20.66 ± 0.90 for AgNPs and 17.25 ± 1.19 for FeNPs), ABTS (% inhibition 86.31 ± 0.21 for AgNPs, 74.94 ± 1.72 for FeNPs), H ₂ O ₂ scavenging (% inhibition 92.14 ± 1.06 for AgNPs and 57.00 ± 0.58 for FeNPs), and total antioxidant assay (% Inhibition 70.10 ± 0.53 for AgNPs and 56.14 ± 0.64% for FeNPs) Antibacterial activity: Against <i>Staphylococcus aureus</i> (ZOI 16.17 ± 2.08 for AgNPs and 13.06 ± 0.57 FeNPs), <i>Bacillus subtilis</i> (ZOI 14.12 ± 1.52 for AgNPs and 12.45 ± 0.52 for FeNPs), <i>Bacillus cereus</i> (ZOI 11.20 ± 1.15 for AgNPs and 10.12 ± 1.02 for FeNPs), and <i>Escherichia coli</i> (ZOI 15.24 ± 1.52 for AgNPs and 11.55 ± 1.18 for FeNPs) Anticancer activity: Against MCF-7 (human breast adenocarcinoma cell line) with % inhibition 15.45, 20.25, and 28.16 at the concentrations 25, 50, and 100 µg/mL, respectively, for AgNPs as well as 11.09, 17.81, and 22.25 at the concentration 25, 50, and 100 µg/mL respectively for FeNPs	[252]

Table 2. Cont.

Plant Name (Part Used)	Extract	Nanoparticles	Findings	Ref.
<i>Artemisia abrotanum</i> (whole plant)	Aqueous	Metal: MgO Shape: spherical Size: 10 nm	Antioxidant activity: Evaluated by using DPPH assay with IC ₅₀ 4.73 µg/mL	[253]
<i>Cnici Benedictus</i> (whole plant)	Aqueous	Metal: Au, CuO, and ZnO Shape: spherical Size: 13 nm for Au-CuONPs and 28 nm for CuO-ZnONPs	Antibacterial activity: Against <i>Staphylococcus aureus</i> (MIC 0.3125), <i>Escherichia coli</i> (MIC 0.625), <i>Pseudomonas aeruginosa</i> (MIC 2.5) Antifungal activity: Against <i>Candida albicans</i> (MIC 1.25). Anticancer activity: Against rat glioma C6 cells with IC ₅₀ 0.907 and 4.91 for Au-CuONP and CuO-ZnONPs, respectively	[254]
<i>Elephantopus scaber</i> (leaves)	Aqueous	Metal: Ag Shape: spherical Size: 37.86 nm	Anticancer activity: Against human skin carcinoma cells on A375 and L929 cell lines with IC ₅₀ values 15.68 ± 0.15 µg/mL and 65.49 ± 0.40 µg/mL, respectively Antioxidant activity: Evaluated by using the DPPH method with an IC ₅₀ value of 6.629 µg/mL Antibacterial activity: Against <i>Bacillus subtilis</i> , <i>Lactococcus lactis</i> , <i>Pseudomonas fluorescens</i> , and <i>Pseudomonas aeruginosa</i> Antifungal activity: Against <i>Aspergillus flavus</i> and <i>Aspergillus penicillioides</i> with ZOI ranges from 12 to 24 mm for all the strains	[255]
<i>Acanthospermum hispidum</i> (leaves)	Aqueous	Metal: Ag Shape: quasi-spherical Size: 20–60 nm	Antibacterial activity: Against <i>Pseudomonas aeruginosa</i> , <i>Streptococcus pyogenes</i> , <i>Staphylococcus aureus</i> , and <i>Escherichia coli</i> with a zone of inhibition of 17–19 at 100 µg/mL concentration Antifungal activity: Against <i>Candida albicans</i> , <i>Aspergillus niger</i> , and <i>Aspergillus clavatus</i> with MIC 500, 250, and 500 MIC µg/mL, respectively Antimicrobial activity: Against <i>Mycobacterium tuberculosis</i> H37RV with MIC 100 MIC µg/mL	[256]
<i>Leucaena leucocephala</i> L. (leaves)	Aqueous	Metal: Ag Shape: quasi-spherical Size: 35–47 nm	Antibacterial activity: Against <i>Pseudomonas aeruginosa</i> , <i>Streptococcus pyogenes</i> , <i>Staphylococcus aureus</i> , <i>Escherichia coli</i> , <i>Salmonella typhi</i> , <i>Bacillus subtilis</i> with ZOI values of 16–19 at 100 µg/mL concentration Antimycobacterial activity: Against <i>Mycobacterium tuberculosis</i> with MIC of 125 µg/mL	[257]

Table 2. Cont.

Plant Name (Part Used)	Extract	Nanoparticles	Findings	Ref.
<i>Silybum marianum</i> (whole plant)	Aqueous	Metal: Ag-ZnO, ZnO Shape: quasi-spherical Size: 31.2 nm for ZnO, and 35.3 nm for Ag-ZnO	Antibacterial activity: Against <i>Staphylococcus epidermidis</i> , <i>Bacillus subtilis</i> , <i>Klebsiella pneumonia</i> , <i>Escherichia coli</i> , and <i>Pseudomonas aeruginosa</i> with MIC values 250, 50, 150, 100, and 250 µg/mL for ZnONPs and 150, 50, 250, 150, and 150 µg/mL for Ag-ZnONPs, respectively Antifungal activity: <i>Fusarium solani</i> , <i>Aspergillus flavus</i> , <i>Aspergillus fumigatus</i> , and <i>Aspergillus niger</i> with MIC values 50, 250, 500, and 100 µg/mL for ZnONPs and 50, 150, 700, and 150 µg/mL for Ag-ZnONPs, respectively Antioxidant activity: Total antioxidant capacity (67.6 ± 1.44 for ZnONPs and 72.6 ± 1.32 for Ag-ZnONPs, at 1000 µg/mL concentration), total reducing power (72.4 ± 2.78 for Ag-ZnONPs and 68.1 ± 1.31 for ZnONPs at 1000 µg/mL concentration) and DPPH (67.22 ± 2.1 for Ag-ZnONPs and 56.31 ± 1.4 for ZnONPs at 1000 µg/mL concentration)	[258]
<i>Nyctanthes arbor-tristis</i> (flowers)	Aqueous	Metal: ZnO Shape: spherical Size: 12–32 nm	Antifungal activity: <i>Alternaria alternata</i> , <i>Aspergillus niger</i> , <i>Botrytis cinerea</i> , <i>Fusarium oxysporum</i> , and <i>Penicillium expansum</i> with MIC values 64, 16, 128, 64, and 128 µg/mL	[259]
<i>Melia azedarach</i> (leaves)	Aqueous	Metal: Ag Shape: spherical Size: 23 nm	Antifungal activity: Against <i>Colletotrichum coccodes</i> , <i>Monilinia</i> sp., and <i>Pyricularia</i> with growth inhibition of 18%, 33%, and 51%, respectively.	[260]
<i>Kleinia grandiflora</i> (leaves)	Aqueous	Metal: Ag Shape: spherical Size: 20–50 nm	Anticancer activity: Against Dalton's lymphoma ascites (DLA) cell lines with 40% cytotoxicity at 10 µg/mL concentration and IC ₅₀ of 500 nM after 6 h of treatment Antimicrobial activity: Against <i>Escherichia coli</i> , <i>Pseudomonas aeruginosa</i> , <i>Candida albicans</i> , and <i>Aspergillus niger</i> with a zone of inhibition as 13 ± 0.7 , 17 ± 1.02 , 13 ± 0.32 , and 15 ± 0.46 , respectively	[261]
<i>Medicago sativa</i> L.	Aqueous	Metal: ZnO Shape: hexagonal Size: 14 nm	Antimicrobial activity: Against <i>Staphylococcus epidermidis</i> , <i>Lactococcus lactis</i> , and <i>Lactobacillus casei</i> with MIC values in the range of 0.58–9.31 µg/mL Antifungal activity: <i>Candida albicans</i> , and <i>Saccharomyces cerevisiae</i> with MIC values of 9.31 and 4.65 µg/mL	[262]

Table 2. Cont.

Plant Name (Part Used)	Extract	Nanoparticles	Findings	Ref.
<i>Tussilago farfara</i> (flower buds)	Aqueous	Metal: Ag, Au Shape: spherical Size: 13.57 ± 3.26 nm for AgNPs and 18.20 ± 4.11 nm for AuNPs	Antibacterial activity: Against <i>Escherichia coli</i> , <i>Enterococcus faecalis</i> , <i>Pseudomonas aeruginosa</i> , and <i>Staphylococcus aureus</i> with MIC values ranging from 10 to 40 $\mu\text{g}/\text{mL}$ for AuNPs and AgNPs samples Anticancer activity: Against PANC-1 cells with IC ₅₀ values 166.1 and 71.2 μM for AgNPs and AuNPs, respectively. Against AGS cell lines with IC ₅₀ values 338 and 77.9 μM for AgNPs and AuNPs, respectively. Against HT-29 cell lines with IC ₅₀ values 275.3 and 87 μM for AgNPs and AuNPs, respectively	[263]
<i>Celastrus paniculatus</i> (leaves)	Aqueous	Metal: Cu Shape: spherical Size: 2–10 nm	Antifungal activity: Against plant pathogenic fungi <i>Fusarium oxysporum</i> with showing 76.29 ± 1.52 maximum mycelial inhibition	[264]
<i>Pechuel-oeschea leubnitziae</i> (roots)	Methanol	Metal: Ag Shape: spherical Size: 100 nm	Anticancer activity: Against the U87 glioma cell line with an IC ₅₀ value in the range of 0.64–0.71 $\mu\text{g}/\text{mL}$	[265]
<i>Centaurea pumilio</i> L. (aerial parts)	Methanol	Metal: Ag Shape: spherical Size: 6 and 8 nm	Antimicrobial activity: Against <i>Staphylococcus aureus</i> , <i>Streptococcus pyogenes</i> , <i>Pseudomonas aeruginosa</i> , <i>Escherichia coli</i> , and <i>Candida albicans</i> with ZOI values 22, 17, 12, 12 mm and no value, respectively. Antioxidant activity: Through estimation of SOD with activity in a dose-dependent-manner on the 4th and 7th days and then decreasing on the 14th day	[266]
<i>Artemisia turcomanica</i> (leaves)	Aqueous	Metal: Ag Shape: spherical Size: 22 nm	Anticancer activity: Against AGS (Human Gastric Adenocarcinoma) and normal L-929 cell lines with the IC ₅₀ value 15.43 and 14.56 $\mu\text{g}/\text{mL}$	[267]
<i>Hagenia abyssinica</i> (Brace) JF. Gmel. (leaves)		Metal: Cu Shape: spherical, hexagonal, triangular, cylindrical, and irregularly shaped Size: 34.76 nm	Antibacterial activity: Against <i>Escherichia coli</i> , <i>Pseudomonas aeruginosa</i> , <i>Staphylococcus aureus</i> , and <i>Bacillus subtilis</i> with ZOI 12.7, 12.7, 14.7, and 14.2 mm, respectively	[268]
<i>Solanum nigrum</i> (leaves)	Aqueous	Metal: CuO Shape: spherical Size: 32 and 25 nm	Antioxidant activity: Evaluated by using DPPH assay with 9–60% inhibition at different concentrations from ranges 15, 30, 60, 125, 250, and 500 $\mu\text{g}/\text{mL}$ Antibacterial activity: Against <i>Bacillus subtilis</i> , <i>Staphylococcus saprophyticus</i> , <i>Escherichia coli</i> , and <i>Pseudomonas aeruginosa</i> with ZOI 13 ± 0.1 , 11 ± 0.2 , 15 ± 0.4 , and 12 ± 0.6 nm, respectively, at a concentration of 100 μg	[269]

Table 2. Cont.

Plant Name (Part Used)	Extract	Nanoparticles	Findings	Ref.
<i>Solanum nigrum</i> (leaves)	Aqueous	Metal: ZnO Shape: spherical Size: 49 nm size	Antioxidant activity: Evaluated by using DPPH (21–94% inhibition) and H ₂ O ₂ scavenging (12–95% inhibition) assays at 15–500 µg/mL concentrations with IC ₅₀ values 130.54 and 126.14 µg/mL, respectively. Antibacterial activity: Against <i>Bacillus Subtilis</i> , <i>Staphylococcus saprophyticus</i> , <i>Escherichia coli</i> , and <i>Pseudomonas aeruginosa</i> with ZOI 17, 15, 19, and 17 nm at 100 µg concentration	[270]
<i>Polyalthia longifolia</i> (leaves)	Aqueous	Metal: CuO Shape: quasi-spherical Size: 5–60 nm	Antibacterial activity: Against <i>Pseudomonas aeruginosa</i> , <i>Staphylococcus aureus</i> , <i>Escherichia coli</i> , and <i>Staphylococcus pyogenes</i> with MIC values 100, 12.5, 25, and 125 µg/mL respectively Antifungal activity: <i>Aspergillus niger</i> , <i>Epidermophyton floccosum</i> , <i>Aspergillus clavatus</i> , and <i>Candida albicans</i> with MIC values 1000, 100, 1000, and 1000 µg/mL, respectively	[271]
<i>Limonia acidissima</i> (fruits)	Aqueous	Metal: MgO Shape: flake-like structure Size: 10–15 nm	Antibacterial activity: Against <i>Escherichia coli</i> , <i>Klebsiella pneumoniae</i> , <i>Pseudomonas aeruginosa</i> , and <i>Staphylococcus aureus</i> with MIC 0.25, 0.025, 0.25, and 0.025 µg/mL, respectively Antifungal activity: Against <i>Alternaria alternate</i> and <i>Phomopsis azadirachtae</i> with 91.48% and 95.33% inhibitions, respectively	[272]
<i>Cardiospermum halicacabum</i> (leaves)	Aqueous	Metal: ZnO Shape: hexagonal quartzite Size: 65, 62, 55, and 48 nm	Antibacterial activity: <i>Staphylococcus aureus</i> , <i>Bacillus subtilis</i> , <i>Escherichia coli</i> , and <i>Pseudomonas aeruginosa</i> with ZOI inhibition 20, 20, 21, and 19 mm at 0.6 mg concentration, respectively	[273]
<i>Oedera genistifolia</i> (leaves)	Aqueous	Metal: Ag Shape: spherical Size: 34.2 nm	Cytotoxicity: No cytotoxicity against HeLa cells Antibacterial activity: Against <i>Listeria ivanovic</i> , <i>Streptococcus uberis</i> , <i>Staphylococcus aureus</i> , <i>Mycobacterium smergatis</i> , <i>Enterobacter cloacae</i> , and <i>Vibrio sp</i> with MIC values 1.0, 0.5, 0.5, 0.25, 0.5, and 0.25 mg/mL, respectively	[274]
<i>Vernonia amygdalina</i> (leaves)	Aqueous	Metal: Cu, Zn Shape: hexagonal wurtzite Size: 34 to 39 nm	Antibacterial activity: Against <i>Staphylococcus aureus</i> , <i>Pseudomonas aeruginosa</i> , and <i>Escherichia coli</i> with ZOI values 21, 24, and 25 mm diameter, respectively	[275]
<i>Moringa oleifera</i> (leaves)	Aqueous	Metal: ZnO Shape: quasi-spherical Size: 35–95 nm	Antifungal activity: Against <i>Candida albicans</i> , <i>Aspergillus niger</i> , <i>Aspergillus clavatus</i> , <i>Trichophyton mentographytes</i> , and <i>Epidermophyton floccosum</i> with MIC values 250, 250, 250, 100, and 100 µg/mL, respectively	[276]

Table 2. Cont.

Plant Name (Part Used)	Extract	Nanoparticles	Findings	Ref.
<i>Wedelia chinensis</i> (leaves)	Aqueous	Metal: Ag Shape: spherical Size: 31.68 nm	Antioxidant activity: Evaluated by using DPPH and reducing power assay with a maximum inhibition at 200 µg/mL and at absorbance 0.81 ± 0.146 Antibacterial activity: Against <i>Escherichia coli</i> and <i>Listeria monocytogenes</i> with ZOI 25.4 and 21.7 mm, respectively Cytotoxic: Showed dose-dependent cytotoxicity against Hep G2 cells with an IC ₅₀ value of 25 µg/mL	[277]
<i>Seripheidium quettense</i> (leaves)	aqueous	Metal: Ag Shape: spherical Size: 49.96–54.36 nm	Antibacterial activity: <i>Bacillus subtilis</i> , <i>Staphylococcus aureus</i> , <i>Staphylococcus epidermidis</i> , <i>Escherichia coli</i> , <i>Pseudomonas aeruginosa</i> , and <i>Klebsiella pneumoniae</i> with MIC 33.3, -, 100, 11.1, 100, and 33.3 µg/mL, respectively Antifungal activity: Against <i>Aspergillus fumigatus</i> , <i>Aspergillus flavus</i> , <i>Aspergillus niger</i> , and <i>Mucor</i> spp., with ZOI 12 ± 0.33 , 10 ± 0.41 , 13.2 ± 0.72 , and 11 ± 0.78 mm diameter, respectively Anticancer activity: Demonstrated cytotoxic effects against HepG2 cells with IC ₅₀ of 62.5 µg/mL	[278]
<i>Albizia procera</i> (leaves)	Aqueous	Metal: Ag Shape: spherical Size: 6.18 nm	Antibacterial activity: <i>Escherichia coli</i> and <i>Staphylococcus aureus</i> with ZOI 13.5 ± 3.1 and 18.5 ± 6.75 at 100 µg concentration dose	[279]
<i>Cynara scolymus</i> (Leaves)	Aqueous	Metal: ZnO Shape: spherical Size: 65.9 nm	Antiproliferative activity: Against human breast cancer cell line (MCF 7) and Vero cells with IC ₅₀ values of 65.31 µg/µL and 957.85 µg/µL, respectively Antimicrobial activity: Against <i>Staphylococcus aureus</i> , <i>Escherichia coli</i> , <i>Pseudomonas aeruginosa</i> , <i>Candida albicans</i> , and <i>Candida tropicalis</i> with MIC ₅₀ > 7, 25, >100, >100, and 0.35 µg/mL concentrations, respectively	[280]
<i>Mangifera indica</i> (leaves)	Aqueous	Metal: ZnO Shape: spherical and hexagonal quartzite Size: 45–60 nm	Antioxidant activity: Evaluated by DPPH assay with 20–90% inhibition at different concentrations Anticancer property: Evaluated cytotoxicity against lung cancer A549 cell lines with 85% cell viability at 1.0 µg/mL concentration	[281]
<i>Cissus arnotiana</i> (leaves)	Aqueous	Metal: Cu Shape: spherical Size: 60–90 nm	Antibacterial activity: Against <i>Escherichia coli</i> , <i>Streptococcus</i> sp., <i>Rhizobium</i> sp., and <i>Klebsiella</i> sp., with 22.20 ± 0.16 , 20.23 ± 0.35 , 16.33 ± 0.13 , and 18.25 ± 0.12 at 75 µg/mL concentration Antioxidant activity: Evaluated by using DPPH assay with % radical scavenging activity 18 ± 1 , 21 ± 2 , 20 ± 8 , 19 ± 6 , 18 ± 2 at 20, 40, 60, 80, and 100 µg/mL concentrations	[282]

Table 2. Cont.

Plant Name (Part Used)	Extract	Nanoparticles	Findings	Ref.
<i>Tridax. procumbens</i> (leaves)	Aqueous	Metal: Ag Shape: spherical Size: 54.34 nm	Antioxidant activity: Evaluated by using DPPH free radical scavenging activity ($60.96 \pm 0.61\%$ inhibition), metal chelating activity ($53.24 \pm 0.56\%$ inhibition), and β -carotene linoleic ($85.26 \pm 0.16\%$ inhibition) assays Antibacterial activity: against <i>Pseudomonas aeruginosa</i> , <i>Serratia marcescens</i> , <i>Shigella flexneri</i> , <i>Salmonella typhi</i> , <i>Escherichia coli</i> , <i>Proteus mirabilis</i> , <i>Klebsiella pneumoniae</i> , <i>Enterococcus faecalis</i> , and <i>Staphylococcus aureus</i> with ZOI inhibition ranges from 11 ± 1.00 to 15.33 ± 0.58 mm diameter and MIC values from 11.43 to 102.8 $\mu\text{g}/\text{mL}$, respectively, for all the strains, respectively	[283]
<i>Taraxacum officinale</i> (leaves)	Aqueous	Metal: Ag Shape: spherical Size: 15 nm	Antioxidant activity: Evaluated by using DPPH radical scavenging ($\text{IC}_{50} = 56.1 \mu\text{g}/\text{mL}$), ABTS radical scavenging ($\text{IC}_{50} = 45.6 \mu\text{g}/\text{mL}$), and nitric oxide (NO) scavenging ($\text{IC}_{50} = 55.2 \mu\text{g}/\text{mL}$) assays Anticancer activity: Against human liver carcinoma cells HepG2 cells with a maximum inhibition at 25 $\mu\text{g}/\text{mL}$ Antimicrobial activity: Against <i>Xanthomonas axonopodis</i> pv. <i>citri</i> and <i>Pseudomonas syringae</i> with ZOI 17.2 ± 0.65 , 20.2 ± 0.84 , 22.0 ± 0.84 mm, and 15.4 ± 0.32 , 17.2 ± 0.65 , 19.5 ± 0.66 mm at 10, 20, and 30 $\mu\text{g}/\text{mL}$ concentrations, respectively	[284]
<i>Tragopogon collinus</i> (whole plant)	Ethanol and methanol	Metal: Ag Shape: spherical Size: 7–18 nm	Antibacterial activity: Against <i>Staphylococcus aureus</i> with ZOI 2, 5, and 10 mm and <i>Escherichia coli</i> with ZOI 4, 7, and 8 mm at 6000, 7000, and 8000 $\mu\text{g}/\text{mL}$ concentrations, respectively	[285]
<i>Deverra tortuosa</i> (aerial part)	Aqueous	Metal: ZnO Shape: hexagonal and Wurtzite structures Size: 9.26–31.18 nm	Anticancer activity: Against cancer cell lines namely human colon adenocarcinoma “Caco-2” with IC_{50} 50.81 $\mu\text{g}/\text{mL}$ and human lung adenocarcinoma “A549” with IC_{50} 83.47 $\mu\text{g}/\text{mL}$, respectively	[286]
<i>Pulicaria vulgaris</i> Gaertn. (aerial part)	Aqueous	Metal: Ag Shape: spherical Size: 28.6 ± 9.0 nm	Antibacterial activity: Against <i>Staphylococcus aureus</i> , and <i>Escherichia coli</i> with MIC values ranging from 60 to 80 $\mu\text{g}/\text{mL}$ and MBC values ranging from 80 to 100 $\mu\text{g}/\text{mL}$ Antifungal activity: Against <i>Candida albicans</i> , and <i>Candida glabrata</i> MIC values ranging from 40 to 60 $\mu\text{g}/\text{mL}$ and MCF values ranging from 80 to 100 $\mu\text{g}/\text{mL}$ Antioxidant activity: Evaluated by using DPPH radical scavenging assay with maximum scavenging activity at 120 $\mu\text{g}/\text{mL}$ concentration	[287]

Table 2. Cont.

Plant Name (Part Used)	Extract	Nanoparticles	Findings	Ref.
<i>Rhododendron arboretum</i> (leaves)	Aqueous	Metal: MgO Shape: spherical Size: NA	Antibacterial activity: <i>Escherichia coli</i> , <i>Spectroscopic mutans</i> , and <i>Proteus vulgaris</i> with ZOI 36 mm, 32 mm, and 24 mm at 10 mg/L concentration, respectively	[288]
<i>Aegle marmelos</i> (leaves)	Aqueous	Metal: ZnFe ₂ O ₄ Shape: spherical Size: NA	Antibacterial activity: Against <i>Escherichia coli</i> , <i>Pseudomonas aeruginosa</i> , <i>Staphylococcus aureus</i> , and <i>Bacillus subtilis</i> with ZOI 17, 25, 22, and 23 nm	[289]
<i>Costus pictus</i> D.(leaves)	Aqueous	Metal: MgO Shape: hexagonal Size: 50 nm	Antibacterial activity: <i>Staphylococcus aureus</i> , <i>Bacillus subtilis</i> , <i>Escherichia coli</i> , and <i>Salmonella paratyphi</i> with ZOI 5.5, 10.0, 12.5, and 15.0 mm Antifungal activity: <i>Candidia albicans</i> and <i>Aspergillus niger</i> with ZOI 10.5 and 12.5 mm Anticancer activity: Against DLA cell line with % inhibition 2 ± 0.152 , 9 ± 0.025 , 18 ± 0.174 , 30 ± 0.035 , and 52 ± 0.0053 at 10, 20, 50, 100, and 200 µg/mL concentrations, respectively	[290]
<i>Tropaeolum majus</i> L. (leaves)	Aqueous	Metal: Ag Shape: spherical Size: 35–55 nm	Antibacterial activity: Against <i>Staphylococcus aureus</i> , <i>Enterococcus faecalis</i> , <i>Escherichia coli</i> , <i>Salmonella typhi</i> , and <i>Pseudomonas aeruginosa</i> with MIC values from 50 to 450 µg/mL Antifungal activity: <i>Aspergillus niger</i> , <i>Candida albicans</i> , <i>Penicillium notatum</i> , <i>Trichoderma viridiae</i> , and <i>Mucor</i> sp. with MIC values from 12 to 170 µg/mL Anticancer activity: Against MCF7 and VERO cells with 50% inhibition at 3–4 and 5–6 µg/mL concentrations, respectively.	[291]
<i>Psidium guajava</i> L. (leaves)	Aqueous	Metal: Ag Shape: spherical Size: 20–35, 25 nm, and 25–35 nm	Antioxidant activity: Evaluated by using DPPH (IC ₅₀ values of 52.53 ± 0.31 µg/mL) and ABTS (IC ₅₀ values of 55.10 ± 0.29 µg/mL) radical scavenging assays Antimicrobial activity: <i>Saccharomyces cerevisiae</i> , <i>Aspergillus niger</i> , <i>Rhizopus</i> , <i>Alcaligenes faecalis</i> , and <i>Escherichia coli</i> with a maximum inhibition at 100 µg/mL concentration.	[292]
<i>Handelia trichophylla</i> (flowers)	Aqueous	Metal: Ag Shape: spherical Size: 20–50 nm	Antibacterial activity: Against <i>Staphylococcus aureus</i> , <i>Bacillus subtilis</i> , <i>Escherichia coli</i> , and <i>Pseudomonas aeruginosa</i> with ZOI 10.2, 9.1, and 8.5 mm for negative control as well as 16.3, 11.3, 11.3, and 9.8 mm for positive control, respectively	[293]

Table 2. Cont.

Plant Name (Part Used)	Extract	Nanoparticles	Findings	Ref.
<i>Pimpinella anisum</i> (seeds)	Methanol	Metal: Ag, Au Shape: spherical Size: ~15 nm	Antioxidant activity: Evaluated by using DPPH assay with IC ₅₀ 45.53 and 191.58 µg/mL for AgNPs and AuNPs samples, respectively Antibacterial activity: Against <i>Staphylococcus aureus</i> and <i>Escherichia coli</i> with ZOI 11 and 13 mm for AgNPs while AuNPs were inactive against these strains Antifungal activity: Against <i>Aspergillus flavus</i> and <i>Candida albicans</i> with ZOI 10 and 11 mm for AgNPs while AuNPs were inactive against these strains	[294]
<i>Gundelia tournefortii</i> L. (leaves)	Aqueous	Metal: Au Shape: spherical Size: 40–45 nm	Antioxidant activity: Evaluated by using DPPH assay with IC ₅₀ 194 µg/mL Antibacterial activity: <i>Pseudomonas aeruginosa</i> , <i>Escherichia coli</i> , <i>Bacillus subtilis</i> , <i>Staphylococcus aureus</i> , <i>Salmonella typhimurium</i> , and <i>Streptococcus pneumonia</i> with MIC values 2 ± 0, 4 ± 0, 2 ± 0, 2 ± 0, 2 ± 0, 4 ± 0 mg/mL, respectively Antifungal activity: <i>Candida albicans</i> , <i>Candida glabrata</i> , <i>Candida krusei</i> , and <i>Candida guilliermondii</i> with MIC values 4 ± 0, 4 ± 0, 2 ± 0, 2 ± 0 mg/mL, respectively	[295]
<i>Plectranthus asirensis</i> (aerial parts)	Ethanol	Metal: Ag Shape: spherical Size: 20 nm	Antioxidant activity: Evaluated by using DPPH assay with IC ₅₀ 12.725 ± 0.326 and 14.541 ± 0.225 µg/mL values for luteolin and stigmaterol in extract, respectively	[296]
<i>Harpagophytum procumbens</i> (roots)	Aqueous	Metal: Ag Shape: spherical Size: 82 nm	Antioxidant activity: Evaluated by chemiluminescence method for short-lived free radicals (inhibition = 73%) and ABTS method for long-lived free radicals (inhibition = 18.3%) respectively	[297]
<i>Hyacinthus orientalis</i> L. and <i>Dianthus caryophyllus</i> L. (leaves)	Aqueous	Metal: Ag Shape: spherical Size: 61.45 and 89.6 nm	Antioxidant activity: Evaluated by chemiluminescence method with inhibition of free radicals ranging between 88.30 and 97.38%	[298] *
<i>Salvia officinalis</i> L. (leaves)	Aqueous	Metal: Ag Shape: spherical Size: 75 nm	Antioxidant activity: Evaluated by chemiluminescence method with 98.6% inhibition of free radicals	[299] *
<i>Anthriscus cerefolium</i> L. (aerial part)	Hydroalcoholic	Metal: Ag Shape: spherical Size: 10–15 nm	Antioxidant activity: Evaluated by DPPH radical scavenging and chemiluminescence method with significant percentage inhibition (55–78%)	[300] *

* References for chemiluminescence method; NA: Not Available; mm: Millimeter; Ag: Silver; Cu: Copper; Fe: Iron; Pd: Palladium; Ni: Nickel; FeO: Ferric oxide; ZnO: Zinc oxide; CuO: Copper oxide; MgO: Magnesium oxide; DPPH: 2,2-diphenyl-1-picrylhydrazyl; FRAP: Ferric ion reducing antioxidant power; F-C: Folin-Ciocalteu; CUPRAC: cupric reducing antioxidant capacity; SNPAC: silver nanoparticle antioxidant capacity method; MIC: Minimum Inhibitory Concentration; IC₅₀: Half maximal inhibitory concentration; H₂O₂: Hydrogen peroxide; AgNPs: Silver nanoparticles; AuNPs: Gold nanoparticles; PdNPs: Palladium nanoparticles; FeNPs: Iron nanoparticles; ZOI: Zone of inhibition; SOD: Superoxide dismutase; NO: Nitric oxide.

7. Future Outlooks and Directions

PDMNPs have a wide range of applications in the regulation of oxidative stress-mediated disorders and diseases, according to recent research advances. Evidence from the published literature suggests that PDMNPs could be used as novel and effective therapeutics to treat diseases caused by oxidative stress. Due to the availability of diverse bioactive compounds, medicinal plants and herbs have been utilized as traditional medicine for thousands of years. This gives patients more treatment alternatives than are available with synthetic medications. Particularly, PDMNPs facilitate the large-scale manufacturing of therapeutic compounds and are environmentally safe, inexpensive, and toxin-free, making this method advantageous for the long-term advancement of nanoscience. PDMNPs also have a wide range of medicinal uses, including as an antioxidant, and with antibacterial, antifungal, anticancer, antiplasmodial, and antidiabetic potentials. Additionally, they have the ability to redox the biomolecular reactions in catalytic amounts. More work in the right direction is needed to address the main problems during the synthesis and implementation of PDMNPs as therapeutic agents, based on pharmacological applications. The key issues are as follows:

- When produced through physical and chemical processes, nanoparticles are uniform and homogeneous. However, synthesized by biological methods, PDMNPs are variable in shape and size. Consequently, logical investigations need to be employed to ensure the uniformity of particles.
- The exact amount of reducing agents (bioactive compounds) in plant extracts is unknown if it is not standardized quantitatively. Therefore, plant extract should be standardized qualitatively and quantitatively in order to maintain the homogeneity of formed PDMNPs.
- PDMNPs are synthesized using metals, which may be toxic to the human body if consumed in large quantities. Most reports do not include the toxicity profile of synthesized PDMNPs, as well as biological studies. To address these issues of the precise mechanism, distribution, toxicity, and adverse effects, comprehensive pharmacokinetic studies are required extensively.
- The majority of PDMNP therapeutic applications and molecular mechanisms are based on ROS generated during biological actions. Despite these studies, the negative effects on normal cells/tissues lack a mode of action, which is one of the most pressing issues that must be addressed accurately.
- Extensive clinical or in vivo research is also required to develop PDMNPs in the appropriate dosage forms for the treatment of a variety of diseases.
- Despite ROS-mediated therapeutic actions, other modes of action of PDMNPs must be investigated further in order to be effective against other diseases.

8. Conclusions

In this review, we summarized the synthesis, characterization techniques, and in-depth evaluation of antioxidant, antimicrobial, and anticancer activities of PDMNPs over the last five years. The challenges experienced in the synthesis of PDMNPs and how they should be overcome, as well as their therapeutic activities mediated by oxidative stress, were the main topics of this review. Moreover, we provided the ideal parameters (extract concentration, incubation time, pH, and temperature) to use at the time of PDMNPs synthesis in order to obtain high-yield, low-cost PDMNPs. Additionally, we have discussed the molecular mechanisms of oxidative stress-mediated therapeutic actions along with their findings in tabulated form. Furthermore, we have also highlighted the future outlooks of metal NPs and the changes that must be made in order to develop PDMNPs as safe biocompatible agents. Considering the above scientific benefits and drawbacks of PDMNPs, researchers may fine-tune their research by simplifying their processes to develop such types of PDMNPs as therapeutics against human diseases. Furthermore, in vivo or clinical studies might be needed to evaluate the toxicity and performance of PDMNPs if they are used as therapeutics for long-term use.

Author Contributions: M.A.K. searched for and compiled the data from the previous literature. M.F.K. contributed to the design of study, supervised the study, and wrote the manuscript. All authors have read and agreed to the published version of the manuscript.

Funding: This research work has been financially supported by intramural funding at Era's Lucknow Medical College & Hospital, Era University, Lucknow-226003, India.

Institutional Review Board Statement: Not applicable.

Informed Consent Statement: No animal or in vitro or in vivo study was performed in this manuscript, and therefore, neither ethics nor informed consent was necessary.

Data Availability Statement: Not applicable.

Acknowledgments: Authors are very thankful to the management team of Era University, Lucknow, India, and the American University of Barbados (AUB) for their assistance during this work. We have sincere thanks to Raj Kazmi for providing figure designing assistance.

Conflicts of Interest: The authors declare no conflict of interest, financial or otherwise.

Abbreviations

Ag: Silver; AgNO₃: Silver nitrate; Au: Gold; AFM: Atomic force microscopy; ABTS: 2,2'-azino-bis(3-ethylbenzothiazoline-6-sulfonic acid); Au-CuONPs: Gold-Copper oxide nanoparticles; Ag-ZnONPs: Silver zinc oxide nanoparticles; AGS: Gastric adenocarcinoma; BHA: Butylated hydroxyanisole; BHT: Butylated hydroxytoluene; Cu: Copper; Co: Cobalt; Cu(NO₃)₂: Cupric nitrate; CuSO₄.5H₂O: Copper sulfate pentahydrate; HAuCl₄: Chloroauric acid; CuO: Copper oxide; CT: Computed tomography; CV: Cyclic voltammetry; CUPRAC: Cupric reducing antioxidant capacity; SKOV3: Cystadenocarcinoma; COLO205: Cellosaurus cell line; CuO-ZnONPs: Copper oxide-zinc oxide nanoparticles; DLS: Dynamic light scattering; DNA: Deoxyribonucleic acid; DPPH: 2,2-diphenyl-1-picrylhydrazyl; DU145: Dihydroflavonols; DLA: Dalton's lymphoma ascites; EDX: Energy dispersive X-ray spectroscopy; EAC: Ehrlich ascites carcinoma; Fe: Iron; FTIR: Fourier-transform infrared; FE-SEM: Field emission scanning electron microscopy; FRAP: Ferric reducing ability of plasma; FeO: Iron oxide; H₂PtCl₆: Chloroplatinic acid; H₂O₂: Hydrogen peroxide; HCT-116: Human colorectal carcinoma; HepG2: Hepatocellular; HT29: Human colorectal; HeLa: Henrietta lacks; H37RV: *Mycobacterium tuberculosis* strain; IC₅₀: Maximal half inhibitory concentration; MgO: Magnesium oxide; MDR: Multidrug resistance; MRI: Magnetic resonance imaging; Mg: Magnesium; MIC: Minimum inhibitory concentration; mmol/g: Milimole per gram; MCF-7: Michigan cancer foundation-7; MM418C: Melanoma; MDA-MB-231: Metastatic breast; MIC: Minimum inhibitory concentration; NPs: Nanoparticles; NiO: Nickel oxide; Ni: Nickel; NSCLC: Non-small cell lung cancer; NCI/ADR: Adriamycin-resistant; NO: Nitric oxide; Pd: Palladium; Pt: Platinum; PDMNPs: Plant-derived metal nanoparticles; PG: Propyl gallate; PET: Positron emission tomography; P53: Protein-53; Pb: Lead; PC-3: Prostatic carcinoma; PANC-1: Pancreatic cancer cell; ROS: Reactive oxygen species; RNA: Ribonucleic acid; RAW264.7: Macrophage cell line; SEM: Scanning electron microscopy; SNPAC: Silver nanoparticles antioxidant capacity method; SOD: Superoxide dismutase; Ti: Titanium; TEM: Transmission electron microscopy; 3D: Three dimensional; TBHQ: Tertiary butyl hydroquinone; WHO: World Health Organization; XRD: X-ray Diffraction; XPS: X-ray photoelectron spectroscopy; Zn: Zinc; ZnSO₄: Zinc sulfate; ZnO: Zinc oxide; ZnNO₃: Zinc nitrate; ZnO: Zinc oxide; ZOI: Zone of inhibition; ZnONPs: Zinc oxide nanoparticles; FRAP: Ferric reducing antioxidant power; TEAC: Trolox equivalent antioxidant capacity; ORAC: Oxygen radical absorbance capacity; TOSC: Total oxy radical scavenging capacity; TRAP: Total radical trapping antioxidant parameter.

References

1. Bayda, S.; Adeel, M.; Tuccinardi, T.; Cordani, M.; Rizzolio, F. The History of Nanoscience and Nanotechnology: From Chemical–Physical Applications to Nanomedicine. *Molecules* **2020**, *25*, 112. [[CrossRef](#)] [[PubMed](#)]
2. Mittal, D.; Kaur, G.; Singh, P.; Yadav, K.; Ali, S.A. Nanoparticle-Based Sustainable Agriculture and Food Science: Recent Advances and Future Outlook. *Front. Nanotechnol.* **2020**, *2*, 579954. [[CrossRef](#)]
3. Gattoo, M.A.; Naseem, S.; Arfat, M.Y.; Dar, A.M.; Qasim, K.; Zubair, S. Physicochemical Properties of Nanomaterials: Implication in Associated Toxic Manifestations. *Biomed Res. Int.* **2014**, *2014*, 498420. [[CrossRef](#)]
4. Mansoori, G.; Fauzi, S.T. *Nanotechnology—An Introduction for the Standards Community*; ASTM International: West Conshohocken, PN, USA, 2005; Volume 2, pp. 1–22.
5. Liu, Y.; Mai, S.; Li, N.; Yiu, C.K.; Mao, J.; Pashley, D.H.; Tay, F.R. Differences between top-down and bottom-up approaches in mineralizing thick, partially demineralized collagen scaffolds. *Acta Biomater.* **2011**, *7*, 1742–1751. [[CrossRef](#)] [[PubMed](#)]
6. Khan, I.; Saeed, K.; Khan, I. Nanoparticles: Properties, applications and toxicities. *Arab. J. Chem.* **2019**, *12*, 908–931. [[CrossRef](#)]
7. Bhardwaj, B.; Singh, P.; Kumar, A.; Kumar, S.; Budhwar, V. Eco-Friendly Greener Synthesis of Nanoparticles. *Adv. Pharm. Bull.* **2020**, *10*, 566–576. [[CrossRef](#)] [[PubMed](#)]
8. Mohamad, N.A.N.; Arham, N.A.; Jai, J.; Hadi, A. Plant extract as reducing agent in synthesis of metallic nanoparticles: A review. *Adv. Mater. Res.* **2013**, *832*, 350–355. [[CrossRef](#)]
9. Logozzi, M.; Di Raimo, R.; Mizzoni, D.; Fais, S. The Potentiality of Plant-Derived Nanovesicles in Human Health—A Comparison with Human Exosomes and Artificial Nanoparticles. *Int. J. Mol. Sci.* **2022**, *23*, 4919. [[CrossRef](#)]
10. Roy, A. Plant Derived Silver Nanoparticles and their Therapeutic Applications. *Curr. Pharm. Biotechnol.* **2021**, *22*, 1834–1847. [[CrossRef](#)]
11. Vippola, M.; Valkonen, M.; Sarlin, E.; Honkanen, M.; Huttunen, H. Insight to Nanoparticle Size Analysis—Novel and Convenient Image Analysis Method versus Conventional Techniques. *Nanoscale Res. Lett.* **2016**, *11*, 169. [[CrossRef](#)]
12. Simpson, D.S.A.; Oliver, P.L. ROS Generation in Microglia: Understanding Oxidative Stress and Inflammation in Neurodegenerative Disease. *Antioxidants* **2020**, *9*, 743. [[CrossRef](#)] [[PubMed](#)]
13. Dröge, W. Free radicals in the physiological control of cell function. *Physiol. Rev.* **2002**, *82*, 47–95. [[CrossRef](#)] [[PubMed](#)]
14. Forrester, S.J.; Kikuchi, D.S.; Hernandez, M.S.; Xu, Q.; Griendling, K.K. Reactive Oxygen Species in Metabolic and Inflammatory Signaling. *Circ Res.* **2018**, *122*, 877–902. [[CrossRef](#)] [[PubMed](#)]
15. Alzoghbi, M.A. Concepts of oxidative stress and antioxidant defense in Crohn’s disease. *World J. Gastroenterol.* **2013**, *19*, 6540–6547. [[CrossRef](#)] [[PubMed](#)]
16. Gilgun-Sherki, Y.; Melamed, E.; Offen, D. Oxidative stress induced-neurodegenerative diseases: The need for antioxidants that penetrate the blood brain barrier. *Neuropharmacology* **2001**, *40*, 959–975. [[CrossRef](#)] [[PubMed](#)]
17. Rasheed, A.; Li, H.; Tahir, M.M.; Mahmood, A.; Nawaz, M.; Shah, A.N.; Aslam, M.T.; Negm, S.; Moustafa, M.; Hassan, M.U.; et al. The role of nanoparticles in plant biochemical, physiological, and molecular responses under drought stress: A review. *Front. Plant Sci.* **2022**, *13*, 976179. [[CrossRef](#)] [[PubMed](#)]
18. Abdal Dayem, A.; Hossain, M.K.; Lee, S.B.; Kim, K.; Saha, S.K.; Yang, G.-M.; Choi, H.Y.; Cho, S.-G. The Role of Reactive Oxygen Species (ROS) in the Biological Activities of Metallic Nanoparticles. *Int. J. Mol. Sci.* **2017**, *18*, 120. [[CrossRef](#)]
19. AshaRani, P.V.; Low, K.M.G.; Hande, M.P.; Valiyaveetil, S. Cytotoxicity and genotoxicity of silver nanoparticles in human cells. *ACS Nano.* **2009**, *24*, 279–290. [[CrossRef](#)]
20. Carlson, C.; Hussain, S.M.; Schrand, A.M.; Braydich-Stolle, L.K.; Hess, K.L.J.R. Unique cellular interaction of silver nanoparticles: Size-dependent generation of reactive oxygen species. *J. Phys. Chem. B.* **2008**, *112*, 13608–13619. [[CrossRef](#)]
21. Baig, N.; Kammakam, I.; Falath, W. Nanomaterials: A review of synthesis methods, properties, recent progress, and challenges. *Mater. Adv.* **2021**, *2*, 1821–1871. [[CrossRef](#)]
22. Nancharaiyah, Y.V.; Mohan, S.V.; Lens, P.N.L. Biological and bioelectrochemical recovery of critical and scarce metals. *Trends Biotechnol.* **2016**, *34*, 137–155. [[CrossRef](#)]
23. Jamkhande, P.G.; Ghule, N.W.; Bamer, A.H.; Kalaskar, M.G. Metal nanoparticles synthesis: An overview on methods of preparation, advantages and disadvantages, and applications. *J. Drug. Deliv. Sci. Technol.* **2019**, *53*, 101174. [[CrossRef](#)]
24. Barhoum, A.; García-Betancourt, M.L.; Jeevanandam, J.; Hussien, E.A.; Mekawy, S.A.; Mostafa, M.; Omran, M.M.; Abdalla, M.S.; Bechelany, M. Review on Natural, Incidental, Bioinspired, and Engineered Nanomaterials: History, Definitions, Classifications, Synthesis, Properties, Market, Toxicities, Risks, and Regulations. *Nanomaterials* **2022**, *12*, 177. [[CrossRef](#)]
25. Jeevanandam, J.; Barhoum, A.; Chan, Y.S.; Dufresne, A.; Danquah, M.K. Review on nanoparticles and nanostructured materials: History, sources, toxicity and regulations. *Beilstein J. Nanotechnol.* **2018**, *9*, 1050–1074. [[CrossRef](#)] [[PubMed](#)]
26. Shehzad, K.; Xu, Y.; Gaoc, C.; Duan, X. Three-dimensional macro-structures of two-dimensional nanomaterials. *Chem. Soc. Rev.* **2016**, *45*, 5541–5588. [[CrossRef](#)]
27. Vollath, D. *Nanomaterials: An Introduction to Synthesis, Properties and Applications*, 2nd ed.; Wiley-VCH: Weinheim, Germany, 2013. ISBN 978-3-527-33379-0.
28. Paras, Yadav, K.; Kumar, P.; Teja, D.R.; Chakraborty, S.; Chakraborty, M.; Mohapatra, S.S.; Sahoo, A.; Chou, M.M.C.; Liang, C.-T.; et al. A Review on Low-Dimensional Nanomaterials: Nanofabrication, Characterization and Applications. *Nanomaterials* **2023**, *13*, 160. [[CrossRef](#)] [[PubMed](#)]

29. Kelly, K.L.; Coronado, E.; Zhao, L.L.; Schatz, G.C. The Optical Properties of Metal Nanoparticles: The Influence of Size, Shape, and Dielectric Environment. *J. Phys. Chem. B* **2003**, *107*, 668–677. [[CrossRef](#)]
30. Yaqoob, A.A.; Ahmad, H.; Parveen, T.; Ahmad, A.; Oves, M.; Ismail, I.M.I.; Qari, H.A.; Umar, K.; Ibrahim, M.N.M. Recent Advances in Metal Decorated Nanomaterials and Their Various Biological Applications: A Review. *Front. Chem.* **2020**, *8*, 341. [[CrossRef](#)]
31. Yaqoob, S.B.; Adnan, R.; Khan, R.M.R.; Rashid, R. Gold, Silver, and Palladium Nanoparticles: A Chemical Tool for Biomedical Applications. *Front. Chem.* **2020**, *8*, 376. [[CrossRef](#)]
32. Chavali, M.S.; Nikolova, M.P. Metal oxide nanoparticles and their applications in nanotechnology. *SN Appl. Sci.* **2019**, *1*, 607. [[CrossRef](#)]
33. Huynh, K.-H.; Pham, X.-H.; Kim, J.; Lee, S.H.; Chang, H.; Rho, W.-Y.; Jun, B.-H. Synthesis, Properties, and Biological Applications of Metallic Alloy Nanoparticles. *Int. J. Mol. Sci.* **2020**, *21*, 5174. [[CrossRef](#)] [[PubMed](#)]
34. Nguyen, T.K.; Thanh, N.M.; Mahiddine, S. Mechanisms of Nucleation and Growth of Nanoparticles in Solution. *Chem. Rev.* **2014**, *114*, 7610–7630.
35. Harish, V.; Ansari, M.M.; Tewari, D.; Gaur, M.; Yadav, A.B.; García-Betancourt, M.-L.; Abdel-Haleem, F.M.; Bechelany, M.; Barhoum, A. Nanoparticle and Nanostructure Synthesis and Controlled Growth Methods. *Nanomaterials* **2022**, *12*, 3226. [[CrossRef](#)] [[PubMed](#)]
36. Ijaz, I.; Gilani, E.; Nazir, A.; Bukhari, A. Detail review on chemical, physical and green synthesis, classification, characterizations and applications of nanoparticles. *Green Chem. Lett. Rev.* **2020**, *13*, 223–245. [[CrossRef](#)]
37. Thakkar, K.; Mhatre, S.S.; Parikh, R.Y. Biological synthesis of metallic nanoparticles. *Nanomed. Nanomed.-Nanotechnol.* **2010**, *6*, 257–262. [[CrossRef](#)] [[PubMed](#)]
38. Dhand, C.; Dwivedi, N.; Loh, X.J.; Ying, A.N.J.; Verma, N.K.; Beuerman, R.W.; Lakshminarayanan, R.; Ramakrishna, S. Methods and strategies for the synthesis of diverse nanoparticles and their applications: A comprehensive overview. *RSC Adv.* **2015**, *5*, 105003–105037. [[CrossRef](#)]
39. Abinaya, S.; Kavitha, H.P.; Prakash, M.; Muthukrishnaraj, A. Green synthesis of magnesium oxide nanoparticles and its applications: A review. *Sustain. Chem. Pharm.* **2021**, *19*, 100368. [[CrossRef](#)]
40. Singh, J.; Dutta, T.; Kim, K.-H.; Rawat, M.; Samddar, P.; Kumar, P. Green' synthesis of metals and their oxide nanoparticles: Applications for environmental remediation. *J. Nanobiotechnol.* **2018**, *16*, 84. [[CrossRef](#)]
41. Viswanath, B.; Kim, S. Influence of nanotoxicity on human health and environment: The alternative strategies. *Rev. Environ. Contam. Toxicol.* **2015**, *240*, 77.
42. Rastogi, A.; Tripathi, D.K.; Yadav, S.; Chauhan, D.K.; Živčák, M.; Ghorbanpour, M.; El-Sheery, N.I.; Bresticet, M. Application of silicon nanoparticles in agriculture. *3 Biotech* **2019**, *9*, 90. [[CrossRef](#)]
43. Abedini, A.; Daud, A.R.; Hamid, M.A.A.; Othman, N.K.; Saion, E. A review on radiation-induced nucleation and growth of colloidal metallic nanoparticles. *Nanoscale Res. Lett.* **2013**, *8*, 1–10. [[CrossRef](#)]
44. Ullah, A.; Lim, S.I. Plant extract-based synthesis of metallic nanomaterials, their applications, and safety concerns. *Biotechnol. Bioeng.* **2022**, *119*, 2273–2304. [[CrossRef](#)] [[PubMed](#)]
45. Zhang, D.; Ma, X.-L.; Gu, Y.; Huang, H.; Zhang, G.-W. Green Synthesis of Metallic Nanoparticles and Their Potential Applications to Treat Cancer. *Front. Chem.* **2020**, *8*, 799. [[CrossRef](#)] [[PubMed](#)]
46. Moghaddam, A.B.; Namvar, F.; Moniri, M.; Tahir, P.M.; Azizi, S.; Mohamad, R. Nanoparticles Biosynthesized by Fungi and Yeast: A Review of Their Preparation, Properties, and Medical Applications. *Molecules* **2015**, *20*, 16540–16565. [[CrossRef](#)]
47. Park, Y.; Hong, Y.N.; Weyers, A.; Kim, Y.S.; Linhardt, R.J. Polysaccharides and phytochemicals: A natural reservoir for the green synthesis of gold and silver nanoparticles. *IET Nanobiotechnol.* **2011**, *5*, 69–78. [[CrossRef](#)]
48. Rónavári, A.; Igaz, N.; Adamecz, D.I.; Szerencsés, B.; Molnar, C.; Kónya, Z.; Pfeiffer, I.; Kiricsi, M. Green Silver and Gold Nanoparticles: Biological Synthesis Approaches and Potentials for Biomedical Applications. *Molecules* **2021**, *26*, 844. [[CrossRef](#)]
49. Das, S.K.; Thatoi, H. *Biotechnological Utilization of Mangrove Resources*, 1st ed.; Academic Press: Cambridge, MA, USA; Elsevier: Amsterdam, The Netherlands, 2020; pp. 355–370.
50. Adeyemi, J.O.; Oriola, A.O.; Onwudiwe, D.C.; Oyediji, A.O. Plant Extracts Mediated Metal-Based Nanoparticles: Synthesis and Biological Applications. *Biomolecules* **2022**, *12*, 627. [[CrossRef](#)] [[PubMed](#)]
51. Marslin, G.; Siram, K.; Maqbool, Q.; Selvakesavan, R.K.; Kruszka, D.; Kachlicki, P.; Franklin, F. Secondary Metabolites in the Green Synthesis of Metallic Nanoparticles. *Materials* **2018**, *11*, 940. [[CrossRef](#)]
52. Xulu, J.H.; Ndongwe, T.; Ezealisiji, K.M.; Tembu, V.J.; Mncwangi, N.P.; Witika, B.A.; Siwe-Noundou, X. The Use of Medicinal Plant-Derived Metallic Nanoparticles in Theranostics. *Pharmaceutics* **2022**, *14*, 2437. [[CrossRef](#)]
53. Gawande, M.B.; Goswami, A.; Felpi, F.X.; Asefa, T.; Huang, X.; Silva, R.; Zou, X.; Zboril, R.; Varma, R.S. Cu and Cu-Based Nanoparticles: Synthesis and Applications in Catalysis. *Chem. Rev.* **2016**, *116*, 3722–3811. [[CrossRef](#)]
54. Rudramurthy, G.R.; Swamy, M.K.; Sinniah, U.R.; Ghasemzadeh, A. Nanoparticles: Alternatives against Drug-Resistant Pathogenic Microbes. *Molecules* **2016**, *21*, 836. [[CrossRef](#)]
55. Khezerlou, A.; Alizadeh-Sani, M.; Azizi-Lalabadi, M.; Ehsani, A. Nanoparticles and their antimicrobial properties against pathogens including bacteria, fungi, parasites and viruses. *Microb. Pathog.* **2018**, *123*, 505–526. [[CrossRef](#)]

56. Benassai, E.; Bubba, M.D.; Ancillotti, C.; Colzi, I.; Gonnelli, C.; Calisi, N.; Salvatici, M.C.; Casalone, E.; Ristori, S. Green and cost-effective synthesis of copper nanoparticles by extracts of non-edible and waste plant materials from *Vaccinium* species: Characterization and antimicrobial activity. *Mater. Sci. Eng. C Mater. Biol. Appl.* **2021**, *119*, 111453. [[CrossRef](#)]
57. Naghdi, S.; Sajjadi, M.; Nasrollahzadeh, M.; Rhee, K.Y.; Sajadi, S.M.; Jaleh, B. *Cuscuta reflexa* leaf extract mediated green synthesis of the Cu nanoparticles on graphene oxide/manganese dioxide nanocomposite and its catalytic activity toward reduction of nitroarenes and organic dyes. *J. Taiwan Inst. Chem. Eng.* **2018**, *86*, 158–173. [[CrossRef](#)]
58. Kumar, B.; Smita, K.; Cumbal, L.; Debut, A. Green approach for fabrication and applications of zinc oxide nanoparticles. *Bioinorg. Chem. Appl.* **2014**, *2014*, 523869. [[CrossRef](#)] [[PubMed](#)]
59. Kesharwani, J.; Yoon, K.Y.; Hwang, J.; Rai, M. Phytosynthesis of silver nanoparticles by leaf extract of *Datura metel*: Hypothetical mechanism involved in synthesis. *J. Bionanoscience* **2009**, *3*, 39–44. [[CrossRef](#)]
60. Patra, J.K.; Baek, K.-H. Green Nanobiotechnology: Factors Affecting Synthesis and Characterization Techniques. *J. Nanomater.* **2014**, *2014*, 417305. [[CrossRef](#)]
61. Pyrzynska, K.; Sentkowska, A. Biosynthesis of selenium nanoparticles using plant extracts. *J. Nanostruct. Chem.* **2022**, *12*, 467–480. [[CrossRef](#)]
62. Gopinath, K.; Arumugam, G.S. Phytosynthesis of silver nanoparticles using *Pterocarpus santalinus* leaf extract and their antibacterial properties. *J. Nanostruct. Chem.* **2013**, *3*, 68. [[CrossRef](#)]
63. Shaikh, W.A.; Chakraborty, S.; Owens, G.; Ul-Islam, R. A review of the phytochemical mediated synthesis of AgNP (silver nanoparticle): The wonder particle of the past decade. *Appl. Nanosci.* **2021**, *11*, 2625–2660. [[CrossRef](#)]
64. Adeyemia, J.O.; Elemikec, E.E.; Onwudiwea, D.C.; Singh, M. Bio-inspired synthesis and cytotoxic evaluation of silver-gold bimetallic nanoparticles using Kei-Apple (*Dovyalis caffra*) fruits. *Inorg. Chem. Comm.* **2019**, *109*, 107569. [[CrossRef](#)]
65. Jain, S.; Mehata, M.S. Medicinal Plant Leaf Extract and Pure Flavonoid Mediated Green Synthesis of Silver Nanoparticles and their Enhanced Antibacterial Property. *Sci. Rep.* **2017**, *7*, 15867. [[CrossRef](#)] [[PubMed](#)]
66. Christopher, J.S.G.; Saswati, B.; Ezilrani, P.S. Optimization of Parameters for Biosynthesis of Silver Nanoparticles Using Leaf Extract of *Aegle marmelose*. *Braz. Arch. Biol. Technol.* **2015**, *58*, 702–710. [[CrossRef](#)]
67. Moosa, A.A.; Ridha, A.M.; Al-Kaser, M. Process Parameters for Green Synthesis of Silver Nanoparticles using Leaves Extract of Aloe Vera Plant. *Int. J. Multidiscip. Curr. Res.* **2015**, *3*, 966–976.
68. Gericke, M.; Pinches, A. Microbial production of gold nanoparticles. *Gold Bull.* **2006**, *39*, 22–28. [[CrossRef](#)]
69. Sangaonkar, G.M.; Pawar, K.D. *Garcinia indica* mediated biogenic synthesis of silver nanoparticles with antibacterial and antioxidant activities. *Colloids Surf. B* **2018**, *164*, 210–217. [[CrossRef](#)] [[PubMed](#)]
70. Krishnaprabha, M.; Pattabi, M. Synthesis of gold nanoparticles using *Garcinia indica* fruit rind extract. *Int. J. Nanosci.* **2016**, *15*, 1660015. [[CrossRef](#)]
71. Dwivedi, A.D.; Gopal, K. Biosynthesis of gold and silver nanoparticles using *Chenopodium album* leaf extract. *Colloids Surf. A* **2010**, *369*, 27–33. [[CrossRef](#)]
72. Dubey, S.P.; Lahtinen, M.; Sillanpää, M. Tansy fruit mediated greener synthesis of silver and gold nanoparticles. *Process Biochem.* **2010**, *45*, 1065–1071. [[CrossRef](#)]
73. Fayaz, A.M.; Balaji, K.; Kalaiichelvan, P.T.; Venkatesan, R. Fungal based synthesis of silver nanoparticles—an effect of temperature on the size of particles. *Colloids Surf. B* **2009**, *74*, 123–126. [[CrossRef](#)]
74. Shaligram, N.S.; Bule, M.; Bhambure, R.; Singhal, R.S.; Singh, S.K.; Szakacs, G.; Pandey, A. Biosynthesis of silver nanoparticles using aqueous extract from the compactin producing fungal strain. *Process Biochem.* **2009**, *44*, 939–943. [[CrossRef](#)]
75. Veerasamy, R.; Xin, T.Z.; Gunasagaran, S.; Xiang, T.F.W.; Yang, E.F.C.; Jeyakumar, N.; Dhanraj, S.A. Biosynthesis of silver nanoparticles using mangosteen leaf extract and evaluation of their antimicrobial activities. *J. Saudi Chem. Soc.* **2011**, *15*, 113–120. [[CrossRef](#)]
76. Ghoreishi, S.M.; Behpour, M.; Khayataকাশani, M. Green synthesis of silver and gold nanoparticles using *Rosa damascena* and its primary applications in electrochemistry. *Phys. E* **2011**, *44*, 97–104. [[CrossRef](#)]
77. Gardea-Torresdey, J.L.; Tiemann, K.J.; Gamez, G.; Dokken, K.; Cano-Aguilera, I.; Furenlid, L.R.; Renner, M.W. Reduction and accumulation of gold(III) by *Medicago sativa* alfalfa biomass: X-ray absorption spectroscopy, pH and temperature dependence. *Environ. Sci. Technol.* **2000**, *34*, 4392–4396. [[CrossRef](#)] [[PubMed](#)]
78. Begum, R.; Farooqi, Z.H.; Naseem, K.; Ali, F.; Batool, M.; Xiao, J.; Irfan, A. Applications of UV/Vis Spectroscopy in Characterization and Catalytic Activity of Noble Metal Nanoparticles Fabricated in Responsive Polymer Microgels: A Review. *Crit. Rev. Anal. Chem.* **2018**, *48*, 506–516. [[CrossRef](#)]
79. Armendariz, V.; Herrera, I.; Peralta-Videa, J.R.; Jose-Yacamán, M.; Troiani, H.; Santiago, P.; Gardea-Torresdey, J.L. Size controlled gold nanoparticle formation by *Avena sativa* biomass: Use of plants in nanobiotechnology. *J. Nanopart. Res.* **2004**, *6*, 377–382. [[CrossRef](#)]
80. Singh, A.K.; Srivastava, O.N. One-step Green synthesis of gold nanoparticles using black cardamom and effect of pH on its synthesis. *Nanoscale Res. Lett.* **2015**, *10*, 353. [[CrossRef](#)]
81. Sathishkumar, M.; Sneha, K.; Won, S.W.; Cho, C.W.; Kim, S.; Yun, Y.S. Cinnamon *zeylanicum* bark extract and powder mediated green synthesis of nano-crystalline silver particles and its bactericidal activity. *Colloids Surf. B* **2009**, *73*, 332–338. [[CrossRef](#)]
82. Vincent, J.; Lau, K.S.; Evyang, Y.C.-Y.; Chin, S.X.; Sillanpää, M.; Chia, C.H. Biogenic Synthesis of Copper-Based Nanomaterials Using Plant Extracts and Their Applications: Current and Future Directions. *Nanomaterials* **2022**, *12*, 3312. [[CrossRef](#)]

83. Marciniak, L.; Nowak, M.; Trojanowska, A.; Tylkowski, B.; Jastrzab, R. The Effect of pH on the Size of Silver Nanoparticles Obtained in the Reduction Reaction with Citric and Malic Acids. *Materials* **2020**, *13*, 5444. [[CrossRef](#)]
84. Bernabé-Antonio, A.; Martínez-Ceja, A.; Romero-Estrada, A.; Sánchez-Carranza, J.N.; Columba-Palomares, M.C.; Rodríguez-López, V.; Meza-Contreras, J.C.; Silva-Guzmán, J.A.; Gutiérrez-Hernández, J.M. Green Synthesis of Silver Nanoparticles Using *Randia aculeata* L. Cell Culture Extracts, Characterization, and Evaluation of Antibacterial and Antiproliferative Activity. *Nanomaterials* **2022**, *12*, 4184. [[CrossRef](#)]
85. Chitra, K.; Annadurai, G. Antibacterial Activity of pH-Dependent Biosynthesized Silver Nanoparticles against Clinical Pathogen. *BioMed Res. Int.* **2014**, *2014*, 725165. [[CrossRef](#)]
86. Suresh, A.P.; Kalarikkal, S.P.; Pullareddy, B.; Sundaram, G.M. Low pH-Based Method to Increase the Yield of Plant-Derived Nanoparticles from Fresh Ginger Rhizomes. *ACS Omega* **2021**, *6*, 17635–17641. [[CrossRef](#)] [[PubMed](#)]
87. Khan, S.A.; Shahid, S.; Sajid, M.R.; Noreen, F.; Kanwal, S. Biogenic synthesis of CuO Nanoparticles and their biomedical applications: A current review. *Int. J. Adv. Res.* **2017**, *5*, 925–946. [[CrossRef](#)] [[PubMed](#)]
88. Pereira, L.; Mehboob, F.; Stams, A.J.M.; Mota, M.M.; Rijnaarts, H.H.M.; Alves, M.M. Metallic nanoparticles: Microbial synthesis and unique properties for biotechnological applications, bioavailability and biotransformation. *Crit. Rev. Biotechnol.* **2013**, *35*, 114–128. [[CrossRef](#)] [[PubMed](#)]
89. Rai, A.; Singh, A.; Ahmad, A.; Sastry, M. Role of halide ions and temperature on the morphology of biologically synthesized gold nanotriangles. *Langmuir* **2006**, *22*, 736–741. [[CrossRef](#)] [[PubMed](#)]
90. Gericke, M.; Pinches, A. Biological synthesis of metal nanoparticles. *Hydrometallurgy* **2006**, *83*, 132–140. [[CrossRef](#)]
91. Lengke, M.F.; Fleet, M.E.; Southam, G. Biosynthesis of silver nanoparticles by filamentous cyanobacteria from a silver (I) nitrate complex. *Langmuir* **2007**, *23*, 2691–2699. [[CrossRef](#)]
92. Andreescu, D.; Eastman, C.; Balantrapu, K.; Goia, D.V.A. Simple route for manufacturing highly dispersed silver nanoparticles. *J. Mater. Res.* **2007**, *22*, 2488–2496. [[CrossRef](#)]
93. Sathishkumar, M.; Krishnamurthy, S.; Yun, Y.S. Immobilization of silver nanoparticles synthesized using the *Curcuma longa* tuber powder extract on cotton cloth for bactericidal activity. *Biores. Technol.* **2010**, *101*, 7958–7965. [[CrossRef](#)]
94. Kumari, M.; Mishra, A.; Pandey, S.; Singh, S.P.; Chaudhry, V.; Mudiam, M.K.R.; Shukla, S.; Kakkar, P.; Nautiyal, C.S. Physico-Chemical Condition Optimization during Biosynthesis lead to development of Improved and Catalytically Efficient Gold Nano Particles. *Sci. Rep.* **2016**, *6*, 27575. [[CrossRef](#)] [[PubMed](#)]
95. Kobylinska, N.; Klymchuk, D.; Khaynakova, O.; Duplij, V.; Matvieieva, N. Morphology-Controlled Green Synthesis of Magnetic Nanoparticles Using Extracts of ‘Hairy’ Roots: Environmental Application and Toxicity Evaluation. *Nanomaterials* **2022**, *12*, 4231. [[CrossRef](#)] [[PubMed](#)]
96. Mittal, J.; Batra, A.; Singh, A.; Sharma, M.M. Phytofabrication of nanoparticles through plant as nanofactories. *Adv. Nat. Sci. Nanosci. Nanotechnol.* **2014**, *5*, 043002. [[CrossRef](#)]
97. Lu, Y.; Foo, L.Y. Polyphenolics of *Salvia*-A review. *Phytochemistry* **2002**, *59*, 117–140. [[CrossRef](#)]
98. Shankar, S.S.; Rai, A.; Ahmad, A.; Sastry, M. Rapid synthesis of Au, Ag, and bimetallic Au core-Ag shell nanoparticles using *Neem* (*Azadirachta indica*) leaf broth. *J. Colloid Interface Sci.* **2004**, *275*, 496–502. [[CrossRef](#)]
99. Prasad, R. Synthesis of Silver Nanoparticles in Photosynthetic Plants. *J. Nanopart.* **2014**, *2014*, 963961. [[CrossRef](#)]
100. Saxena, A.; Tripathi, R.M.; Zafar, F.; Singh, P. Green synthesis of silver nanoparticles using aqueous solution of *Ficus benghalensis* leaf extract and characterization of their antibacterial activity. *Mater. Lett.* **2012**, *67*, 91–94. [[CrossRef](#)]
101. Aziz, N.; Fatma, T.; Varma, A.; Prasad, R. Biogenic Synthesis of Silver Nanoparticles Using *Scenedesmus abundans* and Evaluation of Their Antibacterial Activity. *J. Nanopart.* **2014**, *2014*, 689419. [[CrossRef](#)]
102. Al-Zahrani, S.; Astudillo-Calderón, S.; Pintos, B.; Pérez-Urria, E.; Manzanera, J.A.; Martín, L.; Gomez-Garay, A. Role of Synthetic Plant Extracts on the Production of Silver-Derived Nanoparticles. *Plants* **2021**, *10*, 1671. [[CrossRef](#)]
103. Kutchan, T.M. A role for intra- and intercellular translocation in natural product biosynthesis. *Curr. Opin. Plant Biol.* **2005**, *8*, 292–300. [[CrossRef](#)]
104. Hussain, K.; Saquib, M.; Khan, M.F. *Techniques for Extraction, Isolation, and Standardization of Bio-Active Compounds from Medicinal Plants. Natural Bio-Active Compounds: Volume 2: Chemistry, Pharmacology and Health Care Practices*; Swamy, M.K., Akhtar, M.S., Eds.; Springer: Singapore, 2019; pp. 179–200, ISBN 9789811372056.
105. Teffane, M.; Boudries, H.; Bey, M.B.; Kadi, A.; Boukhalfa, F. Effect of Solvent Type, Extraction Temperature, Agitation Speed and Microwave Power on Phenolic Compound Extraction and Antioxidant Activity of Apricot Kernels (*Prunus armeniaca* L.). *Curr. Bioact. Compd.* **2022**, *18*, e260821191386. [[CrossRef](#)]
106. Ahmed, S.; Ahmad, M.; Swami, B.L.; Ikram, S. A review on plants extract mediated synthesis of silver nanoparticles for antimicrobial applications: A green expertise. *J. Adv. Res.* **2016**, *7*, 17–28. [[CrossRef](#)]
107. Hernández-Pinero, J.L.; Terrón-Rebolledo, M.; Foroughbakhch, R.; Moreno-Limón, S.; Melendrez, M.F.; Solís-Pomar, F.; Pérez-Tijerina, E. Effect of heating rate and plant species on the size and uniformity of silver nanoparticles synthesized using aromatic plant extracts. *Appl. Nanosci.* **2016**, *6*, 1183–1190. [[CrossRef](#)]
108. Deen, G.R.; Hannan, F.A.; Henari, F.; Akhtar, S. Effects of Different Parts of the Okra Plant (*Abelmoschus esculentus*) on the Phytosynthesis of Silver Nanoparticles: Evaluation of Synthesis Conditions, Nonlinear Optical and Antibacterial Properties. *Nanomaterials* **2022**, *12*, 4174. [[CrossRef](#)]

109. Aspé, E.; Fernández, K. The effect of different extraction techniques on extraction yield, total phenolic, and anti-radical capacity of extracts from *Pinus radiata* Bark. *Ind. Crops Prod.* **2011**, *34*, 838–844. [[CrossRef](#)]
110. Hano, C.; Abbasi, B.H. Plant-Based Green Synthesis of Nanoparticles: Production, Characterization and Applications. *Biomolecules* **2022**, *12*, 31. [[CrossRef](#)] [[PubMed](#)]
111. Jiang, J.; Oberdorster, G.; Biswas, P. Characterization of size, surface charge, and agglomeration state of nanoparticle dispersions for toxicological studies. *J. Nanopart. Res.* **2009**, *11*, 77–89. [[CrossRef](#)]
112. Chen, X.; Jensen, L. Understanding the shape effect on the plasmonic response of small ligand coated nanoparticles. *J. Opt.* **2016**, *18*, 074009. [[CrossRef](#)]
113. Soliman, M.K.Y.; Salem, S.S.; Abu-Elghait, M.; Azab, M.S. Biosynthesis of Silver and Gold Nanoparticles and Their Efficacy Towards Antibacterial, Antibiofilm, Cytotoxicity, and Antioxidant Activities. *Appl. Biochem. Biotechnol.* **2023**, *195*, 1158–1183. [[CrossRef](#)]
114. Sun, S.; Murray, C.B.; Weller, D.; Folks, L.; Moser, A. Monodisperse FePt nanoparticles and ferromagnetic FePt nanocrystal superlattices. *Science* **2000**, *287*, 1989–1992. [[CrossRef](#)]
115. Noah, N. *Green Synth Characterizat Applicat Nanoparticles*, 1st ed.; Elsevier: Amsterdam, The Netherlands, 2019; Volume 53, pp. 111–135.
116. Jyoti, K.; Baunthiyal, M.; Singh, A. Characterization of silver nanoparticles synthesized using *Urtica dioica* Linn. leaves and their synergistic effects with antibiotics. *J. Rad. Res. App. Sci.* **2016**, *9*, 217–227. [[CrossRef](#)]
117. Anandalakshmi, K.; Venugob, J.; Ramasamy, V. Characterization of silver nanoparticles by green synthesis method using *Pedaliium murex* leaf extract and their antibacterial activity. *App. Nanosci.* **2016**, *6*, 399–408. [[CrossRef](#)]
118. Krithiga, N.; Rajalakshmi, N.; Jayachitra, A. Green synthesis of silver nanoparticles using leaf extracts of *Clitoria ternatea* and *Solanum nigrum* and study of its antibacterial effect against common nosocomial pathogens. *J. Nanosci.* **2015**, *2015*, 928204. [[CrossRef](#)]
119. Mallikarjuna, K.; Nasif, O.; Ali, A.S.; Chinni, S.V.; Reddy, L.V.; Reddy, M.R.V.; Sreeramanan, S. Phytogenic Synthesis of Pd-Ag/rGO Nanostructures Using Stevia Leaf Extract for Photocatalytic H₂ Production and Antibacterial Studies. *Biomolecules* **2021**, *11*, 190. [[CrossRef](#)] [[PubMed](#)]
120. Khan, S.A.; Shahid, S.; Shahid, B.; Fatima, U.; Abbasi, S.A. Green Synthesis of MnO Nanoparticles Using *Abutilon indicum* Leaf Extract for Biological, Photocatalytic, and Adsorption Activities. *Biomolecules* **2020**, *10*, 785. [[CrossRef](#)] [[PubMed](#)]
121. Baudot, C.; Tan, C.M.; Kong, J.C. FTIR spectroscopy as a tool for nano-material characterization. *Infrared Phys. Technol.* **2010**, *53*, 434–438. [[CrossRef](#)]
122. Kiefer, J.; Grabow, J.; Kurland, H.-D.; Muller, F.A. Characterization of nanoparticles by solvent infrared spectroscopy. *Anal. Chem.* **2015**, *87*, 12313–12317. [[CrossRef](#)]
123. Chithrani, B.D.; Ghazani, A.A.; Chan, W.C.W. Determining the size and shape dependence of gold nanoparticle uptake into mammalian cells. *Nano Lett.* **2006**, *6*, 662–668. [[CrossRef](#)]
124. Ansari, M.A.; Murali, M.; Prasad, D.; Alzohairy, M.A.; Almatroudi, A.; Alomary, M.N.; Udayashankar, A.C.; Singh, S.B.; Asiri, S.M.M.; Ashwini, B.S.; et al. Cinnamomum verum Bark Extract Mediated Green Synthesis of ZnO Nanoparticles and Their Antibacterial Potentiality. *Biomolecules* **2020**, *10*, 336. [[CrossRef](#)]
125. Cherian, T.; Ali, K.; Saquib, Q.; Faisal, M.; Wahab, R.; Musarrat, J. Cymbopogon Citratus Functionalized Green Synthesis of CuO-Nanoparticles: Novel Prospects as Antibacterial and Antibiofilm Agents. *Biomolecules* **2020**, *10*, 169. [[CrossRef](#)]
126. Jain, N.; Jain, P.; Rajput, D.; Patil, U.K. Green synthesized plant-based silver nanoparticles: Therapeutic prospective for anticancer and antiviral activity. *Micro Nano Syst. Lett.* **2021**, *9*, 5. [[CrossRef](#)]
127. Rautela, A.; Rani, J.; Das, M.D. Green synthesis of silver nanoparticles from *Tectona grandis* seeds extract: Characterization and mechanism of antimicrobial action on different microorganisms. *J. Ana. Sci. Tech.* **2019**, *10*, 1–10. [[CrossRef](#)]
128. Utsunomiya, S.; Ewing, R.C. Application of high-angle annular dark field scanning transmission electron microscopy, scanning transmission electron microscopy-energy dispersive X-ray spectrometry, and energy-filtered transmission electron microscopy to the characterization of nanoparticles in the environment. *Environ. Sci. Technol.* **2003**, *37*, 786–791. [[PubMed](#)]
129. Shaik, M.R.; Khan, M.; Kuniyil, M.; Al-Warthan, A.; Alkhathlan, H.Z.; Siddiqui, M.R.H.; Shaik, J.P.; Ahamed, A.; Mahmood, A.; Khan, M.; et al. Plant-Extract-Assisted Green Synthesis of Silver Nanoparticles Using *Origanum vulgare* L. Extract and Their Microbicidal Activities. *Sustainability* **2018**, *10*, 913. [[CrossRef](#)]
130. Gardea-Torresdey, J.L.; Gomez, E.; Peralta-Videa, J.R.; Parsons, J.G.; Troiani, H.E.; Jose-Yacaman, M. Alfalfa sprouts: A natural source for the synthesis of silver nanoparticles. *Langmuir* **2003**, *19*, 1357–1361. [[CrossRef](#)]
131. Sivalingam, D.; Karthikeyan, S.; Arumugam, P. Biosynthesis of silver nanoparticles from *Glycyrrhiza glabra* root extract. *Arch. App. Sci. Res.* **2012**, *4*, 178–187.
132. Joudeh, N.; Linke, D. Nanoparticle classification, physicochemical properties, characterization, and applications: A comprehensive review for biologists. *J. Nanobiotechnol.* **2022**, *20*, 262. [[CrossRef](#)]
133. Srirangam, G.M.; Rao, K.P. Synthesis and characterization of silver nanoparticles from the leaf extract of *Malachra capitata* (L). *Ras. J. Chem.* **2017**, *10*, 46–53.
134. Alexander, V.; Vorontsov, O.; Sergei, V. Tsybulya. Influence of Nanoparticles Size on XRD Patterns for Small Monodisperse Nanoparticles of CuO and TiO₂ Anatase. *Ind. Eng. Chem. Res.* **2018**, *57*, 2526–2536.

135. Tan, Y.; Sun, D.; Yu, H.; Yang, B.; Shi, Y.G.; Chen, Z.; Cai, Q.; Wu, Z. Crystallization mechanism analysis of noncrystalline Ni-P nanoparticles through XRD, HRTEM and XAFS. *CrystEngComm* **2014**, *16*, 9657–9668. [[CrossRef](#)]
136. Gardea-Torresdey, J.; Rodriguez, E.; Parsons, J.G.; Peralta Videa, J.R.; Meitzner, G.; Cruz-Jimenez, G. Use of ICP and XAS to determine the enhancement of gold phytoextraction by *Chilopsis linearis* using thiocyanate as a complexing agent. *Anal. Bioanal. Chem.* **2005**, *382*, 347–352. [[CrossRef](#)] [[PubMed](#)]
137. Velavan, S.; Amargeetha, A. X-ray Diffraction (XRD) and Energy Dispersive Spectroscopy (EDS) Analysis of Silver Nanoparticles Synthesized from *Erythrina Indica* Flowers. *Nanosci Technol.* **2018**, *5*, 1–5.
138. Meva, F.E.; Ntumba, A.A.; Kedi, P.B.E.; Tchoumbi, E.; Schmitz, A.; Schmolke, L.; Klopotoski, M.; Moll, B.; Kökcem-Demir, Ü.; Mpondo, E.A.M.; et al. Silver and palladium nanoparticles produced using a plant extract as reducing agent, stabilized with an ionic liquid: Sizing by X-ray powder diffraction and dynamic light scattering. *J. Mater. Res. Technol.* **2019**, *8*, 1991–2000. [[CrossRef](#)]
139. Bayat, M.; Zargar, M.; Astarkhanova, T.; Pakina, E.; Ladan, S.; Lyashk, M.; Shkurkin, S.I. Facile Biogenic Synthesis and Characterization of Seven Metal-Based Nanoparticles Conjugated with Phytochemical Bioactives Using *Fragaria ananassa* Leaf Extract. *Molecules* **2021**, *26*, 3025. [[CrossRef](#)] [[PubMed](#)]
140. Scimeca, M.; Bischetti, S.; Lamsira, H.K.; Bonfiglio, R.; Bonanno, E. Energy Dispersive X-ray (EDX) microanalysis: A powerful tool in biomedical research and diagnosis. *Eur. J. Histochem.* **2018**, *62*, 2841. [[CrossRef](#)]
141. Carvalho, P.M.; Felício, M.R.; Santos, N.C.; Gonçalves, S.; Domingues, M.M. Application of Light Scattering Techniques to Nanoparticle Characterization and Development. *Front. Chem.* **2018**, *6*, 237. [[CrossRef](#)]
142. Rasmussen, M.K.; Pedersen, J.N.; Marie, R. Size and surface charge characterization of nanoparticles with a salt gradient. *Nat. Commun.* **2020**, *11*, 2337. [[CrossRef](#)]
143. Gurunathan, S.; Qasim, M.; Park, C.; Yoo, H.; Kim, I.D.J.H.; Hong, K. Cytotoxic potential and molecular pathway analysis of silver nanoparticles in human colon cancer cells HCT116. *Int. J. Mol. Sci.* **2018**, *19*, 2269. [[CrossRef](#)]
144. Dikshit, P.K.; Kumar, J.; Das, A.K.; Sadhu, S.; Sharma, S.; Singh, S.; Gupta, P.K.; Kim, B.S. Green Synthesis of Metallic Nanoparticles: Applications and Limitations. *Catalysts* **2021**, *11*, 902. [[CrossRef](#)]
145. Tantra, R.; Schulze, P.; Quincey, P. Effect of nanoparticle concentration on zeta-potential measurement results and reproducibility. *Particuology* **2010**, *8*, 279–285. [[CrossRef](#)]
146. Mourdikoudis, S.; Pallares, R.M.; Thanh, N.T.K. Characterization techniques for nanoparticles: Comparison and complementarity upon studying nanoparticle properties. *Nanoscale* **2018**, *10*, 12871–12934. [[CrossRef](#)] [[PubMed](#)]
147. Phaniendra, A.; Jestadi, D.; Periyasamy, L. Free Radicals: Properties, Sources, Targets, and Their Implication in Various Diseases. *Indian J. Clin. Biochem.* **2015**, *30*, 11–26. [[CrossRef](#)] [[PubMed](#)]
148. Khezerlou, A.; Akhlaghi, A.P.; Alizadeh, A.M.; Dehghan, P.; Malekie, P. Alarming impact of the excessive use of tert-butylhydroquinone in food products: A narrative review. *Toxicol. Rep.* **2022**, *9*, 1066–1075. [[CrossRef](#)] [[PubMed](#)]
149. Galib, B.M.; Mashru, M.; Jagtap, C.; Patgiri, B.J.; Prajapati, P.K. Therapeutic potentials of metals in ancient India: A review through Charaka Samhita. *J. Ayurveda. Integr. Med.* **2011**, *2*, 55–63. [[CrossRef](#)] [[PubMed](#)]
150. Bedlovičová, Z.; Strapáč, I.; Baláž, M.; Salayová, A. A Brief Overview on Antioxidant Activity Determination of Silver Nanoparticles. *Molecules* **2020**, *25*, 3191. [[CrossRef](#)] [[PubMed](#)]
151. El-Shafey, A.M. Green synthesis of metal and metal oxide nanoparticles from plant leaf extracts and their applications: A review. *Green Process. Synth.* **2020**, *9*, 304–339. [[CrossRef](#)]
152. Kumar, M.; Ahmad, A.; Rawat, P.; Khan, M.F.; Rasheed, N.; Gupta, P.; Sathiamoorthy, B.; Bhatia, G.; Palit, G.; Maurya, R. Antioxidant flavonoid glycosides from *Evolvulus alsinoides*. *Fitoterapia* **2010**, *81*, 234–242. [[CrossRef](#)]
153. Akinmoladun, A.C.; Khan, M.F.; Sarkar, J.; Farombi, E.O.; Maurya, R. Distinct radical scavenging and antiproliferative properties of *Spondias mombin* and antioxidant activity-guided isolation of quercetin-3-O- β -D-glucopyranoside and undec-1. *Afr. J. Pharm. Pharmacol.* **2015**, *9*, 506–513.
154. Ansari, J.A.; Khan, A.R.; Ahmad, M.K.; Fatima, N.; Rastogi, N.; Khan, M.F.; Khan, H.J.; Mahdi, A.A. Phytochemicals, Antioxidant and Antiproliferative, Studies of Some Medicinal Plants from Indian Sub-continent. *Br. J. Pharm. Res.* **2016**, *11*, 1–11. [[CrossRef](#)]
155. Ahamad, T.; Khan, M.A.; Ansari, W.A.; Khan, M.F. Antioxidant and Anticancer Activities of Selected Indian Medicinal Plant *Viz.*, *Artocarpus Lakoocha*, *Kigelia Pinnata*, and *Amaranthus Viridis*. *Era's J. Med. Res.* **2020**, *7*, 1–6. [[CrossRef](#)]
156. Ahamad, T.; Negi, D.S.; Khan, M.F. Phytochemical analysis, total phenolic content, antioxidant and antidiabetic activity of *Sansevieria cylindrica* leaves extract. *J. Nat. Prod. Resour.* **2017**, *3*, 134–136.
157. Nelson, B.; Johnson, M.; Walker, M.; Riley, K.R.; Sims, C.M. Antioxidant cerium oxide nanoparticles in biology and medicine. *Antioxidants* **2016**, *5*, 15. [[CrossRef](#)] [[PubMed](#)]
158. Ahamad, T.; Ansari, W.A.; Negi, D.S.; Khan, M.F. Non-Enzymatic Natural Reactive Oxygen Scavengers (Ros): A Review on Structures and Mode of Action. *Era's J. Med. Res.* **2019**, *6*, 103–112. [[CrossRef](#)]
159. Apak, R.; Ozyurek, M.; Guclu, K.; Capanoglu, E. Antioxidant Activity/Capacity Measurement. Reactive Oxygen and Nitrogen Species (ROS/RNS) Scavenging Assays, Oxidative Stress Biomarkers, and Chromatographic/Chemometric Assays. *J. Agric. Food Chem.* **2016**, *64*, 1046–1070. [[CrossRef](#)] [[PubMed](#)]
160. Hirayama, O.; Takagi, M.; Hukamoto, K.; Katoh, S. Evaluation of antioxidant activity by chemiluminescence. *Anal. Biochem.* **1997**, *247*, 237–241. [[CrossRef](#)] [[PubMed](#)]
161. Christodouleas, D.; Papadopoulos, K.; Calokerinos, A.C. Determination of Total Antioxidant Activity of Edible Oils as well as Their Aqueous and Organic Extracts by Chemiluminescence. *Food Anal. Methods* **2011**, *4*, 475–484. [[CrossRef](#)]

162. Bunaciu, A.A.; Danet, A.F.; Fleschin, S.; Aboul-Enein, H.Y. Recent Applications for in Vitro Antioxidant Activity Assay. *Crit. Rev. Anal. Chem.* **2016**, *46*, 389–399. [[CrossRef](#)] [[PubMed](#)]
163. Popa, C.; Farcasanu, I.; Jipa, S.; Zaharescu, T.; Danet, A. Chemiluminescence Determination of the Total Antioxidant Capacity of Rosemary Extract. *Rev. Chim.* **2012**, *63*, 715–719.
164. Popa, C.-V.; Cristea, N.-I.; Farcasanu, I.-C.; Danet, A.F. Total Antioxidant Capacity of Some Fruit Seeds Extracts. *Rev. Chim.* **2013**, *64*, 1377–1380.
165. Popa, C.-V.; Lungu, L.; Savoiu, M.; Bradu, C.; Dinoiu, V.; Danet, A.F. Total antioxidant activity and phenols and flavonoids content of several plant extracts. *Int. J. Food Prop.* **2012**, *15*, 691–701. [[CrossRef](#)]
166. Popa, C.; Danet, A.; Jipa, S.; Zaharescu, T. Determination of Total Antioxidant Activity of Wines Using a Flow Injection Method with Chemiluminescence Detection. *Rev. Chim.* **2010**, *61*, 11–16.
167. Popa, C.V.; Danet, A.F.; Jipa, S.; Zaharescu, T. Determination of Total Antioxidant Capacity of Some Fruit Juices and Noncarbonated Soft Drinks by a FIA-CL Method. *Rev. Chim.* **2012**, *63*, 978–983.
168. Iranifam, M.; Al Lawati, H.A.J. Monitoring the antioxidant capacity in honey and fruit juices using a microfluidic device with a $\text{NaHCO}_3\text{-H}_2\text{O}_2\text{-Co}^{2+}$ chemiluminescence reaction. *Food Chem.* **2019**, *297*, 124930. [[CrossRef](#)] [[PubMed](#)]
169. Fair, R.J.; Tor, Y. Antibiotics and Bacterial Resistance in the 21st Century. *Perspect. Medicin. Chem.* **2014**, *6*, 25–64. [[CrossRef](#)]
170. Verma, N.; Kumar, N. Synthesis and biomedical applications of copper oxide nanoparticles: An expanding horizon. *ACS Biomater. Sci. Eng.* **2019**, *5*, 1170–1188. [[CrossRef](#)]
171. Mba, I.E.; Nweze, E.I. Nanoparticles as therapeutic options for treating multidrug-resistant bacteria: Research progress, challenges, and prospects. *World J. Microbiol. Biotechnol.* **2021**, *37*, 108. [[CrossRef](#)]
172. Eltarahony, M.; Zaki, S.; Elkady, M.; Abd-El-Haleem, D. Biosynthesis, characterization of some combined nanoparticles, and its biocide potency against a broad spectrum of pathogens. *J. Nanomater.* **2018**, *2018*, 5263814. [[CrossRef](#)]
173. Shaikh, S.; Nazam, N.; Rizvi, S.M.D.; Ahmad, K.; Baig, M.H.; Lee, E.J.; Choi, I. Mechanistic Insights into the Antimicrobial Actions of Metallic Nanoparticles and Their Implications for Multidrug Resistance. *Int. J. Mol. Sci.* **2019**, *20*, 2468. [[CrossRef](#)]
174. Kumar, H.; Bhardwaj, K.; Kuča, K.; Kalia, A.; Nepovimova, E.; Verma, R.; Kumar, D. Flower-based green synthesis of metallic nanoparticles: Applications beyond fra-grance. *Nanomaterials* **2020**, *10*, 766. [[CrossRef](#)]
175. Rajeshkumar, S.; Bharath, L.V. Mechanism of plant-mediated synthesis of silver nanoparticles—A review on biomolecules involved, characterisation and antibacterial activity. *Chem. Biol. Interact.* **2017**, *273*, 219–227. [[CrossRef](#)]
176. Sánchez-López, E.; Gomes, D.; Esteruelas, G.; Bonilla, L.; Lopez-Machado, A.L.; Galindo, R.; Cano, A.; Espina, M.; Ettcheto, M.; Camins, A.; et al. Metal-Based Nanoparticles as Antimicrobial Agents: An Overview. *Nanomaterials* **2020**, *10*, 292. [[CrossRef](#)]
177. Khalil, M.M.H.; Ismail, E.H.; El-Baghdady, K.Z.; Mohamed, D. Green synthesis of silver nanoparticles using olive leaf extract and its antibacterial activity. *Arab. J. Chem.* **2014**, *7*, 1131–1139. [[CrossRef](#)]
178. Franci, G.; Falanga, A.; Galdiero, S.; Luciana Palomba, L.; Rai, M.; Morelli, G.; Galdiero, M. Silver nanoparticles as potential antibacterial agents. *Molecules* **2015**, *20*, 8856–8874. [[CrossRef](#)] [[PubMed](#)]
179. Mukunthan, K.; Elumalai, E.; Patel, T.N.; Murty, V.R. *Catharanthus roseus*: A natural source for the synthesis of silver nanoparticles. *Asian Pac. J. Trop. Biomed.* **2011**, *1*, 270–274. [[CrossRef](#)] [[PubMed](#)]
180. Dehnavi, A.S.; Raisi, A.; Aroujalian, A. Control size and stability of colloidal silver nanoparticles with antibacterial activity prepared by a green synthesis method. *Synth. React. Inorg. Met. Nano-Metal Chem.* **2013**, *43*, 543–551. [[CrossRef](#)]
181. Tiwari, V.; Mishra, N.; Gadani, K.; Solanki, P.S.; Shah, N.A.; Tiwari, M. Mechanism of Anti-bacterial Activity of Zinc Oxide Nanoparticle Against Carbapenem-Resistant *Acinetobacter baumannii*. *Front. Microbiol.* **2018**, *9*, 1218. [[CrossRef](#)]
182. Bogdanovič, U.; Lazič, V.; Vodnik, V.; Budimir, M.; Markovič, Z.; Dimitrijevič, S. Copper nanoparticles with high antimicrobial activity. *Mater. Lett.* **2014**, *128*, 75–78. [[CrossRef](#)]
183. Li, Y.; Zhang, W.; Niu, J.; Chen, Y. Mechanism of photogenerated reactive oxygen species and correlation with the antibacterial properties of engineered metal-oxide nanoparticles. *ACS Nano* **2012**, *6*, 5164–5173. [[CrossRef](#)]
184. Lipovsky, A.; Nitzan, Y.; Gedanken, A.; Lubart, R. Antifungal activity of ZnO nanoparticles—the role of ROS mediated cell injury. *Nanotechnology* **2011**, *22*, 105101. [[CrossRef](#)]
185. Romero, M.; Cantón, E.; Pemán, J.; Gobernado, M. Antifúngicos inhibidores de la síntesis del glucano. *Rev. Esp. Quimioter.* **2005**, *18*, 281–299.
186. Kumari, M.; Giri, V.P.; Pandey, S.; Kumar, M.; Katiyar, R.; Nautiyal, C.S.; Mishra, R. An insight into the mechanism of antifungal activity of biogenic nanoparticles than their chemical counterparts. *Pestic. Biochem. Physiol.* **2019**, *157*, 45–52. [[CrossRef](#)]
187. Sun, Q.; Li, J.; Le, T. Zinc Oxide nanoparticle as a novel class of antifungal agents: Current advances and future perspectives. *J. Agric. Food Chem.* **2018**, *66*, 11209–11220. [[CrossRef](#)]
188. Ferlay, J.; Colombet, M.; Soerjomataram, I.; Parkin, D.M.; Piñeros, M.; Znaor, A.; Bray, F. Cancer statistics for the year 2020: An overview. *Int. J. Cancer* **2021**, *149*, 778–789. [[CrossRef](#)]
189. Sung, H.; Ferlay, J.; Siegel, R.L.; Laversanne, M.; Soerjomataram, I.; Jemal, A.; Bray, F. Global Cancer Statistics 2020: GLOBOCAN Estimates of Incidence and Mortality Worldwide for 36 Cancers in 185 Countries. *CA Cancer J. Clin.* **2021**, *71*, 209–249. [[CrossRef](#)] [[PubMed](#)]
190. Falzone, L.; Salomone, S.; Libra, M. Evolution of Cancer Pharmacological Treatments at the Turn of the Third Millennium. *Front. Pharmacol.* **2018**, *9*, 1300. [[CrossRef](#)] [[PubMed](#)]

191. Andra, S.; Balu, S.K.; Jeevanandham, J.; Muthalagu, M.; Vidyavathy, M.; San Chan, Y.; Danquah, M.K. Phytosynthesized metal oxide nanoparticles for pharmaceutical applications. *Naunyn-Schmiedeberg's Arch. Pharmacol.* **2019**, *392*, 755–771. [[CrossRef](#)] [[PubMed](#)]
192. Toy, R.; Bauer, L.; Hoimes, C.; Ghaghada, K.B.; Karathanasis, E. Targeted Nanotechnology for Cancer Imaging. *Adv. Drug Deliv. Rev.* **2014**, *30*, 79–97. [[CrossRef](#)]
193. Khan, M.A.; Ahamad, T.; Saquib, M.; Hussain, M.K.; Khan, M.F. Unmodified household coffee maker assisted extraction and purification of anticancer agents from *Dillenia indica* fruits. *Nat. Prod. Res.* **2021**, *35*, 984–987. [[CrossRef](#)]
194. Mishra, D.P.; Khan, M.A.; Yadav, D.K.; Rawat, A.K.; Singh, R.K.; Ahamad, T.; Hussain, M.K.; Saquib, M.; Khan, M.F. Monoterpene Indole Alkaloids from *Anthocephalus cadamba* Fruits Exhibiting Anticancer Activity in Human Lung Cancer Cell Line H1299. *ChemistrySelect* **2018**, *3*, 8468–8472. [[CrossRef](#)]
195. Verma, V.; Sharma, V.; Singh, V.; Kumar, R.; Khan, M.F.; Singh, A.K.; Sharma, R.; Arya, K.R.; Maikhuri, J.P.; Dalela, D.; et al. Labda-8(17),12,14-trien-19-oic Acid Contained in Fruits of *Cupressus sempervirens* Suppresses Benign Prostatic Hyperplasia in Rat and In Vitro Human Models Through Inhibition of Androgen and STAT-3 Signaling. *Phytother. Res.* **2014**, *28*, 1196–1203. [[CrossRef](#)]
196. Ovais, M.; Khalil, A.T.; Raza, A.; Khan, M.A.; Ahmad, I.; Islam, N.U.; Saravanan, M.; Ubaid, M.F.; Ali, M.; Shinwari, Z.K. Green synthesis of silver nanoparticles via plant extracts: Beginning a new era in cancer theranostics. *Nanomedicine* **2016**, *12*, 3157–3177. [[CrossRef](#)] [[PubMed](#)]
197. Ovais, M.; Raza, A.; Naz, S.; Islam, N.U.; Khalil, A.T.; Ali, S.; Khan, M.A.; Shinwari, Z.K. Current state and prospects of the phytosynthesized colloidal gold nanoparticles and their applications in cancer theranostics. *Appl. Microbiol. Biotechnol.* **2017**, *101*, 3551–3565. [[CrossRef](#)] [[PubMed](#)]
198. Kumari, R.; Saini, A.K.; Kumar, A.; Saini, R.V. Apoptosis induction in lung and prostate cancer cells through silver nano-particles synthesized from *Pinus roxburghii* bioactive fraction. *J. Bio. Inorg. Chem.* **2020**, *25*, 23–37. [[CrossRef](#)] [[PubMed](#)]
199. Sahay, G.; Alakhova, D.Y.; Kabanov, A.V. Endocytosis of nanomedicines. *J. Control. Release* **2010**, *145*, 182–195. [[CrossRef](#)] [[PubMed](#)]
200. Patil, M.P.; Kim, G.-D. Eco-friendly approach for nanoparticles synthesis and mechanism behind antibacterial activity of silver and anticancer activity of gold nanoparticles. *Appl. Microbiol. Biotechnol.* **2017**, *101*, 79–92. [[CrossRef](#)] [[PubMed](#)]
201. Kim, Y.-J.; Perumalsamy, H.; Castro-Aceituno, V.; Kim, D.; Markus, J.; Lee, S.; Kim, S.; Liu, Y.; Yang, D.C. Photoluminescent and self-assembled hyaluronic acid-zinc oxide-ginsenoside Rh2 nanoparticles and their potential caspase-9 apoptotic mechanism towards cancer cell lines. *Int. J. Nano-Med.* **2019**, *14*, 8195–8208. [[CrossRef](#)] [[PubMed](#)]
202. Martínez-Cabanas, M.; López-García, M.; Rodríguez-Barro, P.; Vilariño, T.; Lodeiro, P.; Herrero, R.; Barriada, J.L.; de Vicente, M.E.S. Antioxidant Capacity Assessment of Plant Extracts for Green Synthesis of Nanoparticles. *Nanomaterials* **2021**, *11*, 1679. [[CrossRef](#)] [[PubMed](#)]
203. Flieger, J.; Franus, W.; Panek, R.; Szymańska-Chargot, M.; Flieger, W.; Flieger, M.; Kołodziej, P. Green Synthesis of Silver Nanoparticles Using Natural Extracts with Proven Antioxidant Activity. *Molecules* **2021**, *26*, 4986. [[CrossRef](#)]
204. Djamila, B.; Eddine, L.S.; Abderrhmane, B.; Nassiba, A.; Barhoum, A. In vitro antioxidant activities of copper mixed oxide (CuO/Cu₂O) nanoparticles produced from the leaves of *Phoenix dactylifera* L. *Biomass Conv. Bioref.* **2022**, in press. [[CrossRef](#)]
205. Younis, I.Y.; El-Hawary, S.; Eldahshan, S.O.A.; Abdel-Aziz, M.M.; Ali, Z.Y. Green synthesis of magnesium nanoparticles mediated from *Rosa floribunda* charisma extract and its antioxidant, antiaging and antibiofilm activities. *Sci. Rep.* **2011**, *11*, 16868. [[CrossRef](#)]
206. Keshari, A.K.; Srivastava, R.; Singh, P.; Yadav, V.B.; Nath, G. Antioxidant and antibacterial activity of silver nanoparticles synthesized by *Cestrum nocturnum*. *J. Ayurveda Integr. Med.* **2020**, *11*, 37–44. [[CrossRef](#)]
207. Shah, M.Z.; Guan, Z.H.; Din, A.U.; Ali, A.; Rehman, A.U.; Jan, K.; Faisal, S.; Saud, S.; Adnan, M.; Wahid, F.; et al. Synthesis of silver nanoparticles using *Plantago lanceolata* extract and assessing their antibacterial and antioxidant activities. *Sci. Rep.* **2021**, *11*, 20754. [[CrossRef](#)]
208. Reddy, N.V.; Satyanarayana, B.M.; Sivasankar, S.; Pragathi, D.; Subbaiah, K.V.; Vijaya, T. Eco-friendly synthesis of silver nanoparticles using leaf extract of *Flemingia wightiana*: Spectral characterization, antioxidant and anticancer activity studies. *SN Appl. Sci.* **2020**, *2*, 884. [[CrossRef](#)]
209. Balciunaitiene, A.; Viskelis, P.; Viskelis, J.; Streimikyte, P.; Liaudanskas, M.; Bartkiene, E.; Zavistanaviciute, P.; Zokaityte, E.; Starkute, V.; Ruzauskas, M.; et al. Green Synthesis of Silver Nanoparticles Using Extract of *Artemisia absinthium* L., *Humulus lupulus* L. and *Thymus vulgaris* L., Physico-Chemical Characterization, Antimicrobial and Antioxidant Activity. *Processes* **2021**, *9*, 1304. [[CrossRef](#)]
210. Alfuraydi, A.A.; Devanesan, S.; Al-Ansari, M.; AlSalhi, M.S.; Ranjitsingh, A.J. Eco-friendly green synthesis of silver nanoparticles from the sesame oil cake and its potential anticancer and antimicrobial activities. *J. Photochem. Photobiol. B Biol.* **2019**, *192*, 83–89. [[CrossRef](#)] [[PubMed](#)]
211. Anandan, M.; Poorani, G.; Boomi, P.; Kumar, V.K.; Anand, K.; Chuturgoon, A.A.; Prabu, G.H. Green synthesis of anisotropic silver nanoparticles from the aqueous leaf extract of *Dodonaea viscosa* with their antibacterial and anticancer activities. *Process Biochem.* **2019**, *80*, 80–88. [[CrossRef](#)]
212. Narayanan, A.V.; Jacob, R.; Paulson, J.M.; Kumar, D.B.; Narayana, C.R. Mango leaf extract synthesized silver nanorods exert anticancer activity on breast cancer and colorectal carcinoma cells. *J. Drug Deliv. Sci. Technol.* **2018**, *44*, 8–12.

213. Arintonang, H.F.; Koleangan, H.; Wuntu, A.D. Synthesis of silver nanoparticles using aqueous extract of medicinal plants' *Impatiens balsamina* and *Lantana camara* fresh leaves and analysis of antimicrobial activity. *Int. J. Microbiol.* **2019**, *2019*, 8642303. [[CrossRef](#)]
214. Balasubramanian, S.; Kala, S.M.J.; Pushparaj, T.L. Biogenic synthesis of gold nanoparticles using *Jasminum auriculatum* leaf extract and their catalytic, antimicrobial and anticancer activities. *J. Drug Deliv. Sci. Technol.* **2020**, *57*, 101620. [[CrossRef](#)]
215. Baruah, D.; Yadav, R.N.S.; Yadav, A.; Das, A.M. *Alpinia nigra* fruits mediated synthesis of silver nanoparticles and their antimicrobial and photocatalytic activities. *J. Photochem. Photobiol. B Biol.* **2019**, *201*, 111649. [[CrossRef](#)]
216. Chokkalingam, M.; Singh, P.; Huo, Y.; Soshnikova, V.; Ahn, S.; Kang, J.; Yang, D.C. Facile synthesis of Au and Ag nanoparticles using fruit extract of *Lycium chinense* and their anticancer activity. *J. Drug Deliv. Sci. Technol.* **2019**, *49*, 308–315. [[CrossRef](#)]
217. Desai, M.P.; Sangaokar, G.M.; Pawar, K.D. Kokum fruit mediated biogenic gold nanoparticles with photoluminescent, photocatalytic and antioxidant activities. *Process Biochem.* **2018**, *70*, 188–197. [[CrossRef](#)]
218. Esmail, F.; Koohestani, H.; Abdollah-Pour, H. Characterization and antibacterial activity of silver nanoparticles green synthesized using *Ziziphora clinopodioides* extract. *Environ. Nanotechnol. Monit. Manag.* **2020**, *14*, 100303. [[CrossRef](#)]
219. Govindappa, M.; Hemashekhar, B.; Arthikala, M.-K.; Ravishankar, R.V.; Ramachandra, Y.L. Characterization, antibacterial, antioxidant, antidiabetic, anti-inflammatory and antityrosinase activity of green synthesized silver nanoparticles using *Calophyllum tomentosum* leaves extract. *Results Phys.* **2018**, *9*, 400–408. [[CrossRef](#)]
220. Hamelian, M.; Hemmati, S.; Varmira, K.; Veisi, H. Green synthesis, antibacterial, antioxidant and cytotoxic effect of gold nanoparticles using *Pistacia Atlantica* extract. *J. Taiwan Inst. Chem. Eng.* **2018**, *93*, 21–30. [[CrossRef](#)]
221. Hekmati, M.; Hasanirad, S.; Khaledi, A.; Esmaeili, D. Green synthesis of silver nanoparticles using extracts of *Allium rotundum* L, *Falcaria vulgaris* Bernh, and *Ferulago angulate* Boiss, and their antimicrobial effects in vitro. *Gene Rep.* **2020**, *19*, 100589. [[CrossRef](#)]
222. Dalir, J.B.S.; Djahaniani, H.; Nabati, F.; Hekmati, M. Characterization and the evaluation of antimicrobial activities of silver nanoparticles biosynthesized from *Carya illinoensis* leaf extract. *Heliyon* **2020**, *6*, e03624. [[CrossRef](#)]
223. Khandanlou, R.; Murthy, V.; Wang, H. Gold nanoparticle-assisted enhancement in bioactive properties of Australian native plant extracts, *Tasmania lanceolata* and *Backhousia citriodora*. *Mater. Sci. Eng. C* **2020**, *112*, 110922. [[CrossRef](#)]
224. Kumar, D.; Arora, S.; Abdullah, Danish, M. Plant based synthesis of silver nanoparticles from *Ougeinia oojeinensis* leaves extract and their membrane stabilizing, antioxidant and antimicrobial activities. *Mater. Today Proc.* **2019**, *17*, 313–320. [[CrossRef](#)]
225. Kumar, V.; Singh, S.; Srivastava, B.; Bhadouria, R.; Singh, R. Green synthesis of silver nanoparticles using leaf extract of *Holoptelea integrifolia* and preliminary investigation of its antioxidant, anti-inflammatory, antidiabetic and antibacterial activities. *J. Environ. Chem. Eng.* **2019**, *7*, 103094. [[CrossRef](#)]
226. K p, F. .;  o kun ay, S.; Duman, F. Biosynthesis of silver nanoparticles using leaf extract of *Aesculus hippocastanum* (horse chestnut): Evaluation of their antibacterial, antioxidant and drug release system activities. *Mater. Sci. Eng. C* **2020**, *107*, 110207. [[CrossRef](#)]
227. Lydia, D.E.; Khusro, A.; Immanuel, P.; Esmail, G.A.; Al-Dhabi, N.A.; Arasu, M.V. Photoactivated synthesis and characterization of gold nanoparticles from *Punica granatum* L. seed oil: An assessment on antioxidant and anticancer properties for functional yoghurt nutraceuticals. *J. Photochem. Photobiol. B Biol.* **2020**, *206*, 111868. [[CrossRef](#)]
228. Nagalingam, M.; Kalpana, V.N.; Devi Rajeswari, V.; Panneerselvam, A. Biosynthesis, characterization, and evaluation of bioactivities of leaf extract-mediated biocompatible gold nanoparticles from *Alternanthera bettzickiana*. *Biotechnol. Rep.* **2018**, *19*, e00268.
229. Onitsuka, S.; Hamada, T.; Okamura, H. Preparation of antimicrobial gold and silver nanoparticles from tealeaf extracts. *Colloids Surf. B* **2019**, *173*, 242–248. [[CrossRef](#)]
230. Rajawat, S.; Malik, M.M. Anticancer activity of green silver nanoparticles against He-La cervical cancer cell lines. *Mater. Today Proc.* **2019**, *18*, 841–847.
231. Oves, M.; Aslam, M.; Rauf, M.A.; Qayyum, S.; Qari, H.A.; Khan, M.S.; Ismail, I.M.I. Antimicrobial and anticancer activities of silver nanoparticles synthesized from the root hair extract of *Phoenix dactylifera*. *Mater. Sci. Eng. C* **2018**, *89*, 429–443. [[CrossRef](#)]
232. Pallela, P.N.V.K.; Ummey, S.; Ruddaraju, L.K.; Pammi, S.V.N.; Yoon, S.-G. Ultra-small, mono dispersed green synthesized silver nanoparticles using aqueous extract of *Sida cordifolia* plant and investigation of antibacterial activity. *Microb. Pathog.* **2018**, *124*, 63–69. [[CrossRef](#)]
233. Pirtarighat, S.; Ghannadnia, M.; Baghshahi, S. Green synthesis of silver nanoparticles using the plant extract of *Salvia spinosa* grown in vitro and their antibacterial activity assessment. *J. Nanostruct. Chem.* **2019**, *9*, 1–9. [[CrossRef](#)]
234. Ramadan, M.A.; Shawkey, A.E.; Rabeh, M.A.; Abdellatif, A.O. Promising antimicrobial activities of oil and silver nanoparticles obtained from *Melaleuca alternifolia* leaves against selected skin-infecting pathogens. *J. Nat. Med.* **2019**, *20*, 100289. [[CrossRef](#)]
235. Ravichandran, V.; Vasanthi, S.; Shalini, S.; Shah, S.A.A.; Tripathy, M.; Paliwal, N. Green synthesis, characterization, antibacterial, antioxidant and photocatalytic activity of *Parkia speciosa* leaves extract mediated silver nanoparticles. *Results Phys.* **2019**, *15*, 102565. [[CrossRef](#)]
236. Satpathy, S.; Patra, A.; Ahirwar, B.; Hussain, M.D. Process optimization for green synthesis of gold nanoparticles mediated by extract of *Hygrophila spinosa* T. Anders and their biological applications. *Physica. E Low Dimens. Syst. Nanostruct.* **2020**, *121*, 113830. [[CrossRef](#)]

237. Sriranjani, R.; Srinithya, B.; Vellingiri, V.; Brindha, P.; Anthony, S.P.; Sivasubramanian, A.; Muthuraman, M.S. Silver nanoparticle synthesis using Clerodendrum phlomidis leaf extract and preliminary investigation of its antioxidant and anticancer activities. *J. Mol. Liq.* **2016**, *220*, 926–930. [[CrossRef](#)]
238. Sutan, N.A.; Manolescu, D.S.; Fierascu, I.; Neblea, A.M.; Sutan, C.; Ducu, C.; Fierascu, R.C. Phytosynthesis of gold and silver nanoparticles enhance in vitro antioxidant and mitostimulatory activity of Aconitum toxicum Reichenb. rhizomes alcoholic extracts. *Mater. Sci. Eng. C* **2018**, *93*, 746–758. [[CrossRef](#)]
239. Valsalam, S.; Agastian, P.; Esmail, G.A.; Ghilan, A.-K.M.; Al-Dhabi, N.A.; Arasu, M.V. Biosynthesis of silver and gold nanoparticles using Musa acuminata colla flower and its pharmaceutical activity against bacteria and anticancer efficacy. *J. Photochem. Photobiol. B Biol.* **2019**, *201*, 111670. [[CrossRef](#)]
240. Vijayakumar, S.; Malaikozhundan, B.; Saravanakumar, K.; Durán-Lara, E.F.; Wang, M.-H.; Vaseeharan, B. Garlic clove extract assisted silver nanoparticle—Antibacterial, antibiofilm, antihelminthic, anti-inflammatory, anticancer and ecotoxicity assessment. *J. Photochem. Photobiol. B Biol.* **2019**, *198*, 111558. [[CrossRef](#)]
241. Vijilvani, C.; Bindhu, M.R.; Frincy, F.C.; ALSalhi, M.S.; Sabitha, S.; Saravanakumar, K.; Atif, M. Antimicrobial and catalytic activities of biosynthesized gold, silver and palladium nanoparticles from Solanum nigrum leaves. *J. Photochem. Photobiol. B Biol.* **2020**, *202*, 111713. [[CrossRef](#)]
242. Barani, H.; Aboutorabi, S.N.; Nasiriboroumand, M.; Mohammadi, P.; Sheibani, H. Biosynthesis of silver nanoparticles using safflower flower: Structural characterization, and its antibacterial activity on applied wool fabric. *J. Inorg. Organomet. Polym. Mater.* **2018**, *28*, 2525–2532.
243. Ahn, E.-Y.; Jin, H.; Park, Y. Green synthesis and biological activities of silver nanoparticles prepared by *Carpesium cernuum* extract. *Arch. Pharm. Res.* **2019**, *42*, 926–934. [[CrossRef](#)]
244. Akpomie, K.G.; Ghosh, S.; Gryzenhout, M.; Conradie, J. Ananas comosus peel-mediated green synthesized magnetite nanoparticles and their antifungal activity against four filamentous fungal strains. *Biomass Convers. Biorefinery*, 2021, in press. [[CrossRef](#)]
245. Al-Otibi, F.; Al-Ahaidib, R.A.; Alharbi, R.I.; Al-Otaibi, R.M.; Albasher, G. Antimicrobial potential of biosynthesized silver nanoparticles by Aaronsohnia factorovskyi extract. *Molecules* **2020**, *26*, 130. [[CrossRef](#)]
246. Murthy, A.H.C.; Zeleke, T.D.; Tan, K.B.; Ghotekar, S.; Alam, M.W.; Balachandran, R.; Chan, K.-Y.; Sanaula, P.F.; Kumar, M.R.A.; Ravikum, C.R. Enhanced multifunctionality of CuO nanoparticles synthesized using aqueous leaf extract of Vernonia amygdalina plant. *Results Chem.* **2021**, *3*, 100141. [[CrossRef](#)]
247. Aslany, S.; Tafvizi, F.; Naseh, V. Characterization and evaluation of cytotoxic and apoptotic effects of green synthesis of silver nanoparticles using Artemisia Ciniformis on human gastric adenocarcinoma. *Mater. Today Commun.* **2020**, *24*, 101011. [[CrossRef](#)]
248. Behboodi, S.; Baghbani-Arani, F.; Abdalan, S.; Sadat, S.S.A. Green engineered biomolecule-capped silver nanoparticles fabricated from cichorium intybus extract: In vitro assessment on apoptosis properties toward human breast cancer (MCF-7) Cells. *Biol. Trace Elem. Res.* **2019**, *187*, 392–402. [[CrossRef](#)] [[PubMed](#)]
249. Bethu, M.S.; Netala, V.R.; Domdi, L.; Vijaya, T.; Janapala, V.R. Potential anticancer activity of biogenic silver nanoparticles using leaf extract of Rhynchosia suaveolens: An insight into the mechanism. *Artif Cells. Nanomed. Biotechnol.* **2018**, *46*, 104–114. [[CrossRef](#)] [[PubMed](#)]
250. Bharathi, D.; Preethi, S.; Abarna, K.; Nithyasri, M.; Kishore, P.; Deepika, K. Bio-inspired synthesis of fower shaped iron oxide nanoparticles (FeONPs) using phytochemicals of Solanum lycopersicum leaf extract for biomedical applications. *Biocatal. Agric. Biotechnol.* **2020**, *27*, 101698. [[CrossRef](#)]
251. Chandraker, S.K.; Lal, M.; Shukla, R. DNA-binding, antioxidant, H₂O₂ sensing and photocatalytic properties of biogenic silver nanoparticles using Ageratum conyzoides L. leaf extract. *RSC Adv.* **2019**, *9*, 23408–23417. [[CrossRef](#)]
252. Chavan, R.R.; Bhinge, S.D.; Bhutkar, M.A.; Randive, D. Characterization, antioxidant, antimicrobial and cytotoxic activities of green synthesized silver and iron nanoparticles using alcoholic Blumea eriantha DC plant extract. *Mater. Today Commun.* **2020**, *24*, 101320. [[CrossRef](#)]
253. Dobrucka, R. Synthesis of MgO nanoparticles using artemisia abrotanum herba extract and their antioxidant and photocatalytic properties. *Iran J. Sci. Technol. Trans A Sci.* **2018**, *42*, 547–555. [[CrossRef](#)]
254. Dobrucka, R.; Kaczmarek, M.; Łagiedo, M.; Kielan, A.; Długaszewska, J. Evaluation of biologically synthesized Au-CuO and CuO-ZnO nanoparticles against glioma cells and microorganisms. *Saudi Pharm. J.* **2019**, *27*, 373–383. [[CrossRef](#)]
255. Francis, S.; Joseph, S.; Koshy, E.P.; Mathew, B. Microwave assisted green synthesis of silver nanoparticles using leaf extract of elephantopus scaber and its environmental and biological applications. *Artif. Cells Nanomed. Biotechnol.* **2018**, *46*, 795–804. [[CrossRef](#)]
256. Ghotekar, S.; Pansambal, S.; Pawar, S.P.; Pagar, T.; Oza, R.; Bangale, S. Biological activities of biogenically synthesized fluorescent silver nanoparticles using Acanthospermum hispidum leaves extract. *SN Appl. Sci.* **2019**, *1*, 1342. [[CrossRef](#)]
257. Ghotekar, S.; Savale, A.; Pansambal, S. Phytofabrication of fluorescent silver nanoparticles from Leucaena leucocephala L. leaves and their biological activities. *J. Water Environ. Nanotechnol.* **2018**, *3*, 95–105.
258. Hameed, S.; Khalil, A.T.; Ali, M.; Numan, M.; Khamlich, S.; Shinwari, Z.K.; Maaza, M. Greener synthesis of ZnO and Ag-ZnO nanoparticles using Silybum marianum for diverse biomedical applications. *Nanomedicine* **2019**, *14*, 655–673. [[CrossRef](#)]
259. Jamdagni, P.; Khatri, P.; Rana, J.S. Green synthesis of zinc oxide nanoparticles using fower extract of Nyctanthes arbor-tristis and their antifungal activity. *J. King Saud Univ. Sci.* **2018**, *30*, 168–175. [[CrossRef](#)]

260. Jebril, S.; Jenana, K.B.R.; Dridi, C. Green synthesis of silver nanoparticles using *Melia azedarach* leaf extract and their antifungal activities: In vitro and in vivo. *Mater. Chem. Phys.* **2020**, *248*, 122898. [[CrossRef](#)]
261. Kanagamani, K.; Muthukrishnan, P.; Shankar, K.; Kathiresan, A.; Barabadi, H.; Saravanan, M. Antimicrobial, cytotoxicity and photocatalytic degradation of Norfoxacin using *Kleinia grandiflora* mediated silver nanoparticles. *J. Clust. Sci.* **2019**, *30*, 1415–1424. [[CrossRef](#)]
262. Król, A.; Railean-Plugaru, V.; Pomastowski, P.; Buszewski, B. Phytochemical investigation of *Medicago sativa* L. extract and its potential as a safe source for the synthesis of ZnO nanoparticles: The proposed mechanism of formation and antimicrobial activity. *Phytochem. Lett.* **2019**, *31*, 170–180. [[CrossRef](#)]
263. Lee, Y.J.; Song, K.; Cha, S.-H.; Cho, S.; Kim, Y.S.; Park, Y. Sesquiterpenoids from *Tussilago farfara* flower bud extract for the eco-friendly synthesis of silver and gold nanoparticles possessing antibacterial and anticancer activities. *Nanomaterials* **2019**, *9*, 819. [[CrossRef](#)]
264. Mali, S.C.; Dhaka, A.; Githala, C.K.; Trivedi, R. Green synthesis of copper nanoparticles using *Celastrus paniculatus* Willd. leaf extract and their photocatalytic and antifungal properties. *Biotechnol. Rep.* **2020**, *27*, e00518. [[CrossRef](#)]
265. Mofolo, M.J.; Kadhila, P.; Chinsebu, K.C.; Mashele, S.; Sekhoacha, M. Green synthesis of silver nanoparticles from extracts of *Pechuel-Loeschea leubnitziae*: Their anti-proliferative activity against the U87 cell line. *Inorg. Nano-Metal Chem.* **2020**, *50*, 949–955. [[CrossRef](#)]
266. Mostafa, E.; Fayed, M.A.A.; Radwan, R.A.; Bakr, R.O. *Centaurea pumilio* L. extract and nanoparticles: A candidate for healthy skin. *Colloids Surf. B Biointerfaces* **2019**, *182*, 110350. [[CrossRef](#)]
267. Mousavi, B.; Tafvizi, F.; Zaker, B.S. Green synthesis of silver nanoparticles using *Artemisia turcomanica* leaf extract and the study of anti-cancer effect and apoptosis induction on gastric cancer cell line (AGS). *Artif. Cells Nanomed. Biotechnol.* **2018**, *46*, 499–510. [[CrossRef](#)]
268. Murthy, H.C.A.; Desalegn, T.; Kassa, M.; Abebe, B.; Assefa, T. Synthesis of green copper nanoparticles using Medicinal Plant *Hagenia abyssinica* (Brace) JF. Gmel. leaf extract: Antimicrobial properties. *J. Nanomater.* **2020**, *2020*, 3924081. [[CrossRef](#)]
269. Muthuvel, A.; Jothibas, M.; Manoharan, C. Synthesis of copper oxide nanoparticles by chemical and biogenic methods: Photocatalytic degradation and in vitro antioxidant activity. *Nanotechnol. Environ. Eng.* **2020**, *5*, 14. [[CrossRef](#)]
270. Muthuvel, A.; Jothibas, M.; Manoharan, C. Effect of chemically synthesis compared to biosynthesized ZnO-NPs using *Solanum nigrum* leaf extract and their photocatalytic, antibacterial and invitro antioxidant activity. *J. Environ. Chem. Eng.* **2020**, *8*, 103705. [[CrossRef](#)]
271. Nagore, P.; Ghotekar, S.; Mane, K.; Ghoti, A. Structural properties and antimicrobial activities of *Polyalthia longifolia* leaf extract-mediated CuO nanoparticles. *Bionanoscience* **2021**, *11*, 579–589. [[CrossRef](#)]
272. Nijalingappa, T.B.; Veeraiiah, M.K.; Basavaraj, R.B.; Darshand, G.P.; Sharma, S.C.; Nagabhushana, H. Antimicrobial properties of green synthesis of MgO micro architectures via *Limonia acidissima* fruit extract. *Biocatal. Agric. Biotechnol.* **2019**, *18*, 100991. [[CrossRef](#)]
273. Nithya, K.; Kalyanasundharam, S. Effect of chemically synthesis compared to biosynthesized ZnO nanoparticles using aqueous extract of *C. halicacabum* and their antibacterial activity. *OpenNano* **2019**, *4*, 100024. [[CrossRef](#)]
274. Okaiyeto, K.; Ojemaye, M.O.; Hoppe, H.; Mabinya, L.V.; Okoh, A.I. Phytofabrication of silver/silver chloride nanoparticles using aqueous leaf extract of *Oedera genistifolia*: Characterization and antibacterial potential. *Molecules* **2019**, *24*, 4382. [[CrossRef](#)]
275. Okeke, I.S.; Agwu, K.K.; Ubachukwu, A.A.; Maaza, M.; Ezema, F.I. Impact of Cu doping on ZnO nanoparticles phytochemically synthesized for improved antibacterial and photocatalytic activities. *J. Nanoparticle Res.* **2020**, *22*, 272. [[CrossRef](#)]
276. Pagar, K.; Ghotekar, S.; Pagar, T.; Nikam, A.; Pansambal, S.; Oza, R.; Sanap, D.; Dabhane, H. Antifungal activity of biosynthesized CuO nanoparticles using leaves extract of *Moringa oleifera* and their structural characterizations. *Asian J. Nanosci. Mater.* **2020**, *3*, 15–23.
277. Paul, D.M.; Rebecca, L.J.; Veluswamy, P.; Das, J. Exploration of *Wedelia chinensis* leaf-assisted silver nanoparticles for antioxidant, antibacterial and in vitro cytotoxic applications. *J. Food Drug. Anal.* **2018**, *26*, 917–925. [[CrossRef](#)]
278. Nasar, M.Q.; Zohra, T.; Khalil, A.T.; Saqib, S.; Ayaz, M.; Ahmad, A.; Shinwari, Z.K. *Seripheidium quettense* mediated green synthesis of biogenic silver nanoparticles and their theranostic applications. *Green Chem. Lett. Rev.* **2019**, *12*, 310–322. [[CrossRef](#)]
279. Rafique, M.; Sadaf, I.; Tahir, M.B.; Rafique, M.S.; Nabi, G.; Iqbal, T.; Sughra, K. Novel and facile synthesis of silver nanoparticles using *Albizia procera* leaf extract for dye degradation and antibacterial applications. *Mater. Sci. Eng. C* **2019**, *99*, 1313–1324. [[CrossRef](#)] [[PubMed](#)]
280. Rajapriya, M.; Sharmili, S.A.; Baskar, R.; Balaji, R.; Alharbi, N.S.; Kadaikunnan, S.; Khaled, J.M.; Alanzi, K.F.; Vaseeharan, B. Synthesis and characterization of zinc oxide nanoparticles using *cynara scolymus* leaves: Enhanced hemolytic, antimicrobial, antiproliferative, and photocatalytic activity. *J. Clust. Sci.* **2020**, *31*, 791–801. [[CrossRef](#)]
281. Rajeshkumara, S.; Venkat, K.S.; Ramaiah, A.; Agarwal, H.; Lakshmi, T.; Roopan, S.M. Biosynthesis of zinc oxide nanoparticles using *Mangifera indica* leaves and evaluation of their antioxidant and cytotoxic properties in lung cancer (A549) cells. *Enzyme Microb. Technol.* **2018**, *117*, 91–95. [[CrossRef](#)] [[PubMed](#)]
282. Kumar, R.S.; Menon, S.; Kumar, V.; Tambuwala, M.M.; Bakshi, H.A.; Mehta, M.; Satija, S.; Gupta, G.; Chellappan, D.K.; Thangavelu, K.; et al. Antibacterial and antioxidant potential of biosynthesized copper nanoparticles mediated through *Cissus arnotiana* plant extract. *J. Photochem. Photobiol. B Biol.* **2019**, *197*, 111531.

283. Rani, R.; Sharma, D.; Chaturvedi, M.; Yadav, J.P. Green synthesis of silver nanoparticles using *Tridax procumbens*: Their characterization, antioxidant and antibacterial activity against MDR and reference bacterial strains. *Chem. Pap.* **2020**, *74*, 1817–1830. [[CrossRef](#)]
284. Saratale, R.G.; Benelli, G.; Kumar, G.; Kim, D.S.; Saratale, G.D. Bio-fabrication of silver nanoparticles using the leaf extract of an ancient herbal medicine, dandelion (*Taraxacum officinale*), evaluation of their antioxidant, anticancer potential, and antimicrobial activity against phytopathogens. *Environ. Sci. Pollut. Res.* **2018**, *25*, 10392–10406. [[CrossRef](#)]
285. Seifpour, R.; Nozar, M.; Pishkar, L. Green synthesis of silver nanoparticles using *tragopogon collinus* leaf extract and study of their antibacterial effects. *J. Inorg. Organomet. Polym. Mater.* **2020**, *30*, 2926–2936. [[CrossRef](#)]
286. Selim, Y.A.; Azb, M.A.; Ragab, I.; El-Azim, A.M. Green synthesis of zinc oxide nanoparticles using aqueous extract of *deverra tortuosa* and their cytotoxic activities. *Sci. Rep.* **2020**, *10*, 3445. [[CrossRef](#)]
287. Sharif-Rad, M.; Pohl, P. Synthesis of biogenic silver nanoparticles (AgCl-NPs) using a *pulicaria vulgaris* gaertn. aerial part extract and their application as antibacterial, antifungal and antioxidant agents. *Nanomaterials* **2020**, *10*, 638. [[CrossRef](#)]
288. Singh, A.; Joshi, N.C.; Ramola, M. Magnesium oxide Nanoparticles (MgONPs): Green synthesis, characterizations and antimicrobial activity. *Res. J. Pharm. Technol.* **2019**, *12*, 4644. [[CrossRef](#)]
289. Sriramulu, M.; Shukla, D.; Sumathi, S. Aegle marmelos leaves extract mediated synthesis of zinc ferrite: Antibacterial activity and drug delivery. *Mater. Res. Express* **2018**, *5*, 115404. [[CrossRef](#)]
290. Suresh, J.; Pradheesh, G.; Alexramani, V.; Sundrarajan, M.; Hong, S.I. Green synthesis and characterization of hexagonal shaped MgO nanoparticles using insulin plant (*Costus pictus* D. Don) leave extract and its antimicrobial as well as anticancer activity. *Adv. Powder. Technol.* **2018**, *29*, 1685–1694. [[CrossRef](#)]
291. Valsalam, S.; Agastian, P.; Arasu, M.V.; Al-Dhabi, N.A.; Ghilan, A.K.M.; Kaviyarasu, K.; Ravindran, B.; Chang, S.W.; Arokiyaraj, S. Rapid biosynthesis and characterization of silver nanoparticles from the leaf extract of *Tropaeolum majus* L. and its enhanced in-vitro antibacterial, antifungal, antioxidant and anticancer properties. *J. Photochem. Photobiol. B Biol.* **2019**, *191*, 65–74. [[CrossRef](#)] [[PubMed](#)]
292. Wang, L.; Wu, Y.; Xie, J.; Wu, S.; Wu, Z. Characterization, antioxidant and antimicrobial activities of green synthesized silver nanoparticles from *Psidium guajava* L. leaf aqueous extracts. *Mater. Sci. Eng. C* **2018**, *86*, 1–8. [[CrossRef](#)] [[PubMed](#)]
293. Yazdi, M.E.T.; Amiri, M.S.; Hosseini, H.A.; Reza, K.O.; Mosawee, H.; Pakravanan, K.; Darroudi, M. Plant-based synthesis of silver nanoparticles in *Handelia trichophylla* and their biological activities. *Bull. Mater. Sci.* **2019**, *42*, 155. [[CrossRef](#)]
294. Zayed, M.F.; Mahfoze, R.A.; El-kousy, S.M.; Al-Ashkar, E.A. In-vitro antioxidant and antimicrobial activities of metal nanoparticles biosynthesized using optimized *Pimpinella anisum* extract. *Colloids Surf. A Physicochem. Eng. Asp.* **2020**, *585*, 124167. [[CrossRef](#)]
295. Han, S.; Ahmeda, A.; Jalalvand, A.R.; Lu, W.; Zangeneh, M.M.; Zangeneh, A. Application of silver nanoparticles containing *Gundelia tournefortii* L. leaf aqueous extract in the treatment of microbial diseases and cutaneous wound healing. *Appl. Organomet. Chem.* **2022**, *36*, e6311. [[CrossRef](#)]
296. Amina, M.; Alarfaj, N.A.; El-Tohamy, M.F.; Al-Musayeib, N.M.; Oraby, H.F. Sequential injection-chemiluminescence evaluation of stigmaterol glucoside and luteolin via green synthesis of silver nanoparticles using biomass of *Plectranthus asirensis*. *Green Chem Lett Rev.* **2018**, *11*, 523–533. [[CrossRef](#)]
297. Besliu, D.-V.; Meghea, A. Optimization of green synthesis of silver nanoparticles by using *Harpagophytum procumbens* root extract. *UPB Sci. Bull.* **2021**, *83*, 19–28.
298. Bunghez, R.; Patrascu, M.E.B.; Badea, N.; Doncea, S.M.; Popescu, A.; Ion, R.M. Antioxidant silver nanoparticles green synthesized using ornamental plants. *J. Optoelectron. Adv. Mater.* **2012**, *14*, 1016–1022.
299. Barbinta-Patrascu, M.E.; Bunghez, I.-R.; Iordache, S.M.; Badea, N.; Fierascu, R.-C.; Ion, R.M. Antioxidant properties of biohybrids based on liposomes and Sage silver nanoparticles. *J. Nanosci. Nanotechnol.* **2013**, *13*, 2051–2060. [[CrossRef](#)] [[PubMed](#)]
300. Ortana, A.; Fierascub, I.; Ungureanuc, C.; Fierascub, R.C.; Avramescud, S.M.; Dumitrescuc, O.; Dinu-Pirvue, C.E. Innovative phytosynthesized silver nanoarchitectures with enhanced antifungal and antioxidant properties. *Appl. Surf. Sci.* **2015**, *358*, 540–548. [[CrossRef](#)]

Disclaimer/Publisher's Note: The statements, opinions and data contained in all publications are solely those of the individual author(s) and contributor(s) and not of MDPI and/or the editor(s). MDPI and/or the editor(s) disclaim responsibility for any injury to people or property resulting from any ideas, methods, instructions or products referred to in the content.